الجمهورية الجزائرية الديمقراطية الشعبية

PEOPLE'S DEMOCRATIC REPUBLIC OF ALGERIA

وزارة التعليم العالي و البحث العلمي

Ministry of Higher Education and Scientific Research

جامعة أبي بكر بلقايد – تلمسان –

Abou Bekr Belkaïd University – Tlemcen –
Faculty of TECHNOLOGY

THESIS

Presented to obtain the 3rd Cycle DOCTORATE degree
in **Telecommunication**

Speciality: **Optical and Microwave Telecommunications**

By: **Mébarki Ghada Fatima Elzahra**

Subject

Study and design of conformable absorbers for the control of Electromagnetic waves propagation

Publicly defended on: **05/12/2024**; before the jury composed of:

KAMECHE Samir	Prof	Univ. Tlemcen	**President**
BENMOSTEFA Naima	Prof	Univ. Tlemcen	**Supervisor**
BOUACHA Abdelhafid	Prof	Univ. Tlemcen	**Examiner**
CHAKER Hichem	Prof	Univ. Sidi Bel Abbes	**Examiner**
NOURI Keltouma	Prof	Univ. Saida	**Examiner**

Abstract

This thesis investigates the design, optimization, and fabrication of metamaterial absorbers (MMAs) with a focus on their electromagnetic properties and practical applications. Metamaterial absorbers are of great interest due to their ability to achieve high absorption rates over a broad frequency range and their potential for use in advanced communication and sensing technologies. The research encompasses the theoretical modeling, simulation, and practical implementation of various MMA designs, including spiral wire coil resonator. Key findings reveal how modifications to the absorber design and substrate parameters can significantly enhance performance across different frequency bands. The work provides valuable insights into optimizing metamaterial absorbers for improved functionality in applications such as radar, imaging systems, and stealth technology, advancing the field of metamaterials and their technological applications.

Keyword :Metamaterial absorber;Electromagnetic propriety; Frequency range; spiral wire coil resonator.

Resumé

Cette thèse explore la conception, l'optimisation et la fabrication des absorbants de métamatériaux (MMAs), en mettant l'accent sur leurs propriétés électromagnétiques et leurs applications pratiques. Les absorbants de métamatériaux suscitent un grand intérêt en raison de leur capacité à atteindre des taux d'absorption élevés sur une large gamme de fréquences et de leur potentiel d'utilisation dans les technologies avancées de communication et de détection. La recherche couvre la modélisation théorique, la simulation et la mise en œuvre pratique de divers designs de MMA, y compris le résonateur à bobine de fil en spirale. Les principales conclusions révèlent comment les modifications apportées à la conception de l'absorbants et aux paramètres du substrat peuvent améliorer de manière significative les performances sur différentes bandes de fréquences. Ce travail fournit des perspectives précieuses pour optimiser les absorbants de métamatériaux afin d'améliorer leur fonctionnalité dans des applications telles que le radar, les systèmes d'imagerie et la technologie furtive, faisant progresser le domaine des métamatériaux et leurs applications technologiques.

mots clée : métamatériaux; absorbants; resonateur à bobine de fil en spirale; bande de fréquences.

ملخص:

تتناول هذه الأطروحة تصميم و تحسين وتصنيع ممتصات الميتاميتريال , مع التركيز على خصائصها الكهرومغناطيسية وتطبيقاتها العملية . تحظى ممتصات الميتاميتريال باهتمام كبير نظرًا لقدرتها على تحقيق معدلات امتصاص عالية عبر نطاق واسع من الترددات وإمكانية استخدامها في تقنيات الاتصالات والاستشعار المتقدمة. يشمل البحث النموذج النظري، والمحاكاة، والتنفيذ العملي لتصميم لممتصات الميتاميتريال، بما في ذلك تصميمات تعتمد على الرنانات اللولبية. تكشف النتائج الرئيسية كيف أن التعديلات على تصميم الممتص ومعلمات الطبقة السفلية يمكن أن تعزز الأداء بشكل كبير عبر نطاقات تردد مختلفة. يوفر هذا العمل رؤى قيمة حول كيفية تحسين ممتصات الميتاميتريال لتحقيق أداء أفضل في تطبيقات مثل الرادار، وأنظمة التصوير، وتكنولوجيا التخفي، مما يسهم في تقدم مجال الميتاميتريال وتطبيقاته التكنولوجية.

الكلمات المفتاحية:

ممتصات الميتامتريل, الخصائص الكهرومغناطية,نطاق التردد؛ رنان الملف السلكي الحلزوني.

Acknowledgments

First and foremost, I express my deepest gratitude to God Almighty for granting me the strength and ability to successfully carry out and complete this research. This accomplishment would not have been possible without His blessings.

I am especially indebted to Prof. Benmostefa Naima for her mentorship and guidance as my PhD supervisor. Her willingness to dedicate time and offer assistance whenever needed has been invaluable. I am grateful for her training in writing, presentation skills, and topic selection.I would like to express my deepest gratitude to the examiners, Pr. KAMECHE Samir, Pr.BOUACHA Abdelhafid ,Pr.CHAKER Hichem and Pr.NOURI Keltouma, for graciously accepting and reviewing our dissertation. Their valuable time, constructive feedback, and insightful comments have significantly contributed to the improvement and refinement of this work. Lastly

I am profoundly grateful for the love and support I received from my family. Without the love, support, and education from my parents, this achievement would not have been possible. I extend my deepest thanks to my brothers Mohcine and Ramy, and especially to my sister Aya and my best friend zoubida , who were always beside me, listening, helping, discussing, and providing unwavering support despite the difficulties we faced together.

Words cannot fully express my gratitude to my dear husband, Amine. I am immensely appreciative of his constant love, understanding, encouragement, and patience. His continuous support has been crucial in completing this research work. As my life companion, we have dreamed and planned together, and today we are reaping the fruits of our shared efforts.

Dedecation

To my beloved parents and my wonderful husbandand my litlle angel Yazen; whose endless support, encouragement, and love have been my constant inspiration.

Contents

List of Figures

List of Tables

List of Abbreviations

MM	Metamaterials
MMA	Metamaterial absorber
RCS	Radar cross-section
EMI	Electromagnetic interference
FEM	The finite element method
FDTD	Finite-difference time-domain
MoM	Method of moments
EMW	Electromagnetic wave
LHM	Left-handed materials
NRI MM	Negative refractive index metamaterials
TW	Thin-Wire
ITO	Indium tin oxide
PC	Photonic crystals
FSS	Frequency selective surface
VNAs	Vector network analyzers
FTIR	Fourier-Transform Infrared spectroscopy
HFSS	High Frequency Structure Simulator
HPC	High Performance Computing
PDEs	Partial differential equations
CST	Computer Simulation Technology
MLFMM	Multilevel Fast Multipole Method
RAM	Radar Absorbing Materials
EMC	ElectroMagnetic Compatibility
PCB	Printed Circuit Board
FB	The fractional bandwidth
RES	Reconfigurable Electromagnetic Surfaces
MPA	Metamaterial perfect absorber
TL	Transmission line
PMA	Perfect magnetic absorber
SRRs	Split-Ring Resonators

PMMA	Proposed metamaterial absorber
PET	Polyethylene terephthalate
WFRA	The fractional bandwidth
ADS	Advanced Design System

General Introduction

Metamaterials have revolutionized the field of electromagnetic research by offering unprecedented control over wave propagation, enabling phenomena that are unattainable with natural materials. These engineered structures, designed at sub-wavelength scales, can exhibit extraordinary properties such as negative refractive index, electromagnetic cloaking, and perfect absorption [9]. The ability to manipulate electromagnetic waves at will has led to the development of novel devices and applications that were once considered impossible. Among the various types of metamaterials, absorbers have garnered significant attention due to their versatile applications in stealth technology, electromagnetic shielding, sensors, and energy harvesting. The ability to fine-tune absorption characteristics over a broad frequency spectrum makes metamaterial absorbers essential for numerous technological innovations .

Metamaterial absorbers, in particular, have emerged as a critical area of research due to their potential to achieve near-perfect absorption of electromagnetic waves across specific frequency bands. This is made possible by engineering resonant structures that interact with incident electromagnetic waves in such a way that minimal reflection and transmission occur, thereby maximizing energy dissipation within the material. This characteristic makes metamaterial absorbers highly desirable for applications requiring effective electromagnetic wave manipulation, including radar cross-section (RCS) reduction, electromagnetic interference (EMI) mitigation, and wireless communication systems. The ability to design absorbers that can operate across multiple frequency bands or maintain performance across a wide bandwidth is key to their integration into modern technological systems .

The design and optimization of metamaterial absorbers are complex processes that rely on sophisticated computational simulations to predict their electromagnetic behavior accurately. Techniques like the finite element method (FEM) [10], finite-difference time-domain (FDTD), and method of moments (MoM) are often employed to model how electromagnetic waves interact with the absorber's intricate structure. By adjusting parameters such as geometry, material properties, and layer configurations, researchers can optimize absorption performance to meet specific application requirements. This iterative design approach, often guided by deep theoretical understanding, is key to achieving absorbers with tailored characteristics for a wide range of uses. Additionally, advances in machine learning and optimization algorithms have opened up new pathways for automating and improving the design process, enabling the discovery of absorber configurations that might not be obvious through traditional methods.

Fabrication plays a critical role in realizing the theoretical potential of metamaterial absorbers. The process involves the precise patterning of materials at the micro or nanoscale, which is essential for achieving the designed electromagnetic properties. Techniques such as photolithography, electron-beam lithography, and various etching methods are commonly used to create the intricate designs necessary for manipulating electromagnetic waves. More recent advances in additive manufacturing, such as 3D printing, have introduced new opportunities for fabricating complex metamaterial struc-

tures with greater flexibility and lower costs. The choice of materials and deposition techniques—such as sputtering and evaporation—significantly influence the absorber's performance, particularly in terms of efficiency, bandwidth, and polarization sensitivity. Despite advancements in fabrication technologies, challenges like scalability, material losses, and integration with existing systems remain. Overcoming these hurdles is crucial for enhancing the performance and cost-effectiveness of metamaterial absorbers [11] [12].

In this thesis, we present the design and fabrication of a wideband metamaterial absorber (MMA) optimized for enhanced absorption across a broad frequency range. Utilizing advanced simulation techniques, including parametric optimization and electromagnetic modeling, the MMA is designed to maximize absorption efficiency through careful selection of geometric and material parameters. The absorber is then fabricated using state-of-the-art lithographic methods to replicate the design with high precision at the microscale. A multi-layered design, incorporating both resonant elements and impedance matching techniques, is explored to achieve broad absorption across multiple frequency bands. Through both simulation and experimental validation, the wideband performance of the MMA is demonstrated, highlighting its potential for applications such as electromagnetic interference (EMI) shielding, radar cross-section (RCS) reduction, and wireless communication systems.

This research contributes to the growing body of metamaterial absorber studies by pushing the boundaries of design and fabrication techniques. By exploring the interplay between material properties, structural design, and practical implementation, we aim to develop an absorber that not only performs exceptionally well in simulations but also demonstrates high real-world effectiveness. The successful development and testing of this MMA open new possibilities for high-performance, application-specific absorbers, addressing the growing demand for solutions that operate across wide frequency ranges with minimal signal loss or distortion.

As the field of metamaterials continues to evolve, ongoing research is pushing the boundaries of design, fabrication, and application. Future advancements are expected to further refine the capabilities of metamaterial absorbers, with potential breakthroughs that could impact various sectors of technology, from next-generation communication systems to advanced energy-harvesting devices. By overcoming current limitations such as fabrication scalability and material losses, metamaterial absorbers will undoubtedly play a key role in the technological landscape of the future.

Chapitre 1 Introduction and Background

1.1 Introduction

The study of electromagnetic theory provides the basis for comprehending the characteristics of light and wave propagation in different materials. This chapter starts by investigating the transmission of light in a vacuum, establishing basic rules in the absence of material substances. This serves as a reference point for understanding complex interactions. It explores the phenomenon of wave propagation in material media, taking into account the influence of elements such as absorption, reflection, and refraction on wave behavior. The dispersion relation, which establishes the relationship between phase speed and frequency, is a fundamental idea in classical and contemporary physics.

This chapter goes to discuss metamaterial theory, which explores the interesting world of artificially created materials that possess unique features not seen in natural substances. This text presents a summary of metamaterials, emphasizing their distinct electrical characteristics that have resulted in novel uses in areas such as optics, telecommunications, and sensing.

In addition, we classify various metamaterials based on their specific characteristics and explore how these properties impact their interaction with electromagnetic waves. This classification offers a systematic comprehension of the wide array of metamaterials and their possible uses.

The next sections will examine the characterisation of metamaterials, as well as an analysis of the necessary numerical techniques for modeling these materials. The finite element method (FEM) is a very efficient determining technique that is specifically highlighted for its ability to describe and comprehend the complex behaviors of metamaterials under various conditions.

Finally it ends by examining the practical uses of metamaterials. This part serves as a connection between theoretical concepts and practical implementation. It shows the application of the ideas described in the chapter in real-life situations to create creative technology.Engineered materials possess distinctive features that challenge ordinary comprehension. We provide a comprehensive analysis of their electrical properties, classify different varieties, and explore their importance in modern applications.

1.2 Electromagnetic Theory

1.2.1 Propagation of light in a vacuum

We are primarily concerned with the equations that describe the transmission of waves in a vacuum, without any discussion on their origins. The equations depict the characteristics of the electric fields E and magnetic fields B in an electromagnetic wave. Any electromagnetic wave (EMW) is defined by four fundamental equations, or five if we in-

clude the Maxwell-Lorentz law, known as the Maxwell equations after their creator. The E and B fields of an EMW are the foundation of electromagnetism and illustrate their inter connectedness. Multiple formulations of Maxwell's equations are available, but the most frequent one described here is the vector version using partial derivatives.

Maxwell's Equations

Before exploring the science of metamaterials, it is essential to first outline the basics of electromagnetic theory. This begins with Maxwell's equations, which serve as the cornerstone of all interactions between light and matter. These equations were developed by various scientists over the course of the early 19th century and were unified by James Clerk Maxwell in 1865. Although Maxwell's equations can be expressed in different forms, here they are presented for a linear, isotropic medium without free charges or currents. [13].

$$\nabla \cdot \vec{\mathbf{D}} = 0 \tag{1.1}$$

$$\nabla \cdot \vec{\mathbf{B}} = 0 \tag{1.2}$$

$$\nabla \times \vec{\mathbf{E}} = -\frac{\partial \vec{\mathbf{B}}}{\partial t} \tag{1.3}$$

$$\nabla \times \vec{\mathbf{H}} = \frac{\partial \vec{\mathbf{D}}}{\partial t} \tag{1.4}$$

The signs $\vec{D}$, $\vec{B}$, $\vec{E}$, and $\vec{H}$ represent the electric flux density or electric displacement (measured in C), magnetic flux density (estimated in T), electric field (V/m), and magnetic field (A/m), respectively. Within a uniform and symmetrical material, the electric and magnetic flux densities ($\vec{D}$ and $\vec{B}$) are related according to equations (1.5) and (1.6).

$$\vec{D} = \epsilon \vec{\mathbf{E}} \tag{1.5}$$

$$\vec{B} = \mu \vec{\mathbf{H}} \tag{1.6}$$

The equations of Maxwell in a material that exhibits isotropic nature are as follows:

$$\nabla \cdot (\epsilon \vec{\mathbf{E}}) = 0 \tag{1.7}$$

$$\nabla \cdot (\mu \vec{\mathbf{H}}) = 0 \tag{1.8}$$

$$\nabla \times \vec{\mathbf{E}} = -\mu \frac{\partial \vec{\mathbf{H}}}{\partial t} \tag{1.9}$$

$$\nabla \times \vec{\mathbf{H}} = \epsilon \frac{\partial \vec{\mathbf{E}}}{\partial t} \tag{1.10}$$

In the case of a planar monochromatic wave, the electric and magnetic fields are represented by the equations mentioned in Equation 1.11 and 1.12;

$$\vec{\mathbf{E}}(\omega, \mathbf{k}) = \vec{\mathbf{E}}_0 e^{j(\mathbf{k}\cdot\mathbf{z}-\omega t)} \tag{1.11}$$

$$\vec{\mathbf{B}} = \vec{\mathbf{B}}_0 e^{j(\mathbf{k}\cdot\mathbf{z}-\omega t)} \tag{1.12}$$

By using these relationships, Maxwell's equations may be reformulated. 1.13 and 1.14.

$$\vec{\mathbf{k}} \times \vec{\mathbf{E}} = \omega c \mu \vec{\mathbf{H}} \tag{1.13}$$

$$\vec{\mathbf{k}} \times \vec{\mathbf{H}} = \omega c \epsilon \vec{\mathbf{E}} \tag{1.14}$$

$\vec{k}$ represent the wave vector, ω represent the angular frequency of the electromagnetic wave, and c represent the speed of light in free space. The permittivity and permeability of materials are commonly stated in complicated function

$$\epsilon(\omega) = \epsilon'(\omega) + j\epsilon''(\omega) \tag{1.15}$$

$$\mu(\omega) = \mu'(\omega) + j\mu''(\omega) \tag{1.16}$$

Index of refraction of a material can also be represented in complex function $\tilde{n}$ as in 1.17.

$$\tilde{n} = n + k \tag{1.17}$$

$\vec{k}$ represents the extinction coefficient of an electromagnetic wave in a specific material.

Figure 1.1 illustrates that in an isotropic medium, $\vec{k}$, $\vec{H}$, and$\vec{E}$ are mutually perpendicular, whereas $\vec{H}$ and $\vec{E}$ are in phase. It is evident that when both the electric permittivity and magnetic permeability change signs simultaneously, it has an impact on the signs of Equation 1.15 and 1.16. Figure 1.1 provides a geometric description of the wave vector, magnetic field, electric field, and Poynting vector. If both ϵ and μ have positive signs, equations 1.15 and 1.16) remain unaltered, indicating a "right-handed material". However, when both the signs of ϵ and μ are negative at the same time, equations 1.15 and 1.16 are modified to represent a "left-handed material". The mathematical description of the behaviour of electromagnetic waves propagating through right and left-handed materials may be expressed using equations for energy flow, also known as the Poynting vector 1.18, and wave vector, as seen in Figure 1.1 [14].

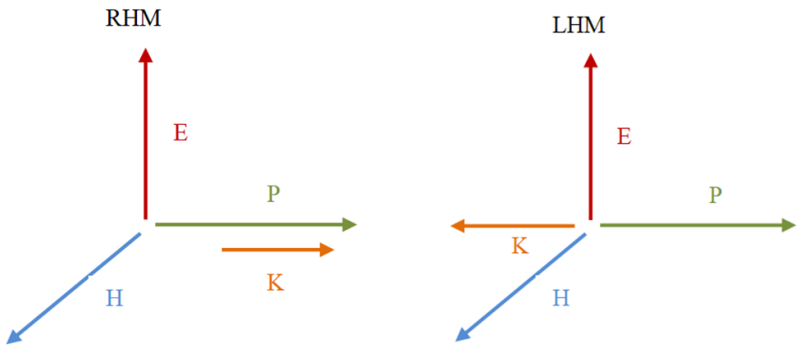

Figure 1.1: Geometric representation of $\vec{P}$, $\vec{K}$, $\vec{H}$, and $\vec{E}$ in: (a) Right handed materials and (b) Left handed materials. [15]

$$\vec{P} = \vec{H} \times \vec{E} \tag{1.18}$$

As per Equation 1.18 in the field of electrodynamics, the Poynting vector $\vec{P}$, together with the fields $\vec{E}$ and $\vec{H}$, have to conform to the right hand rule, and energy must propagate in alignment with the wave vector $\vec{K}$.whereas in materials that demonstrate left-handedness, the two vectors $\vec{K}$ and $\vec{S}$ propagate in opposing directions. In substances with left-handed properties, the flow of energy occurs in the opposite direction of the phase velocity. This is shown by the vector $\vec{K}$, which indicates the direction of the phase velocity. Materials that exhibit left-handed properties are often known as "negative group velocity materials." [14].

1.2.2 Propagation of waves in material media

In a medium other than a vacuum, there exist point charges ρ as well as currents J. Maxwell's equations are therefore slightly different from those of a vacuum [16]:

$$\nabla \cdot \vec{\mathbf{E}} = \frac{\rho}{\epsilon_0} \tag{1.19}$$

$$\nabla \cdot \vec{\mathbf{B}} = 0 \tag{1.20}$$

$$\nabla \times \vec{\mathbf{E}} = -\frac{\partial \vec{\mathbf{B}}}{\partial t} \tag{1.21}$$

$$\nabla \times \vec{\mathbf{B}} = \mu_0 \epsilon_0 \frac{\partial \vec{\mathbf{E}}}{\partial t} + \mu_0 \vec{\mathbf{J}} \tag{1.22}$$

A material medium will also tend to polarize (and magnetize in the case of a magnetic substance) in response to an event Electro-magnetic wave (EMW) because of the charges and currents it carries. After that, its polarization (P) and magnetization (M) must be

considered. Therefore, we must add two new values, the magnetic field $\vec{H}$ and the electric induction $\vec{D}$, which are related to these numbers by:

$$\vec{\mathbf{D}} = \epsilon_0 \vec{\mathbf{E}} + \vec{\mathbf{P}} \tag{1.23}$$

$$\vec{\mathbf{H}} = \frac{1}{\mu_0} \vec{\mathbf{B}} - \vec{\mathbf{M}} \tag{1.24}$$

The relationship between $\vec{E}$, $\vec{H}$, $\vec{B}$, $\vec{D}$, and the parameters of the medium is expressed by the following constitutive relationships in the most general way possible.

$$\begin{bmatrix} \vec{\mathbf{D}} \\ \vec{\mathbf{B}} \end{bmatrix} = \begin{bmatrix} \bar{\bar{\epsilon}} & \bar{\bar{\xi}} \\ \bar{\bar{\zeta}} & \bar{\bar{\mu}} \end{bmatrix} \begin{bmatrix} \vec{\mathbf{E}} \\ \vec{\mathbf{H}} \end{bmatrix} \tag{1.25}$$

The tensors $\bar{\bar{\epsilon}}$, $\bar{\bar{\xi}}$, $\bar{\bar{\zeta}}$, and $\bar{\bar{\mu}}$ describe the permittivity, two polarization transfer components, and permeability of the medium, respectively. Their values are contingent on the presence of dispersion in the medium; otherwise, they stay constant. Without polarization transfer, we assume the diagonal terms are zero, so $\bar{\bar{\xi}} = \bar{\bar{\zeta}}$=0. If the medium is homogeneous and isotropic, the tensors $\bar{\bar{\epsilon}}$ and $\bar{\bar{\mu}}$ become scalar in nature, leading to constitutive relations that are also scalar.

$$\begin{pmatrix} \vec{\mathbf{D}} \\ \vec{\mathbf{B}} \end{pmatrix} = \begin{pmatrix} \epsilon & 0 \\ 0 & \mu \end{pmatrix} \begin{pmatrix} \vec{\mathbf{E}} \\ \vec{\mathbf{H}} \end{pmatrix} \tag{1.26}$$

When there is no current $\mathbf{J} = 0$ and no charge density $\rho = 0$ present, the Maxwell equations are the same as in the preceding section, with the only difference being that ϵ_0 and μ_0 are substituted by ϵ and μ, respectively

$$\nabla \cdot \vec{\mathbf{E}} = 0 \tag{1.27}$$

$$\nabla \cdot \vec{\mathbf{B}} = 0 \tag{1.28}$$

$$\nabla \times \vec{\mathbf{E}} = -\frac{\partial \vec{\mathbf{B}}}{\partial t} \tag{1.29}$$

$$\nabla \times \vec{\mathbf{H}} = \epsilon \frac{\partial \vec{\mathbf{E}}}{\partial t} \tag{1.30}$$

We derive the equation describing the propagation of the electric field $\vec{E}$ in a material medium. (symmetry occurs in field $\vec{B}$)

$$\nabla^2 \vec{\mathbf{E}} - \mu\epsilon \frac{\partial^2 \vec{\mathbf{E}}}{\partial t^2} = 0 \tag{1.31}$$

In a conducting material, when current $\mathbf{J} \neq 0$ is present, the conductivity is described by the same sort of equation.

$$\vec{\mathbf{J}} = \sigma\vec{\mathbf{E}} \tag{1.32}$$

By replacing the expression for $\vec{\mathbf{J}}$ into Equation 1.15, we get the generalized permittivity $\epsilon_e q$ of the medium.

$$\epsilon_{\text{eq}} = \frac{j\sigma}{\omega} + \epsilon \tag{1.33}$$

where ϵ is the permittivity of free space (vacuum permittivity) and ϵ_r is the relative permittivity of the medium.

where $\epsilon_e q$ is the permittivity of the medium considered $\epsilon = \epsilon_0\epsilon_r$ and $\vec{\mathbf{E}}$ the frequency of the incident Electromagnetic wave (EMW)) So we have:

$$\nabla^2\vec{\mathbf{E}} - \mu\epsilon_{\text{eq}}\frac{\partial^2\vec{\mathbf{E}}}{\partial t^2} = 0 \tag{1.34}$$

- **The Dispersion Relation**

  The dispersion relation in a material medium is defined using a monochromatic plane wave that corresponds to Equation 1.11 as a specific solution of the propagation Equation 1.12.

  $$\vec{\mathbf{E}}(r,t) = \vec{\mathbf{E}}_0 e^{j(k\cdot r - \omega t)} \tag{1.35}$$

  The dispersion equation becomes in this case:

  $$k^2 = \omega^2\epsilon\mu \tag{1.36}$$

  In real materials, these values are complicated owing to losses. This drives us to redefine the refractive index using a different .We may begin by defining it and connecting it to wave vectors.

  $$n = \frac{k}{k_0} \tag{1.37}$$

  $$n = \frac{k}{k_0} = \frac{\epsilon\mu}{\epsilon_0\mu_0} = \epsilon_r\mu_r \tag{1.38}$$

  We thus obtain a new definition of the index, solely from the parameters $\epsilon_r$and μ_r of the material medium:

  $$n^2 = \epsilon_r\mu_r \tag{1.39}$$

  The relative permittivity ϵ_r and relative permeability μ_r of common materials are complex with positive real components, ensuring no ambiguity about the sign of the index. However, in the case of a metamaterial when both values are negative at the same time, there is one. When $\mu_r < 0$ and $\epsilon_r < 0$, the equation results in $n < 0$, which may not be immediately apparent. To comprehend this thoroughly, we need to position ourselves on the complicated plane shown in Figure 1.2 , in which we have:

  $$\epsilon_r = |\epsilon_r|e^{j\theta_\epsilon}\ \mu_r = |\mu_r|e^{i\theta_\mu} \tag{1.40}$$

  In this case the refractive index becomes:

$$n = \sqrt{|\epsilon_r||\mu_r|}\, e^{j\frac{1}{2}(\theta_\epsilon+\theta_\mu)} \tag{1.41}$$

As our environments are considered passive, the imaginary parts of ϵ_r and μ_r are necessarily positive, which imposes that $\theta_\epsilon \in [0, \pi]$ and $\theta_\mu \in [0, \pi]$. In fact, the angle of the refractive index n belongs to the same domain: $\frac{\theta_\epsilon+\theta_\mu}{2} \in [0, \pi]$.

In the case of a doubly negative medium, where the real parts of ϵ_r and μ_r are negative simultaneously, the domain of definition of the angle is reduced to $[\frac{\pi}{2}, \pi]$ for ϵ_r, μ_r, and n. We therefore have a real part of the negative index n for $\mathrm{Re}(\epsilon_r) < 0$ and $\mathrm{Re}(\mu_r) < 0$. This is even more obvious if we place ourselves in the limiting case without loss; it just makes θ_ϵ and θ_μ tend towards $\frac{\pi}{2}$. We thus obtain, for the index:

$$n = \sqrt{|\epsilon_r||\mu_r|}\, e^{j\pi} \tag{1.42}$$

which is equivalent to saying that:

$$n = \sqrt{|\epsilon_r||\mu_r|} \tag{1.43}$$

To avoid any possible ambiguity about the existence of a negative index, let us now see how else to define a medium of negative index, not via the relative parameters of the medium, but from the group speed v_g and the phase speed v_ϕ of the incident wave [17].

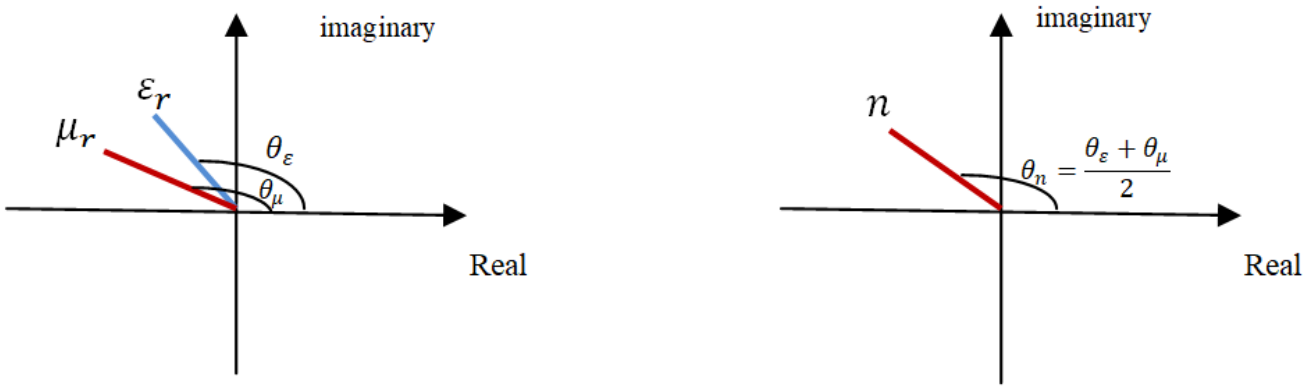

Figure 1.2: Representation in the complex plane of the relative permittivity and of the relative permeability when their real parts are negative (left) and the resulting refractive index n in this configuration (right). Our materials are passive, which is why the angular part is in the upper part of the complex plane: θ_n, θ_ϵ, and $\theta_\mu \in [0, \pi]$. In this case, we understand better why $\mathrm{Re}(n) < 0$ if $\mathrm{Re}(\epsilon_r) < 0$ and $\mathrm{Re}(\mu_r) < 0$ [1].

1.3 Metamaterial Theory

1.3.1 Metamaterial

Natural materials are typically composed of individual atoms and molecules that bond together through a chemical process known as bonding. When these materials interact with light, a form of electromagnetic radiation, three key phenomena occur. First, a portion of the solar radiation is absorbed by the material, a process known as "absorption." Second, some of the radiation that is not absorbed is reflected by the material's surface back into the atmosphere, a phenomenon called "reflection." Lastly, the proportion of radiation that is neither absorbed nor reflected is transmitted through the material, described by the transmittance coefficient. The absorption, reflection, and transmission properties of natural materials are closely linked to their atomic and molecular structures [18]. In recent years, there has been growing interest in creating electromagnetic materials from artificially engineered sub-wavelength structures known as "metamaterials (MM)," which exhibit unique and extraordinary electromagnetic properties.

Metamaterials have been characterized in various manners by numerous references. Broadly, they are identified as synthetic substances with extraordinary electromagnetic properties not typically found in natural materials. This structurally modified material derives its name from the Greek word "meta," meaning "beyond". Metamaterials have attracted considerable attention and are utilized across various global societies. While physicists traditionally investigate natural phenomena, engineers concentrate on the practical application of scientific principles. Metamaterials serve as a link between scientific inquiry and engineering application [19] [20].

Metamaterials are man-made materials that consist of tiny components smaller than the wavelength of light. These components influence the material's optical characteristics, such as its capacity to conduct electricity (electric permittivity) and respond to magnetic fields (magnetic permeability). Usually, they are made up of unit cells, each measuring around $\frac{\lambda}{10}$ or smaller, organized in a vast array. Due to the tiny size of each unit cell compared to the wavelength of light, metamaterials interact with electromagnetic waves as if they were a medium having optical characteristics, rather than diffracting off individual parts. The effective electric permittivity and magnetic permeability are defined as $\epsilon_{\text{eff}}(\omega)$ and $\mu_{\text{eff}}(\omega)$, respectively.

The optical characteristics of metamaterials are mostly influenced by the geometry of their unit cells, rather than their band structure or chemical composition, as is the case for ordinary materials. Metamaterials has the ability to be proportionally variable over a broad band of electromagnetic waves, exhibiting proven reactions from radio frequencies to the optical and visual ranges [16].

1.4 Metamaterials Overview

Metamaterials were not the first medium to effectively use artificial components in order to generate accurate electromagnetic reactions. In 1898, Jagadis Chunder Bose

conducted a microwave experiment on polarization using twisted copper wires. Artificial dielectric materials gained substantial momentum in the 1940s with research done at Bell Labs, specifically with Kock's metallic delay lens, and continued to be influential throughout the century. The concept of artificial magnetism, which does not rely on magnetic components, has a long history that dates back to the same time period. It is described in a conventional textbook on antennas [19]. Artificial plasmas, also known as built media with negative (ω), have been acknowledged since the 1960 s.

One important characteristic of these artificial substances is their ability to exhibit negative refraction, which has led to them being referred to as "left-handed materials" (LHM). These materials refract electromagnetic waves in a manner that goes towards the conventional "right-handed" rule of electromagnetism .When an electromagnetic wave travels through this material, the electric vector, electromagnetic vector, and wave vector do not follow the right-handed law.The idea of these substances was initially proposed in 1968 by Veselago, who suggested that it is theoretically possible for materials to possess both negative permeability and positive permittivity [21].The user performed a theoretical analysis on the propagation of plane waves in a material with negative values for bothϵ (permittivity) and μ (permeability). This uconcluded that the refractive index of a material has to be reevaluated and represented as n. Nevertheless, Veselago's theoretical research on negative refractive index metamaterials (NRI MMs) could not progress to practical implementation because of the absence of a material capable of exhibiting simultaneous negative permittivity and permeability.

Metamaterials are thought to have originated with John Pendry's artificial magnetism in 1999, as well as the groundbreaking work that analyzed the first structure exhibiting both negative (ω) and $\mu(\omega)$ simultaneously. The papers presented a new way of thinking that enabled artificial materials, subsequently named metamaterials by Walser, to exhibit more unique features throughout a wider span of the electromagnetic spectrum, particularly in shorter wavelengths, compared to previous materials; he is devised a practical method to create an LHM that deviated from the conventional right-hand rule.The author presented a design of a Thin-Wire (TW) structure with periodic arrangement, which demonstrates a negative effective permittivity .It was shown that the structure exhibits a lower plasma frequency compared to the wave in the microwave domain. Due to its low plasma frequency, this structure is capable of generating a negative permittivity that is effective in microwave frequencies. Furthermore, it was shown that a group of split-ring resonators may be used to get negative magnetic permeability [22].

In 2000 Smith's [23] design of a negative index material (NIM), a material exhibiting simultaneous negative values of $\epsilon_e f f(\omega)$ and $\mu_e f f(\omega)$, resulting in an index of refraction, $n_{\text{eff}}(\omega)$ can be less than zero, in 2000, represented an important development in metamaterials. Metamaterials have shown many qualities include individualised absorption and emission, multi-band response, and dynamic performance across a wide range of the electromagnetic spectrum. Metamaterials' extensive design flexibility enables their easy integration into many devices, including super lenses, invisibility cloaks, and spatial light modulators.

1.5 Electronic Properties of Metamaterials

Metamaterials are synthetic materials made up of artificial unit structures, referred to as "metal-atoms" or "metal-molecules," which are constructed from existing components and organized in a systematic fashion. The integration of various unit structures results in to a unique material that displays extraordinary characteristics that are different from its separate constituents. The response of a metamaterial structure to an electromagnetic wave and its properties are governed only by the MM unit cell, which is composed of composite materials and their arrangement inside a single cell. Hence, while creating metamaterials, it is crucial to thoroughly evaluate the choice of materials and their distinct physical attributes, including optical and electrical qualities. It is crucial to establish the best suitable material for the intended design, application, and the exact range of wavelengths of interest. Electronics consist of three primary categories of materials: insulators/dielectrics, semiconductors, and conductors/metals. The categorization of materials is defined by their conductivity qualities, which are influenced by the energy band structure or electronic energy levels [14] [24]. Each material has two primary energy bands, known as the valence band and the conduction band, which are distinguished by a gap between them. The conduction band is positioned at the highest energy level and typically has a deficit of electrons, while the valence band is placed at the lowest energy level and includes electrons that are partially filled. The region of space located between these two bands is often known as the "band gap" or "forbidden band," and it has a substantial impact on the conductivity characteristics of materials. The diagram shown in Figure 1.3 provides a visual representation of the electronic energy levels for a conductor, semiconductor, and insulator. In conductors, there is an overlap between the conduction band and the valence band. Thus, when a weak electric field is generated (with a small suppressed voltage), electrons in the valence band readily move to the conduction band (due to the great electrical conductivity of metals). A semiconductor has a band gap that is larger than that of a conductor, but less than the band gap of an insulator. Therefore, semiconductors need a greater electric field strength than conductors in order to enable the transfer of electrons from the valence band to the conduction band. However, the dielectric material has a much wider energy band gap compared to the other two materials. Consequently, electrons are incapable of carrying out this activity and need a much larger amount of energy to go across the empty space between the valence band and conduction band. Dielectrics are incapable of facilitating the flow of electric current, making them ineffective as conductors of electricity. [2].

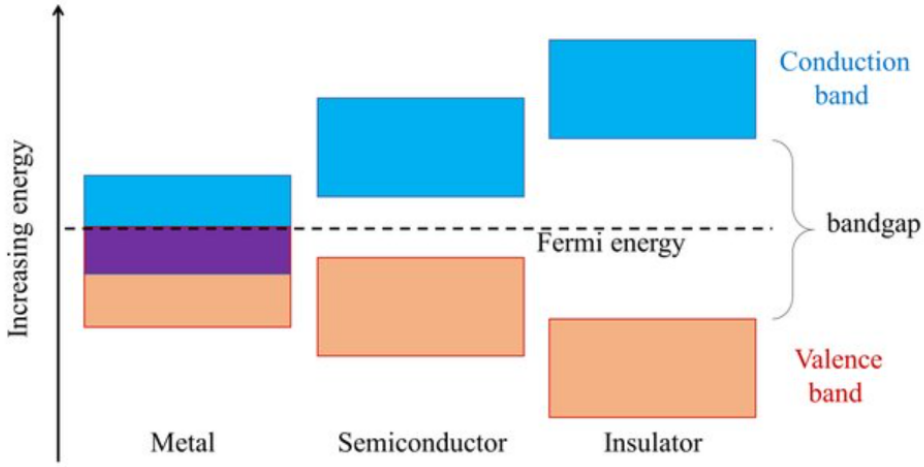

Figure 1.3: Energy band gap diagrams for conductors, semiconductors, and dielectric. The dashed black line between the conduction and valence bands represents the Fermi energy level(EF) [2].

Classifying materials based on their electronic energy band levels is not sufficiently justified, since many compounds exhibit metallic behaviour electronically yet behave as dielectrics optically. Indium tin oxide (ITO) is a compound that exhibits metallic behaviour in terms of its electrical conductivity, while also behaving as a dielectric material in terms of its optical transparency. These unique properties make ITO highly suitable for use in transparent electrodes in the display and lighting industries. Tungsten, a naturally generated metal, has comparable behaviour to lossy dielectric materials in the visible spectrum region. It is often used to transmit current in the filaments of light bulbs and has a positive dielectric constant [25]. Due to their narrow energy band gap, semiconductor materials are commonly employed in metamaterial designs rather than dielectric materials. This is because they are highly effective in manipulating the path of electromagnetic waves. Depending on the wavelength range of interest, semiconductor materials can function as either a lossy/absorber layer or a loss-free substrate [26].

1.6 METAMATERIAL CLASSIFICATION

The response of a system to an electromagnetic field is affected by the properties of the materials it comprises. The characteristics of these materials are defined by specifying the macroscopic parameters of permittivity ϵ and permeability μ. The categorization of metamaterials may be visually shown using the parameters permittivity and permeability, as shown in Figure 1.4 [27].

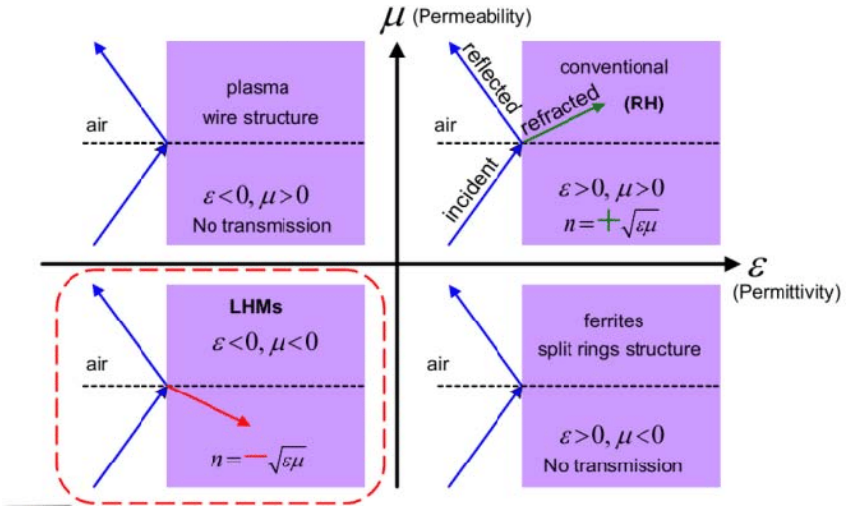

Figure 1.4: metamaterial classification.

1.6.1 Double Positive Material (DPS)

A medium with non-zero permittivity and permeability, specifically $\epsilon > 0$ and $\mu > 0$, is known as a double positive (DPS) media. Media commonly encountered in various applications, such as dielectrics, are classified within this category. Materials with a negative permittivity $\epsilon < 0$ and a positive permeability $\mu > 0$ are commonly known as Epsilon negative (ENG) mediums. These features are commonly observed in various frequency ranges in plasmas. [27].

1.6.2 Epsilon Negative Material(ENM)

If a material has permittivity less than zero and permeability greater than zero $\epsilon < 0$ and $\mu > 0$ it is called as epsilon negative (ENG) material. In certain frequency regimes, many plasmas exhibit these characteristics [27].

1.6.3 Mu Negative Material (MNM)

Mu negative (MNG) media are defined as a medium with a permittivity greater than zero and a permeability less than zero, expressed as $\epsilon > 0$ and $\mu < 0$. This characteristic is exhibited by certain gyrotropic materials within specific frequency ranges. [27].

1.6.4 Double Negative Material (DNM)

A medium having negative values for both permittivity and permeability $\epsilon < 0$ and $\mu < 0$ is referred to as a Double Negative (DNG) media. At this point, this category of materials has only been shown using artificial structures [27].

1.7 Metamaterial Type

1.7.1 Electromagnetic Metamaterials

Metamaterials have emerged as a distinct field of study within the domains of physics and electromagnetism, with a particular focus on optics and photonics.These devices find applications in optical and microwave systems, offering goals such as beam steering, modulation, band-pass filtering, lensing, microwave coupling, and antenna protection. Metamaterials are composed of intricate structures.A metamaterial affects electromagnetic waves by its structural properties, which are smaller in scale than the wavelength of the electromagnetic radiation it interacts with. [28].

Different classes of Electromagnetic Metamaterials.

1. Metamaterials with double negative properties are materials that possess negative values for both permittivity and permeability. These materials are often known as negative index metamaterials (NIM). Alternative terms for DNGs include left-handed media, media with a negative refractive index, and "backward-wave media". [27], [25].

2. Electromagnetic bandgap metamaterials regulate the transmission of light. This may be achieved using either photonic crystals (PC), a kind of metamaterial, or left-handed materials (LHM), another type of metamaterial. Both are a new category of intentionally designed structures that regulate and manage the movement of electromagnetic waves, namely light. As a result, they have gained significant attention in the electromagnetic and antenna research field. Their designs changed and they have investigated a diverse array of materials and shapes. [29].

3. Bi-isotropic and bi-anisotropic metamaterials are categorized according to their distinct electric and magnetic reactions, which are defined by the permittivity and magnetic permeability characteristics. These metamaterials may be classified as either single negative or double negative. However, in some instances of electromagnetic metamaterials, the electric field stimulates magnetic polarization, whereas the magnetic field activates electrical polarization, which is referred to as magneto-electric coupling. Bi-isotropic media are characterized by their anisotropic magneto-electric interaction and are also often referred to as bi-anisotropic. [22].

1.7.2 Terahertz metamaterials

Terahertz metamaterials are a kind of metamaterial that specifically interact at frequencies in the terahertz range. For the study or practical use of the terahertz range in metamaterials and other substances,The frequency range is often characterised as 0.1 to 10 terahertz (THz). This refers to the wavelengths ranging from 3 mm (very high frequency band) to 0.03 mm (far-infrared light's long-wavelength boundary) [30].

1.7.3 Photonic metamaterials

Photonic metamaterials are artificial structures made up of specifically designed micro- or nanostructured metallodielectric subwavelength components. This concept, which seems simple at first look, has the remarkable ability to enable the manifestation of numerous novel and unconventional optical characteristics. These include magnetism occurring at optical frequencies, negative refractive index, significantly high refractive index, complete elimination of reflection through impedance matching, flawless absorption, substantial circular dichroism, and enhanced nonlinear optical properties [31].

1.7.4 Tunable metamaterial

A tunable metamaterial is a structure that intentionally modifies its electromagnetic behaviour over regular use by changing factors such as the effective circuit of the unit cell, material properties of its constituents, or its geometry [32].

1.7.5 Frequency selective surface FSS

FSS is a type of periodic surface that is capable of selectively filtering incoming electromagnetic waves based on their operating frequencies, polarisations, and incidence angles. Because of its filtering characteristic, FSS may be used in several applications. Traditional Frequency Selective Surfaces (FSS) typically include a 2D periodic arrangement of slots or holes that are etched onto a conductive plate or printed on a dielectric substrate using conducting patches or strips [33].

1.7.6 Metamaterial Absorber

A metamaterial absorber MMA has the capacity to manipulate the electrodynamic properties and effects, enabling the development of materials with desirable effective permittivity and permeability values, leading to a very efficient electromagnetic absorber. [34].

1.8 Metamaterial Characterization

The choice of characterisation approach is determined by both the operating wavelength and the specific electromagnetic phenomena that one intends to measure, similar to the fabrication procedure. Vector network analyzers (VNAs) are used at microwave frequencies to produce and detect signals with both phase and amplitude. These signals are then sent via horn antennas into free space. This technology has been expanded to the low THz range with the use of various multipliers, extenders, and filters. However, it is most typically seen in the low RF frequencies to the millimeter-wave regimes. THz time domain spectroscopy is more prevalent in the THz region and allows for amplitude and

phase measurements. A temporal pulse is used for both the sample and reference, while a Fourier transform provides information in the frequency domain. FTIR spectroscopy, short for Fourier-Transform Infrared spectroscopy, is somewhat misleading since it encompasses a wide range of the electromagnetic spectrum, spanning from terahertz (THz) to visible wavelengths. The fundamental concept is using a Michelson Interferometer to get spectral data from a particular sample. Existing systems provide many options for combining sources, detectors, and beam splitters, as well as the capability to perform measurements that include transmission, reflection, and angle dependence. Furthermore, FTIR systems often have the capability to be connected to a microscope equipped with a mobile stage, enabling the use of raster scan microscopy. Other methods, like ellipsometry and optical microscopy, are available to analyse metamaterials throughout the electromagnetic spectrum [22] [35].

1.9 Numerical methods and advice for simulating Metamaterials

1.9.1 The finite element method

Clough introduced the idea of "finite element" in 1960 .During the early 1960s, engineers used this technique to get approximate answers for issues related to stress analysis, fluid flow, heat transfer, and several other domains. Zienkiewicz and Chung released the first book on the Finite Element Method (FEM) in 1967. During the late 1960s and early 1970s, the Finite Element Method (FEM) was used to address a diverse range of engineering challenges. The emergence of many commercial Finite Element Method software packages like as Ansys, Abaqus, Adina, etc., was observed mostly during the 1970s.The concept is easy to understand: the continuous domains, or geometries, are divided into discrete and interconnected areas known as finite elements. The collection of these elements is referred to as a mesh, as shown in 1.5 . Next, a collection of equations at the individual element level is solved to determine the whole response of the entire domain to a certain set of boundary conditions. The Finite Element Method (FEM) offers the benefit of employing a non-uniform mesh, enabling more detailed representation of meshes, particularly for complicated geometries. The precision of the solution improves as the mesh becomes finer. However, this approach demands substantial computational resources, particularly for complex structures.Especially for complicated constructions [36] (Figure 1.5).

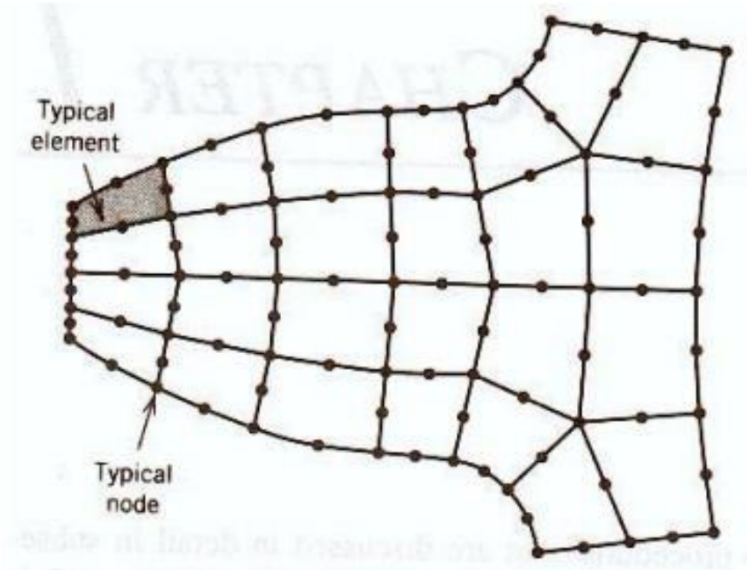

Figure 1.5: Two-dimensional mesh of a non uniform structure.

In general, the solution approach relies on the variational formulation and the weighted residuals. To facilitate comprehension, we will focus our explanation on a one-dimensional system, where the geometric domain is represented by a straightforward interval [a,b] [37] [38]. The system under consideration is defined by a differential equation.

$$L[u(x)] = f(x) \tag{1.44}$$

Let L be a linear differential operator, which in this instance corresponds to Maxwell's equations. Let f be a function, u be an exact solution to the issue, and x be the variable. To ensure the problem's completeness, we take into account the given boundary conditions u(a) and u(b). We seek an approximate solution $\check{u}(x)$ for the function u(x) in the form of a linear combination of linearly independent functions ϕ_i, which together constitute the foundation.

$$\check{u}(x) = \sum_{i=1}^{N} c_i \varphi_i(x) \tag{1.45}$$

Theϕ_i called to as interpolation functions, are typically polynomials with varying degrees. The C coefficients are the weighting factors that need to be found in order to get an approximate solution. By substituting the approximation solution into the differential equation, the resulting value is not equal to f and there is a remaining residue r:

$$L[\check{u}] - f = r(\tilde{u}) \neq 0 \tag{1.46}$$

However, we can evaluate the best possible approximation of u using the weighted residual method. This method consists of minimizing the residue 1 over the definition domain. To do this, we construct the integral R_j of the product of the residue r by a weighting function w_j, and we write:

$$\forall j, \quad R_j = \int_a^b r[\tilde{u}(x)]\, w_j(x)\, dx \tag{1.47}$$

The equality is true for the exact function $u(x)$ regardless of the weighting functions w_j, since the integrand becomes zero for all values of x. For a particular approximation function $\tilde{u}(x)$ and a certain weighting function w_j, the integral disappears only when the residue is minimised (this may be understood intuitively from the explanation of the least squares approach below).Using this integral, we can formulate the approximate answer as:

$$\sum_{i=1}^{N} \int_{a}^{b} \left(L(c_i \phi_i(x)) - f(x)\right) w_j(x)\, dx = 0 \tag{1.48}$$

This results in a matrix system where the coefficients represent the unknown variables. In order to solve a system of equations, we need an equal number of equations as there are unknown variables. Consequently, we must choose a certain number N of weighting functions. The answer, represented as the set of all ci, can be determined using the inverse of the matrix produced by certain methodologies. In the next section, we will describe two distinct weighting functions used in the weighted residuals approach. In the next section, we will describe two distinct weighting functions used in the weighted residuals approach

1. **The Method of Least Squares** :is a strategy that is used to determine the best fit line to data. The proof to this method requires the use of linear algebra and calculus. The primary obstacle is to determine the straight line that best fits the data, y=ax+b, provided that the pairs (x,y) are observed for n = 1,..., N. The procedure rapidly generalizes to the determination of the optimal suit for the shape.Linearity with respect to x is not necessary for the functions fk. Only condition is that y be represented as a linear combination of these functions. [39].

2. **GalerkinMethode** :is more accurately a family of methods, is highly versatile and robust. The approach begins with a variational problem defined in an infinite-dimensional space. To simplify, we first approximate the problem using a sequence of finite-dimensional subspaces. Solving the problem in this finite-dimensional space is generally much easier than tackling it directly in infinite dimensions. Once the approximate solution is obtained, we then take the limit, as the dimension of the approximation spaces approaches infinity, to arrive at a solution to the original problem. Beyond its theoretical value, the Galerkin method also offers, in certain cases, a practical process for constructing approximate solutions. Numerous examples, especially in the context of evolution problems, demonstrate the application of the Galerkin method. [40] [41]

1.9.2 Extraction of effective parameters

Various methodologies may be used to determine the values of permittivity and permeability based on reflection and transmission coefficients. Each of the conversion techniques has specific advantages and limitations. The choice of method relies on several aspects, including whether the S parameters (S11, S21) are simulated or measured, the length of the sample, the required dielectric characteristics, the speed of conversion, and the accuracy of the converted findings. The S parameters are obtained by illuminating a

metamaterial slab with a normally incident wave. They provide information about the effective properties of the metamaterial. This assumes that the boundaries of the slab are clearly defined and that the Fresnel formulas for reflection and transmission are applicable at the interface between air and the metamaterial. S11 represents the reflection coefficient and S21 represents the transmission coefficient [42].

For a homogeneous material of thickness d, the reflection and transmission coefficients of electromagnetic (EM) waves can be expressed as a function of the refractive index n and impedance Z of the material [43] [44].

$$\begin{aligned} \epsilon &= n \cdot z \\ \mu &= n \cdot z \end{aligned} \tag{1.49}$$

The wave vector, represented by $k = \frac{2\pi}{\lambda}$, corresponds to the incidence wavelength in free space. The normalized transmission coefficient, $t' = t^* e^{ikd}$, is used to measure the transmission of the wave. The connections between transmission and reflection are inverted, and the expression for Z is as follows:

$$z = \pm\sqrt{\frac{(1+r^2) - t'^2}{(1-r^2) - t'^2}} \tag{1.50}$$

The fact that the environment is passive implies that:

$$z > 0$$

The refractive index, represented as n, is a mathematical function that depends on two variables, t and r. This relationship may be stated as:

$$\cos(nkd) = X = \frac{1}{2t'}\left(1 - r^2 + t'^2\right) \tag{1.51}$$

The complex refractive index, denoted as n, may be expressed in the following mathematical form:

$$n = n' + jn'' \tag{1.52}$$

Equation ($z > 0$) results

$$e^{-n''kd}\left[\cos(n'kd) + j\sin(n'kd)\right] = Y = X \pm \sqrt{1 - X^2} \tag{1.53}$$

In order for the amplitude of the electromagnetic wave to decrease inside the structure, the absolute value of $|Y|$ must be less than 1. Therefore, the sign of n is determined by the requirement

$$n'' \geq 0. \tag{1.54}$$

The calculations of a quadrupole (two waveports, i.e., two inputs/two outputs) result in the parameters S being written in the form of a 2×2 matrix:

$$S = \begin{pmatrix} S_{11} & S_{21} \\ S_{21} & S_{22} \end{pmatrix} \tag{1.55}$$

The diagonal parameters S_{11} and S_{22} represent the reflection of the structure, whereas the extra-diagonal parameters S_{12} and S_{21} represent its transmission. Furthermore, it is assumed that the system is reciprocal, meaning that $S_{11} = S_{22}$ and $S_{12} = S_{21}$.

The values S_{11} and S_{12} represent the coefficients of reflection (r) and transmission (t') for our structure. The equations are given by:

$$z = \pm\sqrt{\frac{(1 + S_{11}^2) - S_{21}^2}{(1 - S_{11}^2) - S_{21}^2}} \tag{1.56}$$

$$X = \cos(nkd) = \frac{1}{2S_{21}}(1 - S_{11}^2 + S_{21}^2) \tag{1.57}$$

$$e^{jnkd} = X \pm i\sqrt{1 - X^2} \tag{1.58}$$

The expression $n'' \geq 0$ allows for the determination of both the real and imaginary components of the refractive index, as well as the sign of $\mathrm{Re}(n)$. This is particularly important when using materials that may contain regions exhibiting Left-Hand characteristics, meaning regions where $\mathrm{Re}(n)$ can be negative. The complex number n may be decomposed into its imaginary portion and real part, which are determined by:

$$n'' = -\frac{1}{kd}\left[\mathrm{Re}\left(\ln(Y)\right)\right] \tag{1.59}$$

$$n' = \frac{\arctan\left(\frac{\mathrm{Im}(Y)}{\mathrm{Re}(Y)}\right) \pm m\pi}{kd} \tag{1.60}$$

Where m is an integer.

1.9.3 HFSS

High Frequency Structure Simulator (HFSS) is a software programme that simulates electromagnetic phenomena in three dimensions. It employs the finite element approach to analyse electromagnetic behaviour in the frequency domain. The software has an intuitive graphical interface that allows for the construction of the simulation structure and the presentation of results. Studying parameters allows the answer to be visualised. To compute the electromagnetic field and extract the parameters, the user just has to provide the shape, materials, and set the frequency range. The structure is meshed using tetrahedral volume components. Furthermore, it is also applicable to homogeneous structures, as well as heterogeneous ones. This programme also enables the creation and optimisation of meshes. In order to address such issues, It is important to find solutions to Maxwell's equations, which enable the calculation of electric and magnetic fields. HFSS uses a direct solver as the default method for solving the resolution component of the linear system that results from discretization. This direct solver is quick but may

have constraints when dealing with extremely large problem sizes. Alternatively, an iterative solver may be used . After being created, HFSS immediately produces the near field and distant field [45] [46]. HFSS, or High Frequency Structure Simulator, employs adaptable solutions and a simple to use interface to provide exceptional performance and comprehensive understanding of all 3D electromagnetic issues. By integrating with ANSYS thermal, structural, and fluid dynamics tools, HFSS offers strong and extensive multi-physics analysis for electronic goods, verifying their thermal and structural dependability. HFSS utilizes an automated adaptive meshing approach and advanced solvers to ensure precise and reliable results. Additionally, the use of High Performance Computing (HPC) technology may further enhance the speed and efficiency of HFSS. Finite element codes may be categorized into two groups: general codes and specialized codes. The first method provides the resolution of any system of EDPs, but it is not optimised in terms of the IT resources used. The specialised systems' codes enable the efficient resolution of the partial differential equations (PDEs) specific to a given system. In our situation, we use the specialised code HFSS®.The differential Equation 1.61 solved by its finite element code is the equation Following wave:

$$\nabla \times \left[\mu_r^{-1} \nabla \times \vec{\mathbf{E}}\right] - k_0^2 \epsilon_0 \vec{\mathbf{E}} = 0 \tag{1.61}$$

This equation is a frequency code because it has to be solved for each value of $k_0 = \frac{2\pi\nu}{c}$ which directly associated with the frequency value ν.This code is designed to generate a three-dimensional mesh using a mesh adaptable tetrahedral approach. The use of finite element analysis in these constructions, in conjunction with an integrated calculator, enables the visualisation of many fields and physical parameters. Most HFSS mistakes are caused by incorrect usage of excitations and boundary conditions. Boundary conditions play an important role since they have significant impacts on the electromagnetic solution. HFSS advises using "perfect E" and "perfect H" boundary conditions on the unit cell surfaces in the x and y axes for simulating infinite structures. Boundary conditions define the limits of the model and have the ability to simplify the model and reduce the time and resources needed for obtaining a solution. The boundary conditions are properly set on the symmetry and antisymmetry planes of the unit cell. The electric field is perpendicular to any electrical antisymmetry plane, while the magnetic field is perpendicular to the magnetic symmetry planes. This allows us to simulate the periodicity of the network and minimise the size of the simulated region. To accurately replicate the design, it is necessary to generate or allocate a minimum of one port excitation for simulation purposes [47].

1.9.4 CST - Microwave Studio

The Computer Simulation Technology (CST) tool had many modules known as "solvers".
• A transient solver is a versatile 3D module that enables real-time simulations, useful for analyzing the propagation of fields in an electrical component as time progresses. A frequency solver is a broad solution that operates based on a frequency technique, similar to the transient solver. The mesh might be Cartesian or tetrahedral, depending on the structure being analyzed.
• A modal solver specifically designed for simulating resonant closed structures. Possible outcomes consist of mode distribution and resonance frequencies of the structure. •

Integral solver: This solution is designed for complex electrical systems. The approach depends on the Method of Moments using an integral formulation of electric and magnetic fields. The Multilevel Fast Multipole Method(MLFMM) technique is used to decrease numerical complexity.

The CST program provides several options for analyzing electromagnetic structures. Analysis may be conducted in either the time domain or the frequency domain. CST examines the possibility of a non-uniform mesh. This tool is suitable for time-domain analysis as well as wideband analysis. However, its use is restricted to structures of modest dimensions, typically a few wavelengths in size. Modeling propagation in a tunnel is not feasible because of limitations in calculating time [46]

1.10 Metamaterial application

1.10.1 Metamaterial as antenna

Metamaterial coatings were previously used to enhance the radiation and coupling properties of electrically small electric and magnetic dipole antennas. Apply metamaterials to amplify the radiated power. The most recent Metamaterial antenna achieves a 95% efficiency in capturing the incoming radio signal at a frequency of 350 MHz. Metamaterial antennas used in research typically have diameters that are around one-fifth of a wavelength. The inclusion of a metamaterial cover improves the directivity of a patch antenna. The use of a zero index metamaterial in the construction of a flat horn antenna with a flat aperture offers the advantage of enhanced directivity. Zero-index metamaterials enable the realization of antennas with exceptional directivity. In a zero-index metamaterial, the propagation of a signal results in the generation of a time-varying, but spatially fixed, field structure. Once the system reaches a steady state, the phase at any given place inside the metamaterial remains constant. Metamaterial has the ability to amplify the signal strength and minimize the amount of signal reflected back in a patch antenna. The following is a comparison of I-shaped antennas inspired by metamaterials, as conducted by M.A. Wan Nordin et al. in 2012 as seen in figure(1.6) [3].

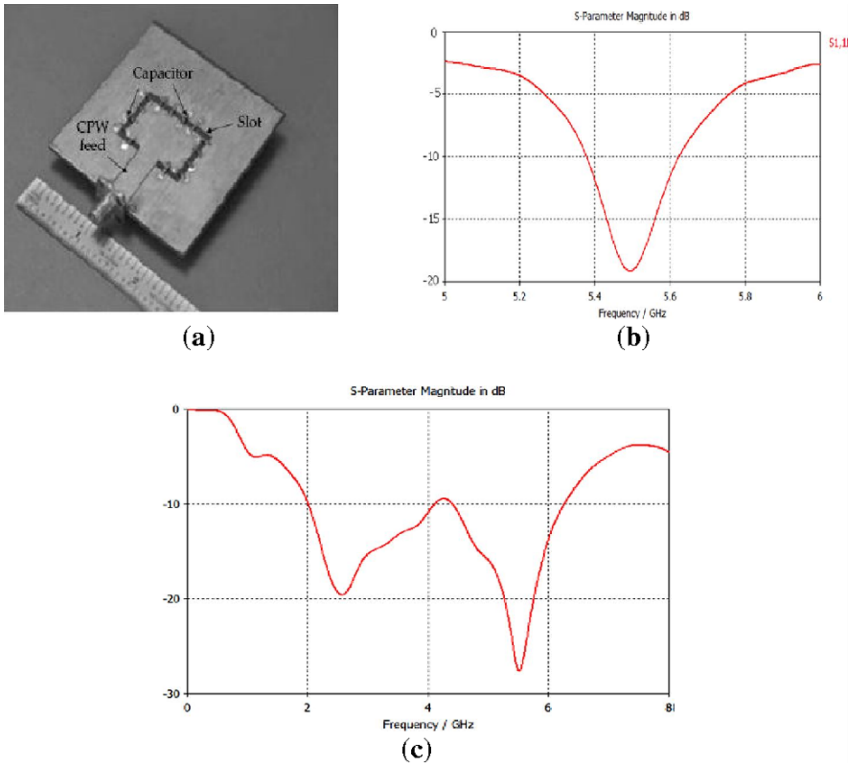

Figure 1.6: (a) three-dimensional graphic depicting the coplanar waveguide (CPW) feeding mechanism of an antenna. (b) Outcome of a basic patch antenna.(c) The results of the Metamaterial antenna.

1.10.2 Metamaterial absorber

In 2008, Gangwar and Gangwar created the first metamaterial absorber, which consisted of a dielectric layer placed between two metal layers [3]. The absorber, which operated at a frequency of 22,984 Hz, demonstrated an absorption rate of 22%. In contrast, Landy's research achieved a greater absorption rate of 44%.Figure 1.7 depicts the absorber and its unique cell. Hossain et al. [4] designed an efficient metamaterial absorber consisting of two metal layers separated by a gallium arsenide dielectric substrate, with the aim of harnessing solar energy. The solar cells of this adsorbent have the capacity to increase the performance of the system by enhancing the solar electromagnetic pulse. The adsorbent metamaterial has achieved optimal adsorption in both the electric and transverse magnetic modes. Results suggested that altering the thickness of different absorbent layers, the polarization angle, and the size and shape of the resonators had the ability to change the rate at which absorption occurs. Figure 1.8 shows the absorbent material that was built, whereas figure 1.9 demonstrates how the absorption rate changes depending on the frequency for several shapes of patches (hexagonal, octagonal, pentagonal, and circular) that were made throughout the research. The study data showed that the hexagonal shape was more efficient in collecting solar energy due to its higher absorption rate.

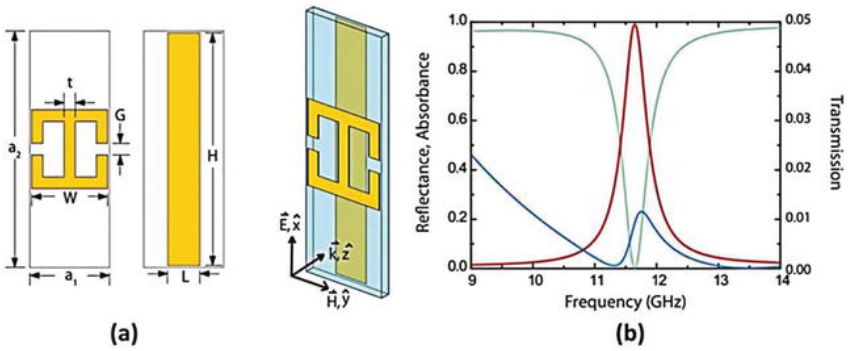

Figure 1.7: Metamaterial absorber and its unit cell [3]

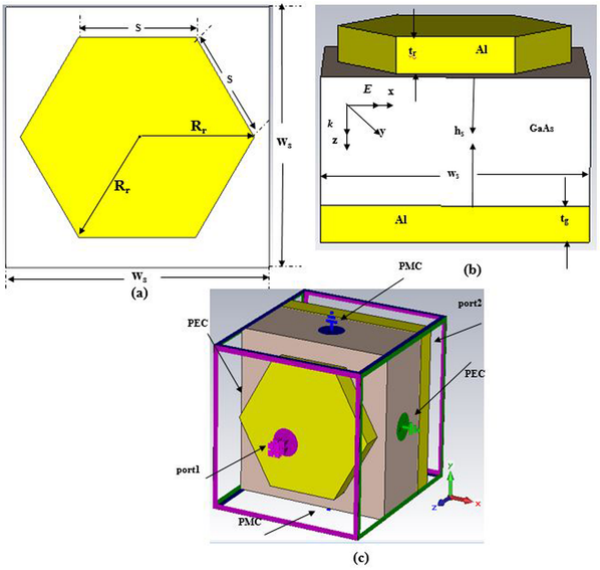

Figure 1.8: An ideal metamaterial absorber and its basic structural unit [4]

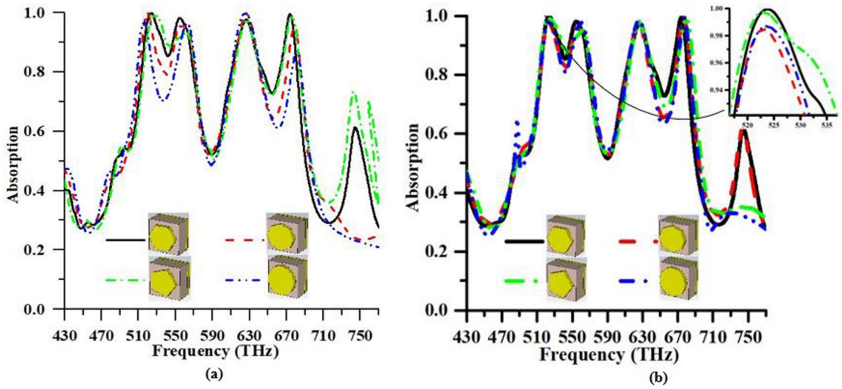

Figure 1.9: Changing of the absorption rate in frequency for patches with varying configurations (a) with a varied effective area and (b) with the same operational area [4]

Using two dielectric layers that were specifically designed for adsorption on the k-band, Tran and Phuong [48] created an exceptional metamaterial absorber. The absorption rate was examined in relation to the dimensions of the structure and the distance

between the two level after the researchers made adjustments. The structure's efficacy was significantly correlated with its size, as indicated by the experimental and simulation results. [49].

1.10.3 Invisibility cloaks

One popular application of metamaterials and transformation optics is the development of an invisibility cloak, which causes an object undetectable to external observation. A cloak is a space that contains various types of media. The cloak enables an incident wave to pass around the object effectively, maintaining its original form to obtaining the opposite side. The incident wave will perceive the entire covered area as if it were open space. The initial prototype of the invisibility cloak is a 2D cylindrical design that functions within the microwave frequency range, as observed in the laboratory setting. The mechanism involves the polarization of the electric field along the axis of the cylinder. The cloak was fabricated using printed SRR arrays, as depicted in Figure 1.10, and evaluated in a parallel-plate waveguide operating at X-band frequencies (8 to 12 GHz). The experiment showed that using a cloak reduces scattering from the concealed item while also minimizing its shadow, resulting in a cloak and object that resembles empty space. Initially, cloaking devices focused on cylindrical or spherical shapes for ease of analysis and implementation. However, they are not always effective in hiding irregularly shaped things. As a result, several forms of cloaking devices were later developed. Cloak invisibility has been created for inverse design ,as well as other sections of the electromagnetic spectrum, including optical and terahertz frequencies (figure1.10) [50].

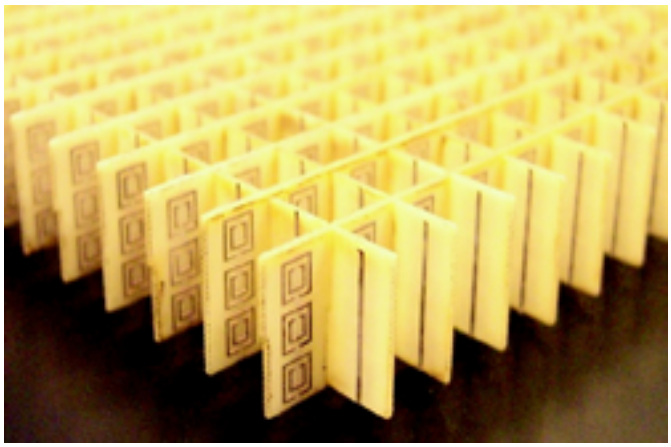

Figure 1.10: (Color online) The first prototype of NIM metamaterial.

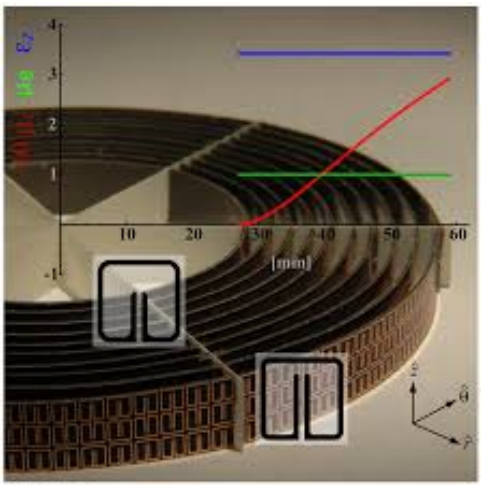

Figure 1.11: The first 2D cloak at microwave frequencies has been developed, with a plot illustrating the material parameters used in its implementation.

1.10.4 Metamaterial as sensor

Metamaterial offers the creation of sensors with precise sensitivity; it provide a means to greatly amplify the sensitivity and precision of sensors. Metamaterial sensors have use in several areas such as agriculture and medicinal sciences. Agricultural sensors use resonant material and utilize SRR technology to provide improved sensitivity. In the context of biomedical applications, wireless strain sensors are often utilized. Researchers, such as Goran Kiti et al. (2012), have created nested SRR-based strain sensors to boost sensitivity [5].

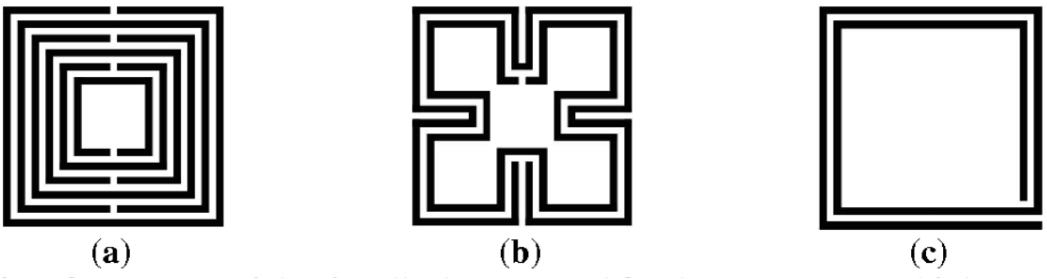

Figure 1.12: The sensor utilizes metamaterial unit cells (a). This research focuses on the multiple SRR,(b) Sierpinski SRR, (c) Spiral Resonator [5].

1.10.5 Metamaterial as superlens

Metamaterials are used in superlens technology to exceed the diffraction limit. Ramakrishna (2005) demonstrated that it has resolution capabilities beyond those of traditional microscopes. Conventional optical materials are restricted by diffraction since they can only transmit the propagating components of light emitted by a source. The non-transmitting elements, referred to as evanescent waves, are not conveyed. Increasing the resolution may be accomplished by raising the refractive index. However, this method

is limited by the lack of high-index materials. The primary characteristic of the super lens is its capacity to significantly magnify and retrieve the evanescent waves that convey information at very small scales. At now, there is no lens that can completely recreate all the transient waves produced by an object. Our next objective is to create an advanced lens that can effectively capture and use all evanescent waves, resulting in a clear and high-quality image [6].

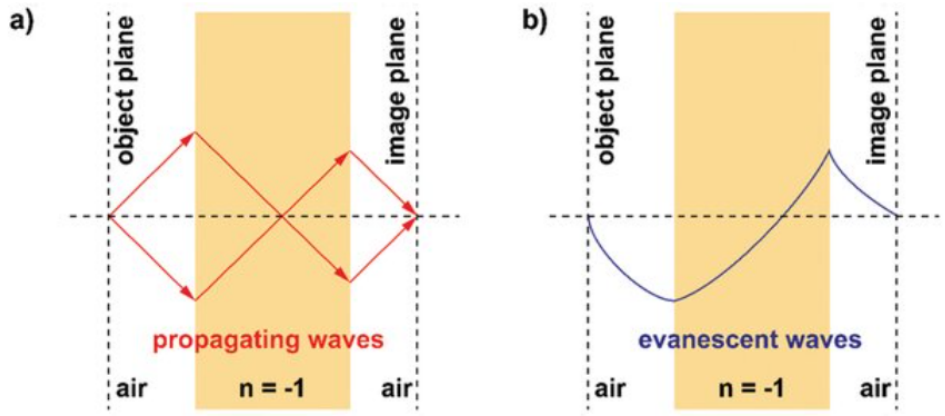

Figure 1.13: (a)Propagation wave recovery (b) Enhancement of Evanescent wave [6].

1.10.6 Metamaterial as cloaks

A metamaterial cloak is a device that can provide invisibility for objects by modifying the propagation of electromagnetic waves. This is accomplished by using metamaterials, which bend the electromagnetic waves around the object, essentially rendering it invisible. The underlying idea of this cloaking method relies on the notion of coordinate transformation, in which the spatial coordinates are altered in such a way that the electromagnetic field inside the cloak becomes nonexistent [5]. Pendry, Schurig, and Smith (2006) [51] provided a description of this notion (Figure 1.14).

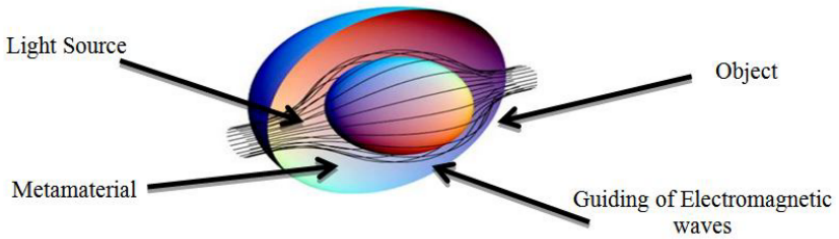

Figure 1.14: Cloaking

1.11 Conclusion

In conclusion, this chapter laid the groundwork for understanding the key principles of electromagnetic theory, starting with the behavior of light in a vacuum and progressing to the intricate dynamics of wave propagation in various materials. By exploring the dispersion relation and its implications, we have gained insight into how different media influence wave behavior, which is essential for advancing into more complex topics such as metamaterials. This foundational knowledge is critical as we transition to the next chapter, where we delve into metamaterial absorbers. In the upcoming section, we will build on the concepts introduced here to explore how engineered structures, like metamaterial absorbers, interact with electromagnetic waves, allowing for tailored absorption properties and innovative applications in various fields.

Chapitre 2 Metamaterial Absorbers

2.1 Introduction

Metamaterial absorbers (MMAs) have emerged as a cutting-edge technology in the field of electromagnetic wave absorption, offering significant advantages over traditional absorbers. This chapter begins by exploring the origins and evolution of metamaterial absorbers, focusing on the foundational theories that underpin their design and operation. Key principles such as impedance matching and resonance are discussed to provide a clear understanding of how MMAs achieve high absorption rates over specific or broad frequency ranges. Furthermore, the chapter introduces figures of merit, which are critical benchmarks for assessing the performance of different types of absorbers. Beyond the theoretical framework, this chapter also provides an in-depth overview of the primary industrial absorbers, including dielectric, magnetic, and adaptive absorbers, highlighting their unique mechanisms and applications. Finally, we categorize various types of metamaterial absorbers, emphasizing their diverse structures and functionalities, thereby paving the way for the development of advanced applications in modern technology.

2.2 Background and History

Electromagnetic absorbing materials, often known as Radar Absorbing Materials (RAM), were developed in both the United States and Germany during the Second World War. An ideal absorbent is characterized by its ability to function as an efficient paint or coating that can absorb all polarizations over a broad frequency range and a wide range of incident angles. Such a substance does not exist in actuality, and it seems challenging to create a prototype that precisely answers this specification. The primary uses of absorbents are mostly in the domains of ElectroMagnetic Compatibility (EMC) and radar stealth. They act in order to mitigate the issues of interference that arise between the frequency bands of terrestrial and/or space telecommunications systems. For instance, they may be used in electromagnetic properties testing rooms, such as anechoic chambers [52] [53].

The MMA counts among the electromagnetic (EM) wave absorbers that have been manufactured in the last century. The primary goal of these absorbers is to create a material with little transmission and reflection, hence achieving high absorption. Absorbers were first introduced in the 1930s, but their full potential was realized in the 1940s when they were used to improve radar performance and provide defense against radar detection [54].Famous absorbers that have been created and are now used include the Salisbury Screen, the Jaumann absorber, the crossed grating absorber, and circuit analog absorbers. Electromagnetic wave absorbers find use in several radar applications, as well as in the mitigation of electromagnetic interference (EMI), waveguides, and other military applications. [55] [56].

The MMA, which was established in 2008 [57], used a three-layer design and operated inside the microwave range of the electromagnetic spectrum .The outcome was an experimental absorption rate of 88% at a frequency of 11.5 GHz .Following to the

publication of , significant advancements have been made in the design of the MMA. Currently, there are absorbers available that function throughout a wide range of frequencies, from microwave to optical. These absorbers possess various features, such as being omnidirectional, sensitive or insensitive to polarization, and having either broadband, narrowband, or multiband capabilities. Additionally, they may be either passive or dynamic in nature [35].Metamaterials that exhibit numerous responses have also influenced the development of absorbers. As a result, multi-band metamaterial absorbers (MMAs) are now capable of operating over a wide range of frequencies, from microwave to optical wavelengths [50].

2.3 MMA Theory

The absorption of a material, which depends on frequency, may be defined using the transmission and reflection properties. It can be expressed as [58]:

$$A(\omega) = 1 - T(\omega) - R(\omega) \tag{2.1}$$

This equation does not take into account scattering effects or the re-radiation of light caused by surface electromagnetic waves. Hence, it is essential to concurrently establish a frequency range that exhibits both minimal transmission and reflection in order to optimize absorption. To reduce reflection, the impedance of the metamaterial must be adjusted to match that of free space. The impedance is determined by the equation:

$$Z = \sqrt{\frac{\mu}{\epsilon}} \tag{2.2}$$

where μ and ϵ represent the permeability and permittivity of the substance, respectively. The permeability (μ) may be calculated as the product of μ_0 and μ_r, while the permittivity (ϵ) can be calculated as the product of ϵ_0 and ϵ_r. The reflection at normal incidence may be expressed using the following equation:

$$R(\omega) = \left| \frac{Z(\omega) - Z_0}{Z(\omega) + Z_0} \right|^2 \tag{2.3}$$

All parameters in this context are dependent to the frequency of the receiving radiation, denoted as ω, as well as the impedance of the vacuum, which is represented $Z_0 = 120\pi\,\Omega$ [59]. Beer's Law states that the transmission through a slab may be described by the equation:

$$T(\omega) = e^{-\frac{2n_2 d\omega}{c}} \tag{2.4}$$

where $T(\omega)$ represents the transmission, n is the refractive index, d is the thickness of the slab, ω is the angular frequency, and c is the speed of light.

As the limit of $Z(\omega)$ approaches Z_0, in the above equation, n_2 represents the imaginary part of the index of refraction ($n = n_1 + in_2$), d represents the thickness of the slab, ω represents the frequency of the incoming light, and c represents the speed of light in a vacuum. Thus, by adjusting the values of ϵ and μ such that $Z = \sqrt{\frac{\mu}{\epsilon}} = 120\pi\,\Omega$,

and ensuring that $n_2 d$ is much larger than $\frac{c}{\omega}$,, it is theoretically possible to achieve complete absorption of both reflection and transmission, resulting in a nearly perfect absorber [16]. For Equation 2.1, all the absorbers that have been created are covered by a metallic plate at the bottom that completely eliminates any transmission, resulting in $T = 0$. This reduces Equation 2.1 to Equation 2.5.

$$A(\omega) = 1 - R(\omega) \tag{2.5}$$

Therefore, in order to achieve complete absorption, it is necessary to ensure that there is no reflection. This state or situation. Impedance matching is the term used to describe this. It is important to explain that R represents the reflectance, which is the ratio of power between the reflected and incident waves. The expression may be formulated using the complex reflection coefficient Γ, as shown in equation (2.6a), or the complex reflection coefficient represented by the scattering parameter S11, as shown in Equation [60]. BothΓ and S11 are represented as ratios of voltages.

$$R = |\Gamma|^2 \tag{2.6a}$$
$$R = |S_{11}|^2 \tag{2.6b}$$

Considering Equation 2.6, Equation 2.5 can be written as:

$$A(\omega) = 1 - |\Gamma|^2 = 1 - |S_{11}|^2 \tag{2.7}$$

In order to comprehend the impedance matching condition, we consider the example of a plane wave propagating through free space at a perpendicular angle and encountering a medium situated above a metal plate, as seen in Figure 2.1.

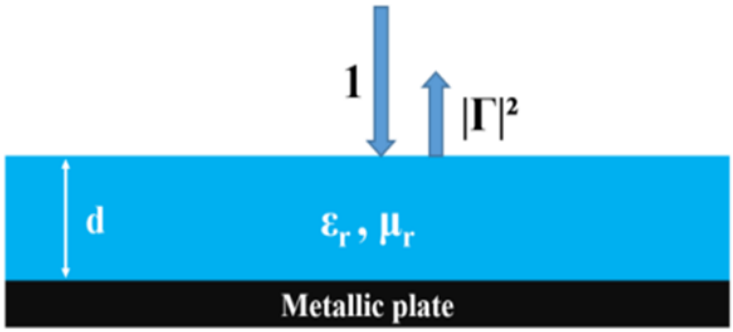

Figure 2.1: illustrates the geometric arrangement of a single dielectric slab positioned on a metallic plate. The incident power, shown as 1, is the quantity of power that may either be reflected or absorbed. The metallic plate ensures complete absence of transmission.

When the reflection coefficient in equation (2.8) becomes zero, the material losses result in a unitary absorptivity indicated by equation (2.7). This results because the transmission is zero below the metal plate [61].

$$\Gamma = \frac{\eta - \eta_0}{\eta + \eta_0} \tag{2.8}$$

Here, η represents the intrinsic impedance of the medium, while η_0 represents the intrinsic impedance of free space (air), which is equal to 377 ohms. When the value of η is equal to η_0, the condition for impedance matching is met since the reflection coefficient (Γ) is zero. The inherent impedance of a generic material η is only affected by the constitutive properties of the medium, as outlined in 2.9

$$\eta = \sqrt{\frac{\mu}{\epsilon}} = \sqrt{\frac{\mu_0\mu_r}{\epsilon_0\epsilon_r}} = \eta_0\sqrt{\frac{\mu}{\epsilon}} \tag{2.9}$$

The variables ϵ and μ represent the permittivity and permeability , respectively. These quantities are complicated and may be characterized by equations 2.10a and 2.10b, respectively.

$$\mu = \mu_0\mu_r = \mu_0(\mu_r' - j\mu_r'') \tag{2.10a}$$
$$\epsilon = \epsilon_0\epsilon_r = \epsilon_0(\epsilon_r' - j\epsilon_r'') \tag{2.10b}$$

The imaginary component of the constitutive parameters is linked to the dissipation of energy inside the medium. Therefore, the magnetic and dielectric losses of a certain medium may be quantified using the loss tangent, which is represented by Equations 2.11a and 2.11b correspondingly.

$$\tan\delta_m = \frac{\mu_r''}{\mu_r'} \tag{2.11a}$$
$$\tan\delta_e = \frac{\epsilon_r''}{\epsilon_r'} \tag{2.11b}$$

An ideal absorber is achieved when the values of ϵ_r and μ_r are equal, satisfying equation (2.9). Meeting this requirement is difficult, particularly when dealing with a broad range of frequencies. However, it is feasible to achieve for absorbers that operate within a limited frequency range. The preceding study of the electromagnetic field using a transmission line model (voltage and current method) allows us to investigate two situations for the medium presented in Figure 2.1: lossless and lossy. We can then evaluate the input impedance at the interface between the air and the absorber [12]. The use of a lossless medium is used to address the need for an RF absorber with a gradient of absorptivity. This is achieved by adding resistive sheets on top of the lossless medium. The impedance experienced by an incoming wave on a lossless medium that is grounded and has a thickness of d may be expressed as:

$$Z_{\text{in}} = j\eta\tan(kd) \tag{2.12a}$$

The sign η represents the intrinsic impedance of the lossless material, where the imaginary components of permittivity and permeability are both zero. The symbol k represents the wave vector in the medium. When dealing with a medium that causes loss, it is necessary to take into account the imaginary components of the constitutive parameters.

$$Z_{\text{in}} = \eta\,\tanh\left(j\frac{2\pi}{\lambda_0}\sqrt{\mu\epsilon}\,d\right) = \eta_0\sqrt{\frac{\mu_r' - j\mu_r''}{\epsilon_r' - j\epsilon_r''}}\,\tanh\left(j\frac{2\pi}{\lambda_0}\sqrt{(\mu_r' - j\mu_r'')(\epsilon_r' - j\epsilon_r'')}\,d\right) \tag{2.12b}$$

λ_0 represents the wavelength in open space, whereas η is a complex variable. Perfect absorption may be achieved in both lossless and lossy media when the condition $Z_{\text{in}} = \eta_0$ is met. This can be accomplished by adjusting the thickness d and the real parts (ϵ_r and μ_r) in equations (2.12a) and (2.12b), as well as the imaginary parts (ϵ_r'' and μ_r'').in equation (2.12b). Here, we have included some essential formulae for analyzing the absorbance of a particular structure. The next part will offer an analysis of the physical absorption processes.

2.4 Absorption mechanisms

Energy dissipation takes place inside a material when it is subjected to electromagnetic waves due to the damping effects on polarized atoms and molecules. The use of vector calculus allows for the development of an equation in electromagnetism that describes the conservation of energy, which is often referred to as the complex Poynting vector theorem. This theorem establishes a correlation between the amount of power into a certain volume V, via a closed surface S, and the electromagnetic fields and material properties inside that volume. The actual origin of power found on a particular surface is the power that has been dispersed or absorbed. In order support this theory, we provide the conservation-of-energy equation (2.13) derived from [61].

$$-\frac{1}{2}\iiint \left(\vec{H}^* \cdot \vec{M}_i + \vec{E} \cdot \vec{J}_i^{\,*}\right) dv = \oint \left(\frac{1}{2}\vec{E} \times \vec{H}^*\right) \cdot ds + \frac{1}{2}\iiint \left(\sigma|\vec{E}|^2\, dv + j2\omega \iiint \left(\frac{1}{4}\mu|\vec{H}|^2 - \frac{1}{4}\epsilon|\vec{E}|^2\right) dv\right) \tag{2.13}$$

where:

- H is the magnetic field intensity in amperes per meter (A/m).
- M_i is the impressed magnetic current density in volts per square meter (V/m^2).
- E is the electric field intensity in volts per meter (V/m).
- J_i is the impressed electric current density in amperes per square meter (A/m^2).
- σ is the conductivity in siemens per meter (S/m).
- ϵ is the complex permittivity in farads per meter (F/m).
- μ is the complex permeability in henries per meter (H/m).
- ω is the angular frequency in radians per second (rad/s).

Equation (2.13) may be expressed as (2.13a)

$$P_s = P_e + P_d + j2\omega\left(\vec{W}_m + \vec{W}_e\right) \tag{2.13a}$$

where:

$$P_s = -\frac{1}{2}\iiint \left(\vec{H}^* \cdot \vec{M}_i + \vec{E} \cdot \vec{J}_i^{\,*}\right) dv \tag{2.13b}$$

(The supplied complex power (W)).

$$P_e = \oint \left(\frac{1}{2} \vec{E} \times \vec{H}^* \right) \cdot ds \tag{2.13c}$$

(The excited complex power (W)).

$$P_d = \frac{1}{2} \iiint \sigma |\vec{E}|^2 \, dv \tag{2.13d}$$

(The dissipated real power (W)).

$$W_m = \iiint \frac{1}{4} \mu |\vec{H}|^2 \, dv \tag{2.13e}$$

(The time-average magnetic energy (J)).

$$W_e = \iiint \frac{1}{4} \epsilon |\vec{E}|^2 \, dv \tag{2.13f}$$

(The time-average electric energy (J)).

Although P_s and P_e can frequently be complicated, P_s is always a real number. However, the two variables mentioned are consistently imaginary and represent the reactive power associated with magnetic and electric fields.. It is important to note that when dealing with complex permeability and permittivity, the imaginary portions of the integrals in equations (2.13e) and (2.13f) should be added to equation (2.13d). This is because all three equations indicate the losses related to the permeability and permittivity, as shown in equation (2.13g).

$$P_d = \frac{\omega}{2} \iiint \left(\mu'' |\vec{H}|^2 + \epsilon'' |\vec{E}|^2 + \frac{\sigma}{\omega} |\vec{E}|^2 \right) dv \tag{2.13g}$$

Therefore, it can be inferred that for full absorptivity, one must use either conductivity (σ), imaginary permittivity (ϵ''), and imaginary permeability (μ''). This will happen when the impedance matching criteria is satisfied. This assertion is of utmost importance for the structures analyzed in the present investigation. As an example, two prototypes are created using 3D printing technology with layers that have relatively low conductivity, in contrast to Printed Circuit Board(PCB) technology structures that have layers with strong conductivity.

2.5 Figures of merit

The fractional bandwidth (FB) is the most often used metric to evaluate the performance of a broadband absorber. The calculation is performed using the equation (2.12).

$$FB = \frac{f_{\max} - f_{\min}}{f_c} = \frac{2(f_{\max} - f_{\min})}{f_{\max} + f_{\min}} \tag{2.14}$$

The variables fmax and fmin correspond to the greatest and lowermost frequencies., respectively, inside a band where an absorption coefficient over 90% is achieved. The value of fc corresponds to the center frequency of this band. There are three key factors that need to be emphasized at this juncture, which will be taken into account it:

- FB is often referred to as having a rate of absorption over 90%, unless otherwise specified.
- The presented data refers to the frequency dependence of the absorbance. The reflection coefficient is sometimes used in relation to the scattering parameter S11, which is measured in decibels (dB). When the absorption level is 90% (0.9), the corresponding S11 value is -10 dB.
- Absorber is classified as broad-band if its fractional bandwidth is 0.67, which is comparable to one octave.

2.6 Principal Industrial Absorber Types

2.6.1 Dielectric Absorber

Dielectric absorbers exhibit loss behavior that is completely attributed to their dielectric properties, without any magnetic characteristics. The loss might originate from several sources inside the dielectric material. Dielectric absorbers have the benefits of being cost-effective and lightweight when used with elastomers. Furthermore, due to their limited ability to absorb magnetic fields, dielectric absorbers are not suitable for most cavity resonance applications, which is a disadvantage [62]. This absorber is basic. These structures consist of foams, polymers, or honeycombs that include particles of carbon or metals such as iron, aluminum, or copper...
These materials have a high dielectric loss constant, which means they efficiently convert the incident wave into heat. The impedance of this substance is not well matched to the impedance of open space. Consequently, they have the ability to exhibit an effective reflection at their boundary. These materials are available in the industrial sector. Current studies on dielectric absorbers are increasingly emphasizing the use of conductive polymer materials. They possess the characteristic of having a low relative permittivity and a very evident dielectric loss. The production of this particular material is quite complex often including the deposition of layers onto material in order to achieve a certain level of strength [52].

2.6.2 Structural Absorbers

The reflection of a wave at the surface of a material is directly correlated with the impedance of the substance. Three kinds of absorbers (pyramidal, progressively loaded, and impedance matching layers) were developed to improve the dispersion of

the wave in a dielectric absorbing layer, based on this discovery. This specific material requires a significant thickness to effectively reduce signal intensity over a wide range of frequencies, which therefore leads to a high weight. The primary focus of our study was the pyramidal absorber construction used in the anechoic chamber.

a)Paramydical strecture

Pyramidal absorbers are often composed of thick materials that include regularly spaced structures in the shape of pyramids or cones, which are oriented at a right angle to the surface.The pyramidal absorbers have been specifically engineered to provide a smooth change between the impedance of air and the impedance of the absorber at the interface. The height and frequency of the pyramids often coincide with the wavelength. These absorbers have exceptional performance. Pyramidal absorbers have the disadvantage of being large and prone to fragility [63].

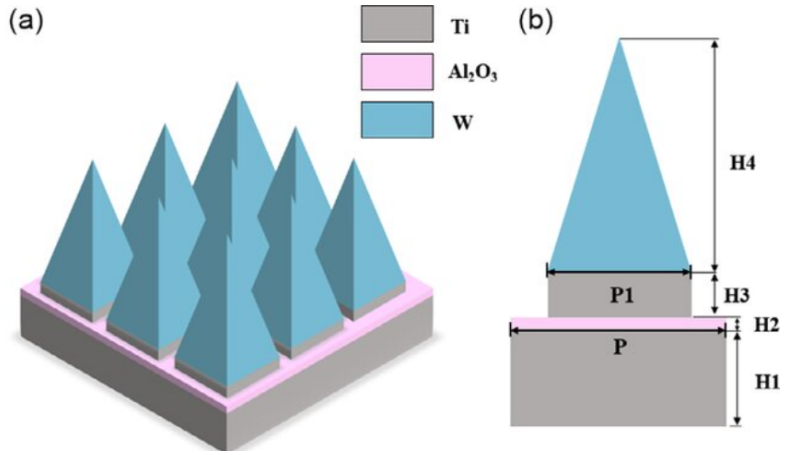

Figure 2.2: Model of Pyramidal Dielectric Absorber. a) three-dimensional schematic diagram. b) Two-dimensional cross-sectional view. [7]

b)Taped loading absorber

This material typically consists of a low-loss plate combined with a high-loss plate. There are two separate categories of structures that we may specify. The first ideal component is uniformly distributed along to the surface of the item to be protected, with a perpendicular gradient and progressive distribution inside the material. Reproducibly fabricating a gradient in this way is challenging and costly. The second kind of structure, which is more prevalent, consists of uniform layers that have an increasing load in the direction of propagation (i.e., the gradient is formed as a step function). These materials provide the benefit of being thinner compared to pyramid absorbers. However, their efficiency is lower [52].

c)Matching Layer Absorber

Matching Layer has objective of an absorber is to decrease the necessary thickness for materials that are subjected to increasing loads. This absorber type has an absorption change layer that acts as a barrier between the incoming wave and the absorbent materials. The impedance value of the transition layer is intermediate between the impedances of the two media. The idea is to provide a variation in impedance between different configurations. The phenomenon of matching arises when the thickness of the matching layer is precisely one-fourth of the wavelength of the incoming wave [52].

$$Z_1 = \sqrt{Z_0 \times Z_2} \tag{2.15}$$

Impedance matching only takes place at the specific frequency that is wanted. Thus, this particular absorbent material has a limited frequency range and is much thicker at low frequencies, as seen in Figure 2.3.

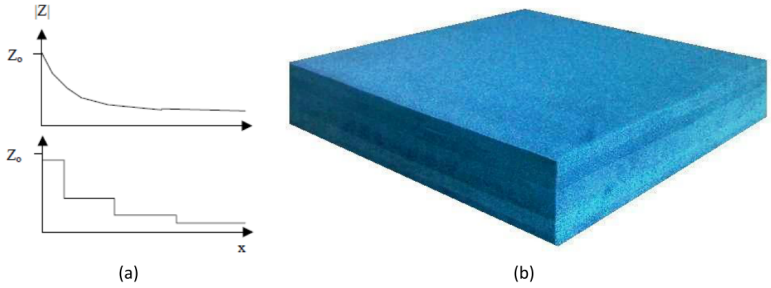

Figure 2.3: (a) Ideal impedance curve and typical impedance curve, and (b) example of a progressively charged absorbing material

2.7 Resonant Absorber

These absorbers are also known as tuned absorbers or quarter wave absorbers. Specifically, they consist of the Dällenbach layers [64], the Salisbury screens [65], and the Jaumann layers [66]. With this specific category of substances, the impedance may not be precisely adjusted to align with both the incoming wave and the absorbing medium. These materials have a thin structure and can only absorb a limited amount of energy. The technique used utilizes both reflection and transmission at the first interaction. The reflected wave experiences a phase inversion of a certain magnitude. The wave travels through the absorbing medium and experiences reflection when meeting a metallic surface. Due to the propagation of the wave towards the center of the incident wave, a phase inversion takes place during this second reflection. Destructive interference happens when the distance traveled by the emitted wave is a precise multiple of half the wavelengths, causing the two reflected waves to be in phase opposition. If the amplitude of two waves reflected is the same, then the combined intensity of the reflected waves is zero.

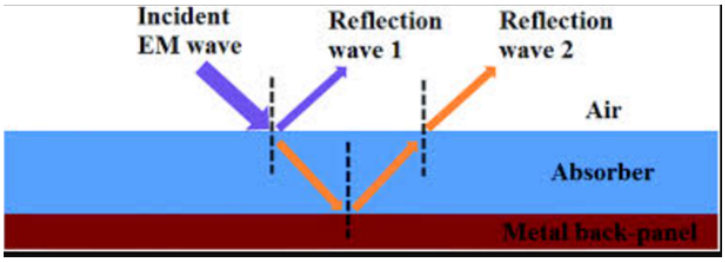

Figure 2.4: The representation of the Destructive Interference Phenomenon.

a)Dällenbach layer

A Dällenbach layer refers to a uniform absorption layer that is positioned on a flat surface driver. The layer thickness, permittivity, and permeability are manipulated in order to decrease the reflectance at a certain wavelength. The Dällenbach layer is supported by a process of destructive interference, which occurs when waves reflected from the first and second interfaces cancel each other out. In order to achieve lowest reflectivity, the effective impedance of the layer ZL must be equivalent to the impedance Z0 of the incident material. When designing a layer, there are five adjustable properties: ϵ',ϵ'',μ', μ'', and the layer thickness is often set at $\lambda/4$. Applying many layers with distinct absorption bands enhances the absorption bandwidth.

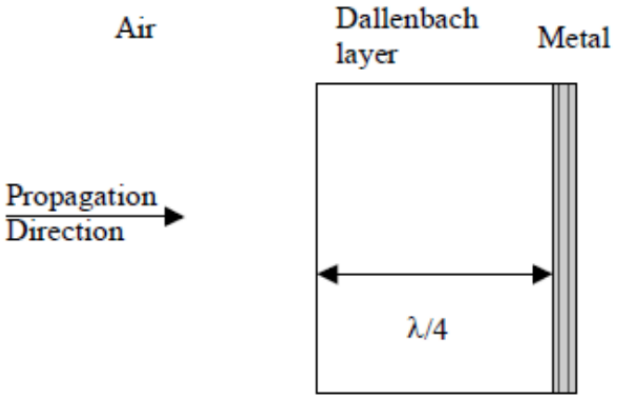

Figure 2.5: Illustration of the layout of a Dällenbach layer

2.7.1 Salisbury Screen

The Salisbury screen operates as a resonant absorber, which sets it apart from absorbent materials that count on the permittivity and permeability of their main layer. The Salisbury screen consists of a resistive sheet placed at a distance equal to an odd multiple of one-fourth of the wavelength of the metallic ground plane, with an empty space in between. Substituting an air blade with a material that has a high permittivity may decrease the necessary thickness, but it will result in a reduced on

bandwidth. The quarter-wave transmission line theoretically transforms a short circuit at the metal into an open circuit at the resistive sheet. Impedance matching is good when the resistance of the screen is comparable to the impedance of the air.

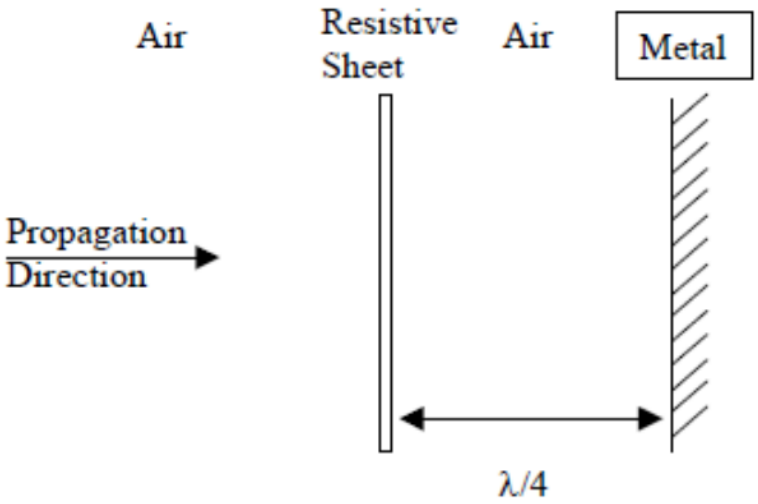

Figure 2.6: Illustration of a Salisbury screen layout

The original constructions consisted of a plywood frame covered with canvas, which was then coated with colloidal graphite. Next, conductive polymers were used in the creation of the Salisbury screen. The ideal thickness of the Salisbury screen may be determined by equating the screen resistance to the impedance of free space (Zo). The absorbent's thickness is determined by:

$$d = \frac{1}{Z_0 \sigma} \tag{2.16}$$

The resistive layer's thickness is denoted by d, while the sheet's conductivity is represented by σ. Two assumptions are made regarding the resistive layer:

1. The layer is thin in terms of its electrical properties, which means $k_0 d\sqrt{|\epsilon'|} \ll 1$, where $k_0 = \frac{2\pi}{\lambda_0}$ is the free-space wavenumber.
2. The losses in the layer are primarily due to the conductivity σ and $\epsilon'' \gg \epsilon'$.

These approximations provide values that can be obtained through measurement. Typically, a transition towards lower frequencies is observed as the resistive layer thickness or ϵ' increases.

To minimize reflections at the material entry, the resistance of the resistive layer should closely match the impedance of air, which is $Z_0 = 377\,\Omega$. The ideal resistance R_{spot} can be achieved to provide the desired reflectivity by:

$$R_{\text{spot}} = Z_0 \frac{1 - \Gamma_{\text{cutoff}}}{1 + \Gamma_{\text{cutoff}}} \tag{2.17}$$

where Γ_{cutoff} represents the maximum acceptable reflectivity.

Research has shown that as the permittivity of the spacer layer increases, the bandwidth decreases. The bandwidth of the Salisbury screen may be enhanced by creating absorber multi-screens, which are referred to as Jaumann layers.

a)Jaumann layer

Type absorbents were developed in Germany during the Second World War. Jaumann used the concept of the Salisbury screens, but with the implementation of several resistive screens. This was done to cover a range of frequencies and generate absorption bands. The resistivity of screens rises in the direction of the ground plane and is separated by low-loss dielectric layers. The first device was outfitted with two resistive layers that were separated by air, resulting in the creation of two adjacent frequency minima to enhance the bandwidth. Resistors are typically composed of layers of elastomer that contain carbon powder.

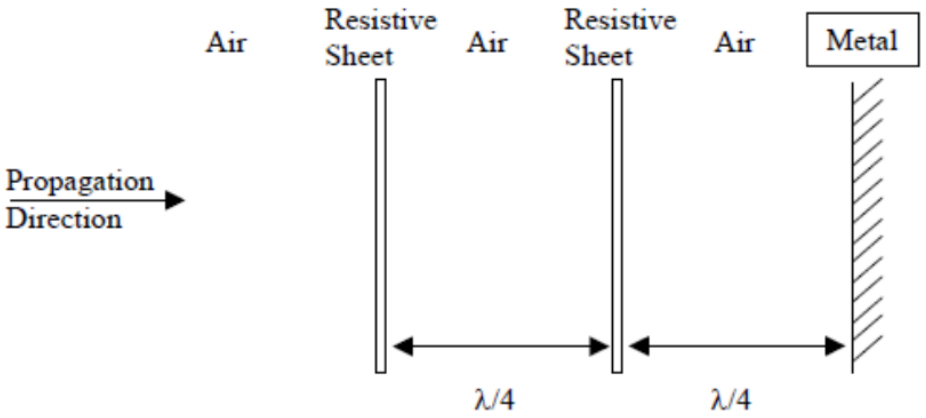

Figure 2.7: Illustration of Jaumann's layer arrangement

2.8 Adaptatif Absorber

Adaptive absorbers use Reconfigurable Electromagnetic Surfaces (RES) by expanding around the concept of resonant absorbers and absorbers using analog circuitry.

Numerous studies has been conducted on this particular absorbent material in order to attain commercial use. An illustrative instance involves the use of a high permittivity liquid inside a layer composed of a porous matrix with low permittivity. By doing so, it becomes feasible to regulate the absorbent characteristics by managing the volume of liquid. Regrettably, the absorbent in question has a somewhat prolonged reaction time. Applying a regulated magnetic field may vary the permittivity

of Dällenbach layers. However, implementing this technology on large surfaces is difficult.

2.9 Magnetic Absorber

Magnetic absorbers use iron or ferrite particles attached to a dielectric material, such as polymer, foam, or honeycomb structure. The uniformity of particle dispersion in the absorbent is an essential factor in the design of this material. Alternative particles may be used, however they are less prevalent.

Although the magnetic absorber is heavy due to its constituent particles, its greatest benefit is in its thinness, which may be as small as one tenth of the wavelength at its initial resonance.

These materials function across a broad frequency range spanning from megahertz (MHz) to gigahertz (GHz). The operating frequency of these particles is solely determined by their size. The physical and chemical characteristics of iron and ferrite particles were measured and computed. The preceding materials have a capacity that is similar to that of space. In order to get more flexibility in the absorbent design, we will adapt the parameter specific to these materials. The relative permeability of a material is as significant as the relative permittivity for designing an absorber, considering the expression of the characteristic impedance and refractive index.

$$Z = \sqrt{\frac{\mu_r}{\epsilon_r}} Z_0 \tag{2.18}$$

$$n = \sqrt{\mu_r \epsilon_r} \tag{2.19}$$

2.10 Metamaterial absorber

Metamaterial is a medium that allows the designer to manipulate electromagnetic characteristics by manipulating the geometry of the material, resulting in unique and exceptional capabilities. These materials often consist of dielectric and metallic components that are formed at scales far lower than the wavelength. They possess unique dispersion characteristics, such as negative permittivityϵ_{eff} and effective permeability μ_{eff} [67] [68].Due of these characteristics, the metamaterial has the ability to modify electromagnetic waves by absorption, filtration, amplification, or bending. Therefore, there are many possible uses for this technology, such as microwave and optical filters, very sensitive detectors, compact directional antennas, phase shifters that work with both right and left-handed signals, invisibility cloaks, extremely thin total absorbers, and more [69] .The branch of metamaterial perfect absorber (MPA) has gained significant attention due to its ability to produce complete absorption of electromagnetic waves at scales much lower than the wavelength. Since its first experimental demonstration in 2008 by N. I. Landy et al [57], several efforts [70] have been dedicated

to the development of Metamaterial absorbers with the aim of achieving multi-band absorption, broadband absorption, polarization-insensitive absorption, and wide incident angle absorption. Metamaterials are often created using many types of structures, including photonic crystal structures[26][27] ,transmission line (TL) based structures [71] [72] ,resonant structures , and complete dielectric materials [73] . MPA is a component of the resonant structure, meaning it functions within a limited frequency range.

2.11 Categories of Metamaterial Absorber

Literature frequently highlights metamaterial absorbers that are categorized according on many criteria, primarily resonance. In this part, we will discuss the fundamental principles of metamaterial absorbers. We will specifically focus on their efficiency in terms of absorption level, sensitivity to incoming angles, and sensitivity to polarization. A literature evaluation of several models will be provided to do this.

2.11.1 Plasmonic Resonance

This design is the most basic one reported in the existing research. It is considered the essential element for a resonant absorber. Plasmonic resonant-based MPAs have made significant progress in the last ten years because of their capacity to demonstrate wide-ranging behaviors and other advantages for real-world applications. Most MPAs are composed of three layers: (i) periodically spaced metallic patterns, (ii) a dielectric layer, and (iii) a solid metallic plate [73]. The metallic layers must be carefully planned to achieve a certain resonance at the desired frequency. The impedance matching requirement for open space is achieved by modifying the dimensions of the resonators, which may take various shapes such as ring, cross, patch, circular, snowflake, and others. When the impedance matching condition is satisfied, the reflectivity of the device is removed and all incident electromagnetic waves are efficiently coupled to the device.

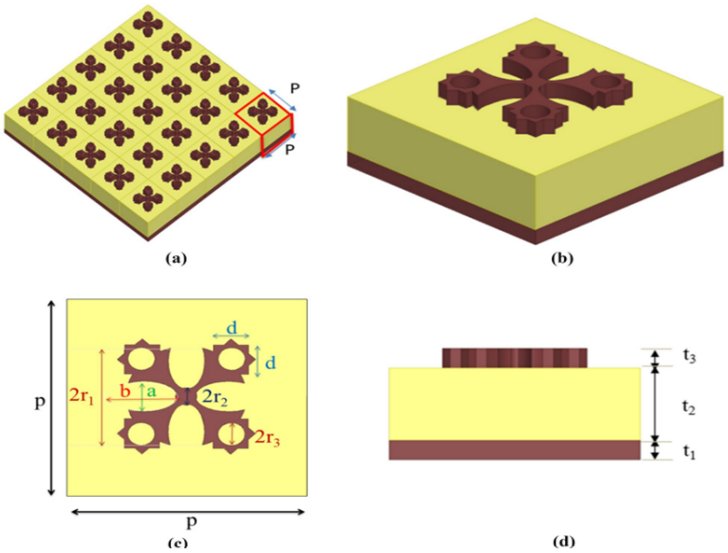

Figure 2.8: Proposed metamaterial absorber. (a) Three-dimensional representation of a 5×5 unit cell, (b) Three-dimensional model of a nanostructure composed of unit cells, (c) Top view, (d) the front views of the structure of unit cells [8].

The main objective of the second dielectric layer is to effectively capture the incoming electromagnetic wave. When the absorber is at its resonant frequency, the electromagnetic waves bounce back and forth within the resonator, causing the electromagnetic energy to be effectively absorbed.

In basic terms, the metal-dielectric-metal structure directly influences the lifespan of the resonant cavity, which subsequently impacts the frequency selectivity of its resonance via its quality parameter. The primary purpose of the third metallic layer is to reduce the transmission of the affecting wave. Furthermore, the next sections focused on plasmonic-type structures will illustrate that the metallic regions adjacent to the structured top metal layers facilitate the flow of reverse backside local currents.

To summarize, when an electromagnetic wave interacts with a tri-layered medium, the lack of transmission and reflection at the resonance point signifies that all of the electromagnetic energy is absorbed. This supports the term of "perfect magnetic absorber" (PMA) for such a material.

2.11.2 Broadband metamaterial absorbers

Broadband metamaterial absorbers are designed with precision to provide optimal absorption over a wide range of frequencies. These absorbers use advanced designs, such as multi-resonant structures and gradient index materials, to expand their ability to absorb electromagnetic waves over a range of frequencies, rather than just one unlike classic absorbers which are confined to certain frequencies. This characteristic make them effective in many applications, including stealth technology and energy harvesting [74].

a)Multi-resonant structures

Multi-resonant structures use many resonant components, each adjusted at different frequencies, To gain broad-spectrum absorption. An instance of this is the use of Split-Ring Resonators (SRRs) of diverse diameters, which may generate several resonance peaks over a broad frequency spectrum. The superimposition of these peaks leads to a wide absorption range, which is especially advantageous in applications that need efficient electromagnetic interference (EMI) protection. The research conducted by Liu et al. (2011) [75] is titled "Broadband Metamaterial Absorber Based on Multi-Resonant Structures". The researchers in this study devised an absorber by employing multiple concentric square rings of varying sizes. Every square ring resonates at a distinct frequency, resulting in numerous absorption peaks that overlap with each other. The distinctive design led to a wide-ranging absorption spectrum that covered frequencies from 2 GHz to 18 GHz. The broad absorption range is attained by precisely adjusting the dimensions of each resonator element to resonate at specific target frequencies, providing a uniform overlap of absorption bands. The absorber showcased in Liu et al.'s research is especially advantageous For applications require thorough absorption over a broad spectrum of frequencies, such as reducing radar cross-section and enhancing thermal imaging capabilities.

2.11.3 Frequency-Selective Metamaterial Absorbers

Frequency-Selective Surfaces (FSS) are designed surfaces made up of regular arrangements of resonant features, such as patches, dipoles, or loops, that resonate at certain frequencies. When an electromagnetic wave comes into contact with a Frequency Selective Surface (FSS), the resonant components of the FSS interact with the wave. This interaction causes the wave to be highly absorbed at the resonant frequency, while allowing other frequencies to either pass through or be reflected. The specific capacity of FSS absorbers to absorb just a restricted range of frequencies makes them very suitable for applications like antenna radomes. These absorbers effectively protect the antenna while permitting the transmission of certain frequencies. The study authored by Huang et al. [75] (Figure 2.9) describe the creation of an ultra-wideband Frequency Selective Surface (FSS) absorber that can function over a broad spectrum of frequencies. The absorber employs innovative resistive patterns to provide exceptional absorption over the whole range of wavelengths, showcasing substantial enhancements compared to conventional FSS designs. The design exhibits polarization insensitivity and consistently delivers excellent performance at different incidence angles, giving it ideal for practical use in electromagnetic interference (EMI) shielding and stealth technologies. The paper provides comprehensive models and experimental data that demonstrate the efficacy of the proposed FSS absorber in accomplishing absorption over a broad range of frequencies. This enhances its potential for many electromagnetic applications.

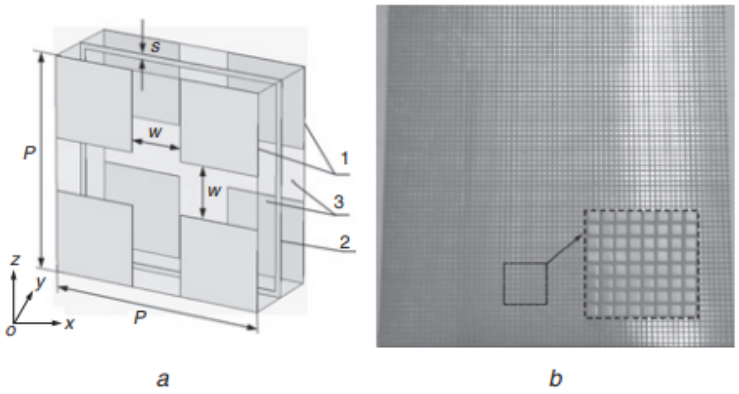

Figure 2.9: FSS structure (a)3D view of FSS Design; (b) Prototype of fabricated FSS.

2.11.4 Multilayer Metamaterial Absorbers

Multi-layer metamaterial absorbers uses multiple layers of diverse metamaterials, each specifically designed to absorb electromagnetic waves across different frequency ranges. This approach increases the absorption across a wider range of frequencies or enhances efficiency specifically at certain frequencies. H Xiong, wt all in 2013 [76](Figure2.10)article showcases the design and effectiveness of a highly thin and broad metamaterial absorber employing a multi-layered configuration. The absorber consists of multiple layers of resonant metamaterial structures, with each layer contributing to the absorption at distinct frequencies. Through meticulous layer design and stacking, the authors successfully achieve a wide absorption spectrum that spans from microwave to terahertz frequencies.

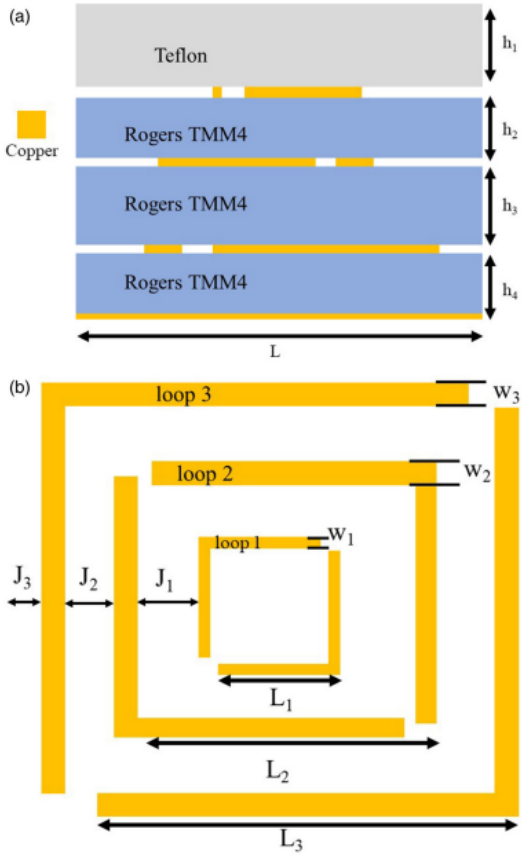

Figure 2.10: (a) A vertical perspective of a unit cell. (b) A upward view of the cell.

2.11.5 Angle-insensitive metamaterial absorbers

Angle-insensitive metamaterial absorbers are designed to exhibit consistent absorption characteristics regardless of the incident angle. This capability is accomplished by utilizing symmetric designs or specialized structures which ensure consistent impedance matching, regardless of the angle at which the electromagnetic wave arrives. These absorbers are essential in applications that demand consistent performance across different orientations, such as cloaking devices and antennas that can be used in multiple orientations.

Metasurface absorbers are a notable illustration of designs that are not affected by the angle of incidence. These absorbers utilize flat, engineered surfaces made up of sub-wavelength structures to efficiently control electromagnetic waves at various angles of incidence. An example of such an article is In the study conducted by Y. Fan, (2020) [77], an innovative approach is examined for the design of phase-controlled metasurfaces, utilizing an optimized genetic algorithm. The study highlights the utilization of genetic algorithms to optimize the geometric configurations and material properties of metasurfaces. This optimization allows for precise control of the phase of electromagnetic waves. The metasurfaces created using this technique have the ability to precisely control wave phases, making them well-suited for applications that demand precise beam steering, focusing, and wave manipulation. This technique demonstrates

the capacity of genetic algorithms to improve the functionality and adaptability of metasurfaces in different electromagnetic applications.

2.11.6 Flexible and Printable Metamaterial Absorbers

Metamaterial absorbers that are both flexible and printable are developed to be flexible and compatible with different surfaces and devices through the utilization of flexible materials or additive manufacturing techniques. These absorbers have the property of being adaptable and capable of being incorporated into various applications, such as wearable technology and flexible electronics. By utilizing materials and techniques that enable flexibility, elasticity, or printing, these absorbers may maintain their functionality while conforming to various shapes and surfaces. Illustrations:

- The research conducted in 2017 [78] investigates the highly flexible metamaterial absorber figure 2.11 and its potential application in sensing. The research shows that the metamaterial absorber maintains exceptional absorption performance while also being highly flexible, able to adapt to different surfaces and structures. The absorber's high degree of flexibility enables it to undergo substantial deformation without compromising its effectiveness, making it especially suited for installation into sensing platforms. This study emphasizes the application of the ultra-flexible absorber in sensing technologies for detecting variations in environmental conditions, such as pressure or strain. It demonstrates the adaptability and potential of this absorber for use in wearable and flexible electronic devices.

- Stretchable metamaterials are designed using flexible and stretchable substrates, enabling their integration into soft electronics or flexible screens. An illustration can be found in the article studied by Z. Xu et all (2019) [79] introduces a stretchable metamaterial with a parabolic shape that is specifically designed for terahertz applications as seen in figure 2.12. The research demonstrates that this metamaterial consistently maintains its performance even when subjected to various deformations, such as stretching and bending. The parabolic design enables improved control and absorption of terahertz waves, while the stretchable properties ensure that the metamaterial can adapt to different surfaces and structures without affecting its performance. This novel method showcases the capacity to develop versatile and flexible metamaterials that are well-suited for modern terahertz technologies.

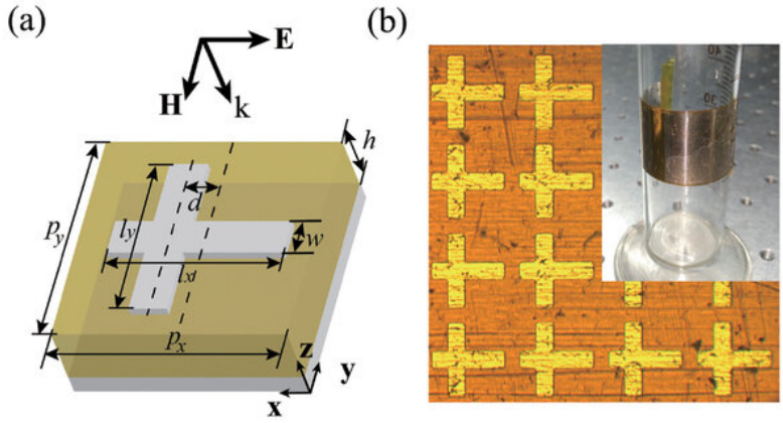

Figure 2.11: (a) Diagram depicting the construction of the asymmetric cross MPA. (b) A top-down optical microscope picture of the sample. The sample that was created is very flexible and can be readily wrapped around a measuring cylinder, as seen in the inset .

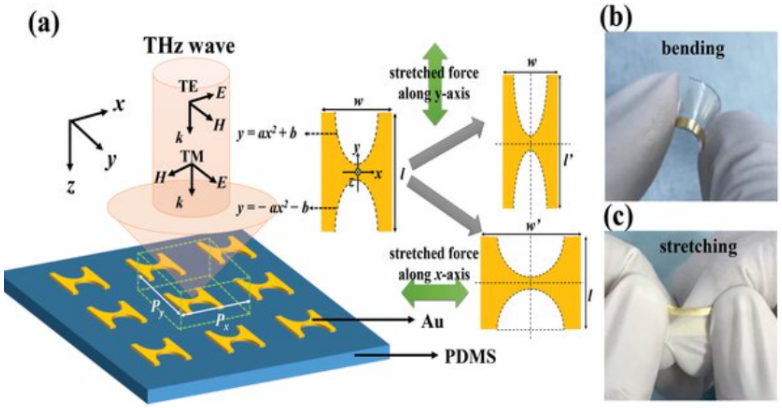

Figure 2.12: (a) Diagrams depicting the proposed PSM (Piezoelectric Strain Microscopy) device in operation, with a stretching force applied in the x- and y-axis directions. b,c) The photographs depict the PSM (Photonic Crystal Structure) that was created on a PDMS (Polydimethylsiloxane) substrate, highlighting its fundamental flexibility .

2.12 Conclusion

In conclusion, this chapter has explored the various types of metamaterial absorbers (MMAs) and their unique ability to manipulate electromagnetic radiation, distinguishing them from traditional absorbers. By classifying MMAs into resonant, broadband, frequency-selective, and flexible absorbers, we have highlighted their versatility and potential for a variety of applications. Each category offers a different approach to achieving high absorption efficiency, whether through fine-tuning resonant structures

or using flexible materials suited for diverse environments. These classifications underscore the transformative role MMAs play in controlling electromagnetic waves, providing tailored solutions for fields such as stealth technology and energy harvesting.

As we transition to the next chapter, we will shift focus from the broad categorization of MMAs to the theoretical modeling, design simulation, and parametric optimization of these absorbers. Building on the foundational understanding of MMAs' absorption mechanisms, the upcoming chapter will delve into how precise design and simulation techniques can optimize absorber performance, paving the way for enhanced functionality and practical applications.

Chapitre 3 Theoretical Model of MMA and Simulation Approaches

3.1 Introduction

In this chapter, we examine theoretical designs of MMAs, focusing on the significance of geometric structure and material qualities in achieving certain absorption characteristics. Following that, a comprehensive parametric analysis is provided, specifically examining the influence of several design parameters, such as the angle of incidence.unit cell parameters and the thickness of the substrate, on the performance of the absorber. We present a specialized ultrathin metamaterial absorber designed for conformal applications in the Ka frequency region. We explain the approach used to construct it and examine the theoretical foundations behind it. In addition, we analyze a modified wideband metamaterial absorber that includes a resistor element to improve absorption bandwidth and conformal flexibility. Our objective is to get a thorough grasp of the design and optimization methodologies for future metamaterial absorbers by using theoretical insights and simulation data.

3.2 Flexible and ultrathin metamaterial absorber for microwave application

3.2.1 Design Methodology

Figure 3.1 illustrates the structure of the unit cell for the proposed MA Its design consists of S shape in the middle and two rectangular positioned perpendicular to each other, empty inside are implemented on the four corners of these unit cell and It comprises copper layers on both sides. Additionally, there is a flexible silicone rubber layer with a thickness of t3 = 3 mm. The silicone rubber has a relative permittivity of 2.9 and a loss tangent of 0.08. The polyimide material, with a thickness of 0.25mm, is characterised as a lossy polymer with a dielectric constant of 3.5.The electrical conductivity of the top and bottom copper layers, with a thickness of t1 = 0.017mm, is adjusted at $\sigma = 5.8 \times 10^7\,\mathrm{S\,m^{-1}}$ The absorber was optimised to have a broad acceptable absorption band. The dimensions of the indicated absorber are $10 \times 10 \times 2.284$ $\mathrm{mm^3}$, as shown in Figure 3.1.The optimal parameters of the MMA are shown in Table 3.1.

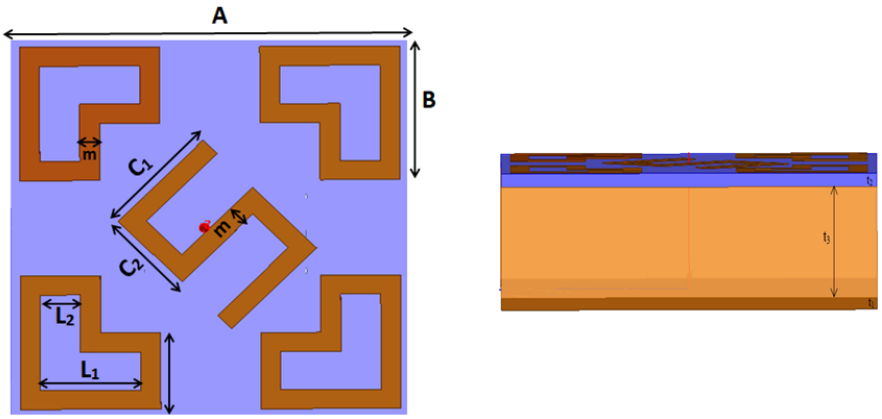

(a) (b)

Figure 3.1: The provided diagram illustrates the structural arrangement of the unit cell for the suggested (MA). (a) A view from above, and (b) perspective view of a unit cell.

Table 3.1: Geometric parameter of the Proposed MMA

Parameter	**Value (mm)**
A	10
B	3.5
C1	3
C2	2
L1	2.5
L2	1
m	0.5

3.3 Parametric Analysis

Figure 3.2a a demonstrates the simulated absorption effects while varying the incidence angle from 0° to 45°. The absorption band exhibits a constant behavior through the frequency range of 8 to 11.5 GHz across different incident angles, maintaining a similar absorption rate of above 90%. This stability in absorption performance indicates that the proposed metamaterial structure exhibits excellent angle-insensitive characteristics. Such a feature is highly desirable for practical applications where the angle of incidence may vary, ensuring reliable and efficient absorption across a range of conditions. Furthermore, the minimal shift in peak frequencies and the preservation of high absorption rates underscore the robustness of the design. This property enhances the potential of the metamaterial absorber in real-world scenarios, such as in stealth technology [80] and electromagnetic shielding [81], where consistent performance is crucial regardless of the incident angle (theta).

Additionally, Figure 3.2b depicts the simulated absorption rates as a variation of frequency at different polarization angles. With the polarization angle varying from 0° to 60°, the absorption band consistently approximately between 8 to 11.5 GHz with high absorption rates. This indicates that the metamaterial absorber exhibits excellent polarization-insensitive characteristics. The stable absorption performance across a wide range of polarization angles ensures that the absorber can effectively operate in diverse electromagnetic environments. Such polarization insensitivity is particularly advantageous for applications in stealth technology , where the orientation of incoming waves can vary unpredictably.

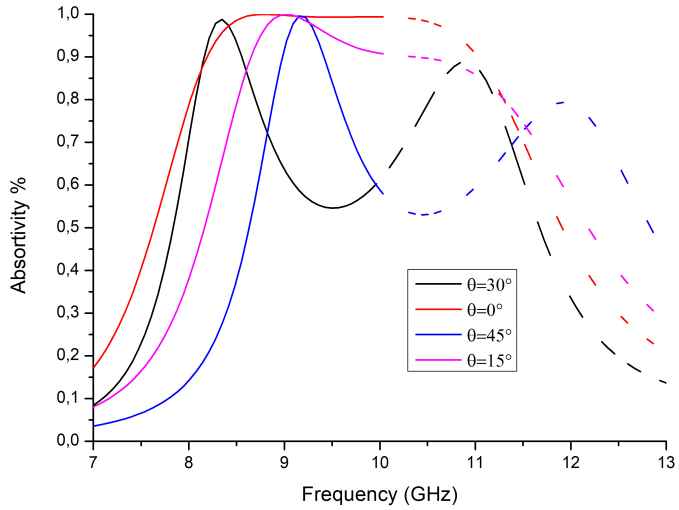

(a)

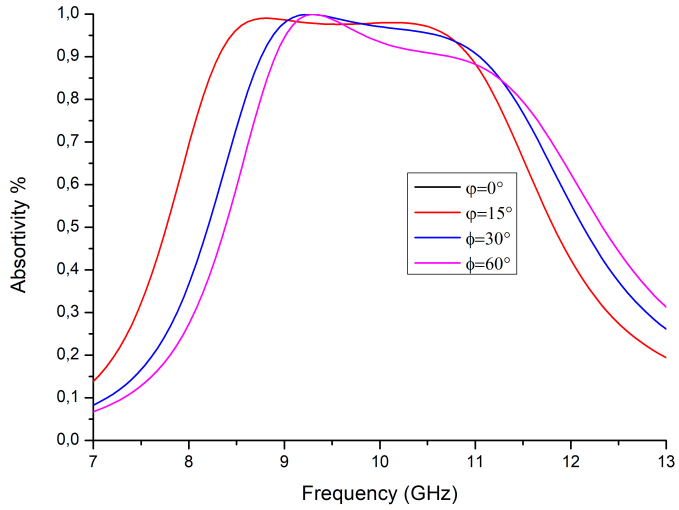

(b)

Figure 3.2: (a) Simulated absorption rates at different angles of incidence (b) The absorption rates of the MMA at different polarization angles.

Figure 3.3a demonstrates the absorptivity at different substrate thicknesses (t3). Increasing t3 thickness affects the absorption frequency bands differently. Thicker substrates extend the absorption band to lower frequencies, while thinner substrates enhance absorption in higher frequency bands.Therefore, there is a balance between the ability to absorb light and the range of frequencies that can be absorbed. [82]. Based on the analysis, t3 = 3 mm is identified as the optimized value.

Figure 3.3b illustrates the absorptivity at various thicknesses of polymide, where the parameter t2 represents the thickness. As t2 increases, there is a noticeable decrease in the percentage of absorptivity. This trend indicates that thicker layers of polymide result in reduced efficiency in absorbing electromagnetic waves across the tested frequency range. The optimal thickness, identified as 0.25 mm, exhibits the highest absorptivity percentage, suggesting that this thickness is most effective in attenuating incident electromagnetic radiation. This finding underscores the critical role of material thickness in determining absorber performance, emphasizing the importance of optimizing thickness parameters for achieving desired absorption characteristics in practical applications such as antenna design.

As illustrated in Figure 3.3c , increasing the thickness of the FSS affects its resonant frequency and absorption characteristics. In general, thicker FSS structures tend to lower the resonant frequency due to increased inductance and capacitance effects within the rings. This change in resonant frequency alters the absorption spectrum, potentially broadening or narrowing the bandwidth over which effective absorption occurs. In contrast, thinner FSS can exhibit higher resonant frequencies and narrower absorption bands. Therefore, the optimal FSS thickness balances these factors to achieve desired absorption performance over specific frequency ranges. This understanding highlights the importance of precise manufacturing control and design optimization to tailor FSS structures for applications in metamaterials, electromagnetic absorbers, and related technologies.

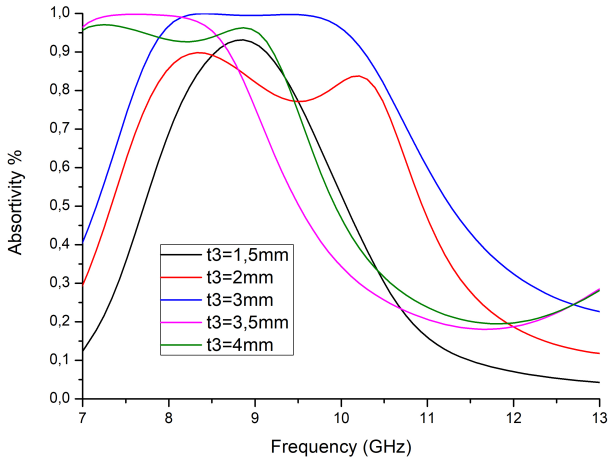

(a)

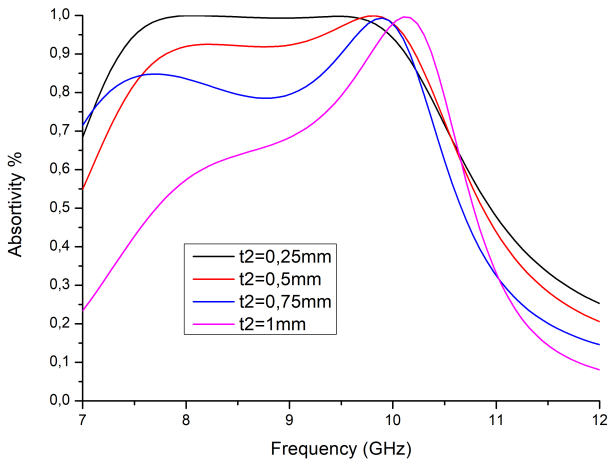

(b)

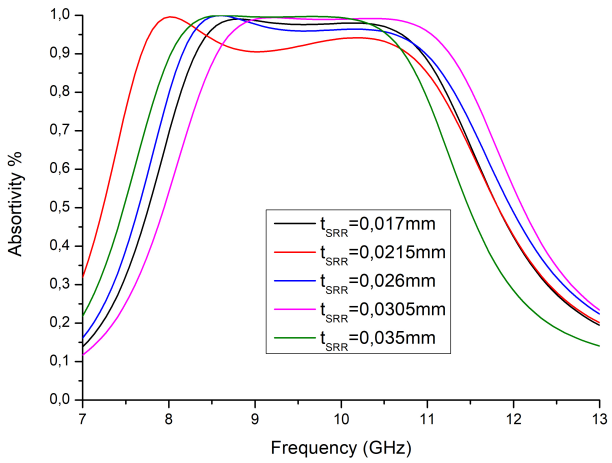

(c)

Figure 3.3: Absorber unit cell simulated absorption vs (a) silicone rubber, (b) polyimide substrate, and (c) FSS surface thickness.

Figure 3.4a displays the spatial arrangement of the electric field at 8.3 GHz. The electric field exhibits significant concentration along the outside border of the S-shaped structure and the rectangular components. The high concentration seen in these areas suggests a strong capacitive coupling, which plays a important part in the overall resonance of the absorber. The areas regarding the S-shape and the corners of the rectangular parts exhibit high-intensity electric fields, indicating that these locations are particularly efficient in absorbing and dispersing the energy of incoming electromagnetic waves. The electric field is uniformly circulate all over the surface of the absorber, hence enhancing the general effectiveness of the device.

Figure 3.4b depicts the spatial arrangement of the electric field with a frequency of 8.3 GHz. At this frequency , the electric field is mostly focused on the margins of both the S-shaped structure and the rectangular elements, similar to the observed distribution. The persistent focus of the electric field suggests that these areas are essential for capacitive coupling and the resonance of the absorber at various frequencies. The high-intensity zones around the S-shape and rectangular components effectively collect and dissipate incoming electromagnetic waves, hence improving the performance and efficiency of the absorber at this frequency.

Figure 3.4 illustrates the electric field distribution of the FSS. It shows an S-shaped structure in the centre and two rectangular components placed at right angles to each other. The four corners are left vacant. The presence of high electric field intensity in these regions emphasises the need of including S-shaped and rectangular features in the design, as they greatly enhance the overall performance of the absorber.

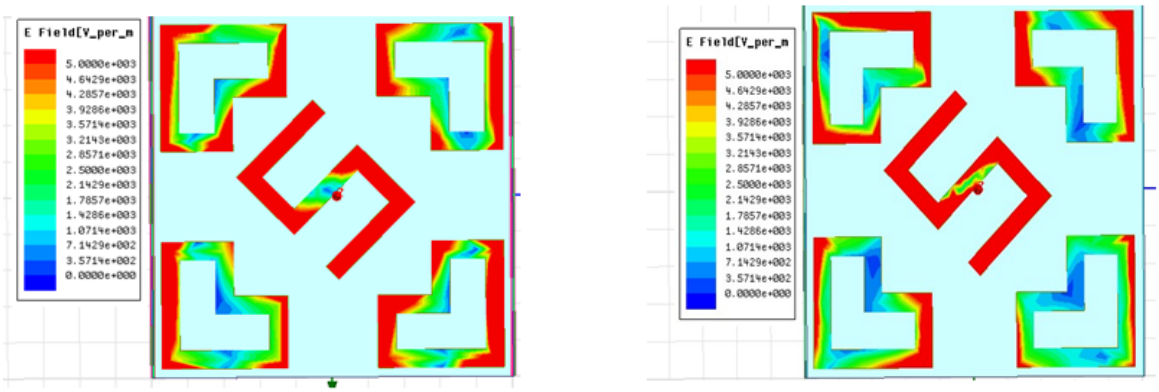

(a) (b)

Figure 3.4: Electric Field distribution (a) for f=8.3 GHz (b) for f= 10.8 GHz.

3.4 An Ultrathin Metamaterial Absorber for Conformal Applications at Ka Frequency Band.

3.4.1 Architectural Design of the PMMA

The PMMA has an absorption peak of 98% is obtained for resonance frequency at 32.3 GHz. The optimal values for the structural parameters are shown in Table 3.2, and the simulated structure is shown in Figure 3.5. As depicted in Figure 3.5, copper was deposited on the upper and lower surfaces of the flexible silicone rubber substrate with a dielectric constant of 2.90, a loss coefficient of 0.08, and a thickness of 2 mm.Silicone rubber is a polymer with high flexibility, low density, exceptional resistance to high and low temperatures (50 °C to 250 °C), high tensile strength, and excellent chemical resistance [83]. The upper surface consists of two cross circles with a small void printed on a 0.25 mm-thick of flexible polyimide film. Where the background is composed of metals, making the transmittivity nil.The unit cell parameters are correctly optimised so that the incident wave is properly coupled. The proposed absorbers are simulated using ANSOFT HFSS with Master-Slave boundary condition.

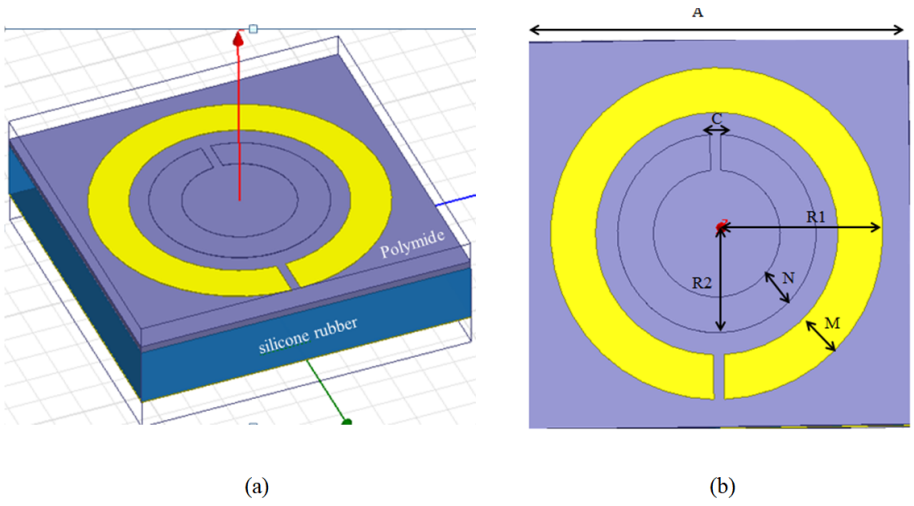

Figure 3.5: a)Schematics view b) topview of the absorber unit cell.

Table 3.2: Parameters list of the designed structure.

Parameter	Value (mm)
A	10.5
R1	4
R2	2.39
C	0.28
N	0.97
M	1.21

3.4.2 Results and Discussion

Figure 3.6 depicts the absorptivity values of the simulated structure witch has one absorptivity peaks where the absorption is greater than 98%, and it is calculated at resonance frequency of 32.3 GHz, where the absorption values at these peaks are 0.9841.

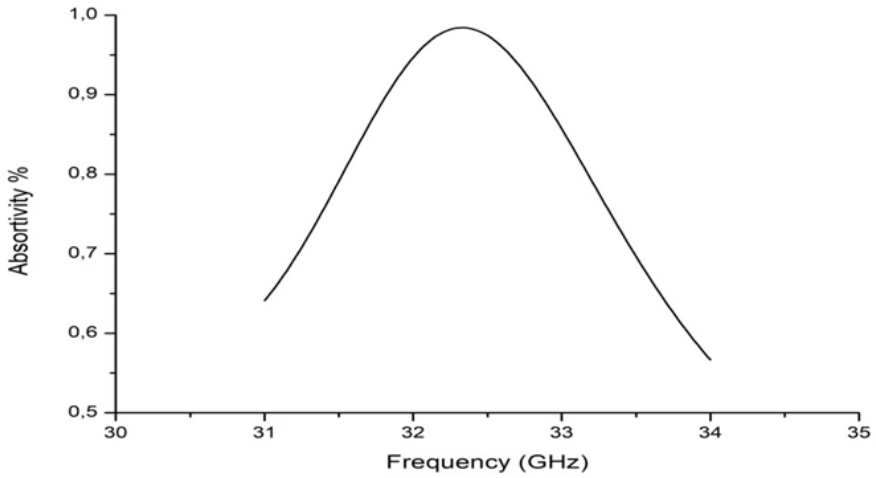

Figure 3.6: Simulated absorption and S11 of the Ka Frequency Band flexible absorber.

Figure 3.7 illustrates the electric field distribution in the proposed absorber at frequency of 32 GHz. The picture unambiguously demonstrate the existence of a powerful electric field focused on the cross-ring resonator, especially in the middle area of the device. The strong concentration of the electric field suggests that the structure exhibits resonant activity. The absorption peaks seen at these resonance frequencies are mostly attributed to the frequency selective surface (FSS) resonator, as shown by the concentrated electric field strength. This elucidates the exceptional efficacy of the absorber at the designated frequency.

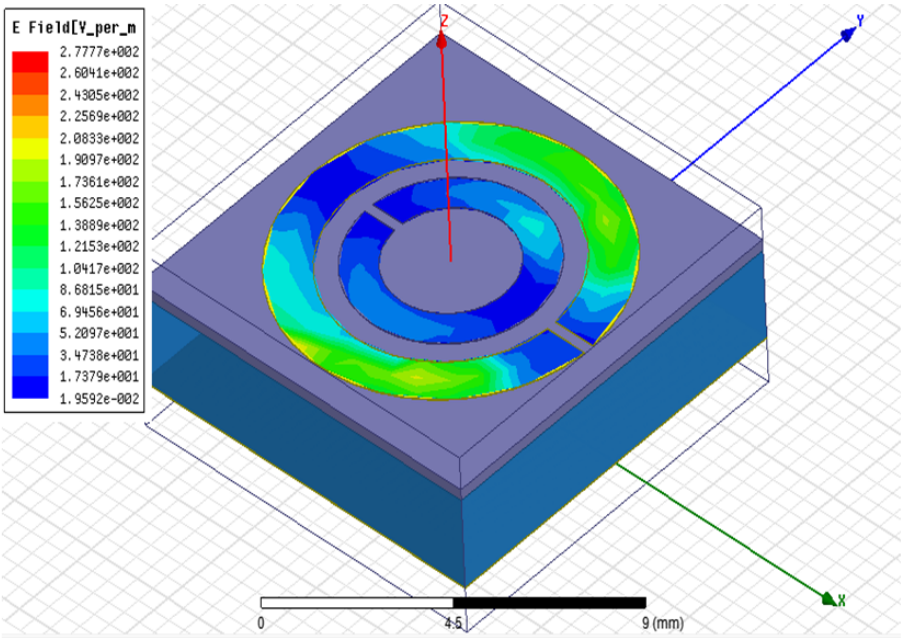

Figure 3.7: The absolute arrangement of electric fields in the MMA for TE polarization at 32 GHz.

Figure 3.8 depicts the surface current density of the design. The current is mostly focused in the inner arcs, notably in the right and bottom regions of the structure, as seen in the illustration. In addition, the currents flow in a certain direction within the absorber design and reach a maximum value of 16.37 A/m.

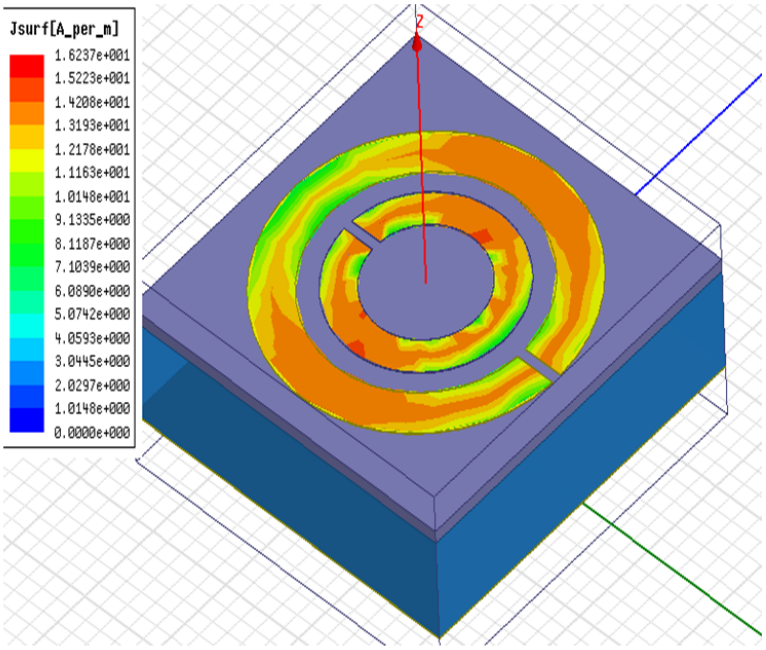

Figure 3.8: Analysis of the suggested design's surface current density at the Absortivity frequency.

The figure 3.9a illustrates how altering the diameter of the first ring affects the absorption properties of the absorber. It is evident that decreasing the diameter of the first ring leads to a significant reduction in the maximum absorption rate. Decreasing the diameter of the ring changes its resonance frequency. Reducing the diameter of the resonator alters its inductance and capacitance, resulting in a frequency shift in the resonance and a decrease in the efficiency of energy absorption.

The figure 3.9b illustrates that as the radius of the inner ring increases, there is a significant reduction in the absorption rate. This is attributed to changes in resonance characteristics, inefficient field distribution, and impedance mismatching. This emphasizes the susceptibility of the absorber's efficiency to the geometric characteristics of the resonant components According to the figure 3.9c , the ideal height for the absorber's substrate is 2 mm. At this elevation, the absorber functions with optimal efficiency, delivering the highest level of absorption. Deviation from the ideal height leads to reduced absorption efficiency, suggesting that the substrate height has a substantial influence on the performance of the absorber ; from here the best best valeu is R1=4mm and R2=2.39mm.

The diagram 3.9d illustrates that the gap C in each ring has an impact on the absorption efficiency. The absorption efficiency is maximized when the gap size is set at 0.3 mm. Any deviations from this value result in decreased absorption, suggesting that the size of the gaps inside each ring is crucial for attaining optimum performance.

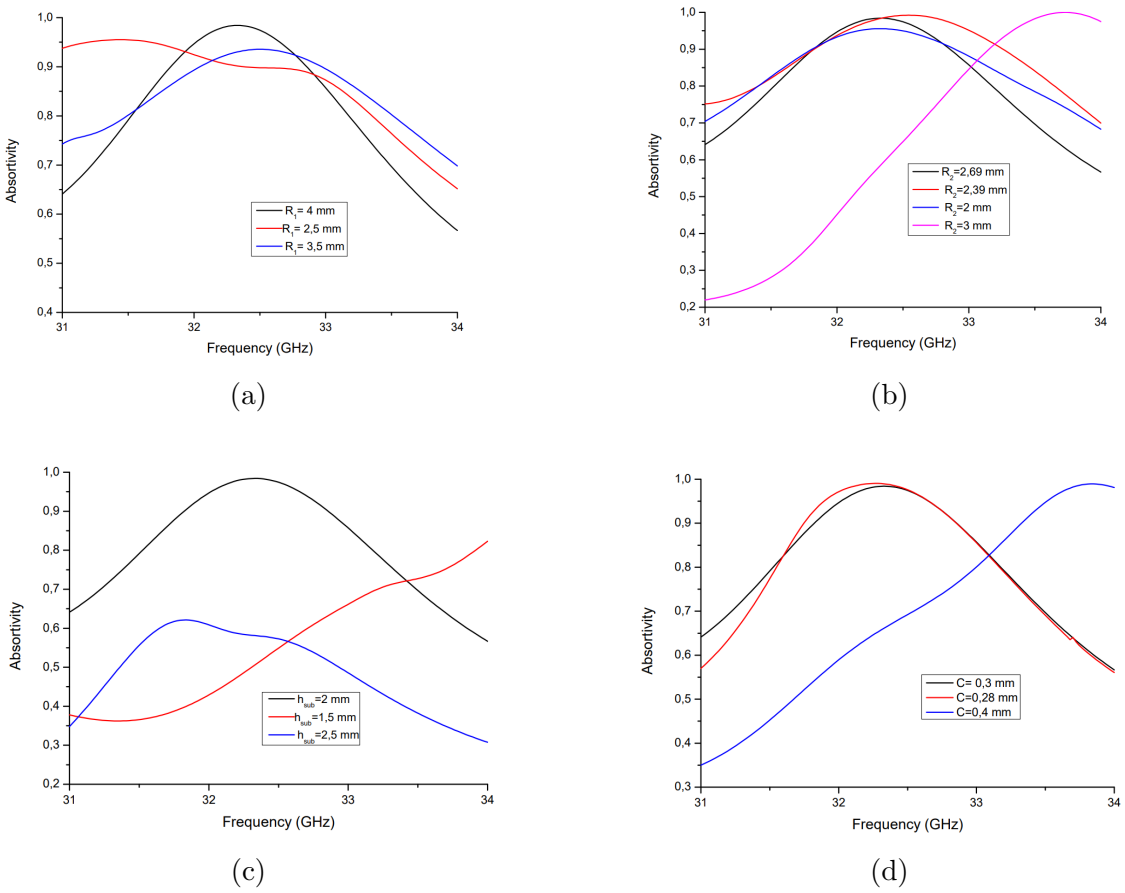

Figure 3.9: Simulated absorption rates: (a) for various outer diameter rings, (b) for different inner diameter rings, (c) for multiple substrate heights, and (d) for varied gap values.

3.5 Modified Resistor loaded wideband conformal metamaterial absorber

3.5.1 Unit cell design

In this part, we devlpe a compact structure of SachinKalraiya and all [84] to produce an ultrathin, inexpensive MMA that is polarization-insensitive and functional throughout a wide frequency range. The estimated bandwidth for effective absorption (more than 90%) ranges from 4 to 18 GHz. Achieving an improved ultrathin design, featuring compact broadband polarization insensitivity and wide-angle absorption, specifically optimized for transverse electric (TE) incident waves. This advanced structure demonstrates exceptional performance in maintaining consistent absorption across a broad range of incident angles and frequencies, while ensuring minimal sensitivity to the polarization of incoming waves, making it ideal for applications requiring compact and efficient energy absorption. The MMA structure confirms that its absorption is indifferent to polarization angles. Furthermore, when TE-polarized waves are encountered

at 50° angles of incidence, the suggested MA absorbs more than 85%. Different geometrical characteristics and their effect on the spectral absorption were studied.In Figure 3.10 we see the unit cell design of The absorber. The design consisting tree layer a metallic layer, a resistive layer , and a layer of flexible polyethylene terephthalate (PET) substrate ($\varepsilon_r = 3.5$ and $\tan\delta = 0.015$). A metallic cross-shaped resonator, which is equipped with lumped resistors, is used for the top layer.

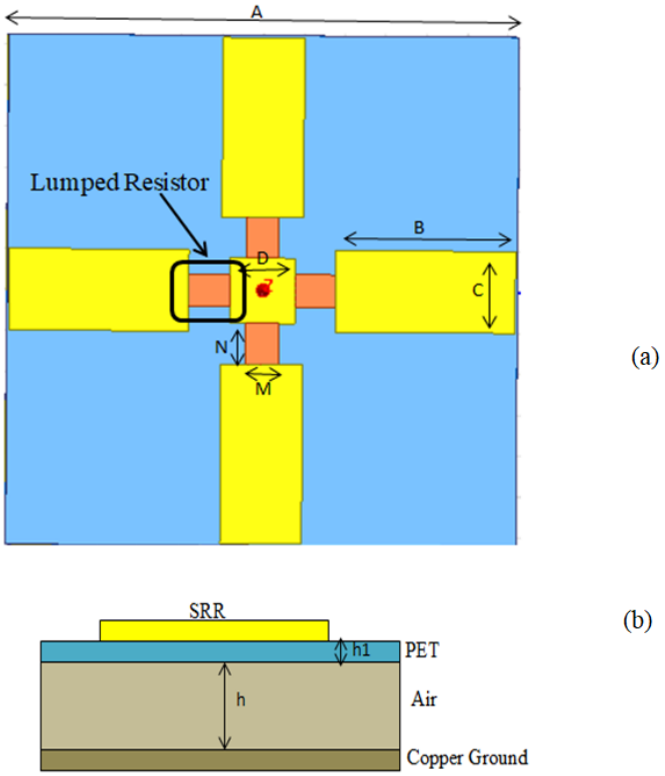

Figure 3.10: a)Schematics view of the absorber structure ; b) side view.

The suggested geometrical structure of the unit cell is constructed on a polyethylene terephthalate (PET) substrate with a thickness of 6 mm, which contributes to the absorber's overall compactness. The absorber's absorption is defined by A = 1-R-T, where the background is made up of metals, resulting in a zero transmissivity. The unit cell's characteristics are suitably tuned so that the incident wave is properly linked. The suggested absorbers are simulated using Ansoft HFSS with Master-slave boundary condition and The MMA optimal unit cell parameters are shown in Table 3.3.

3.5.2 Simulation Results

Figure 3.11 illustrates the theoretical absorptivity values of the absorber, which demonstrates over 90% absorption all over the frequency range of 4 GHz to 18 GHz when the incident angle is normal.

Table 3.3: Geometric parameters list of The proposed design.

Parameter	Value
A	12.5 mm
B	4.4 mm
C	2 mm
D	1.6 mm
R	90 Ohm
N	1 mm
M	0.8 mm
h	6 mm
h1	0.16 mm

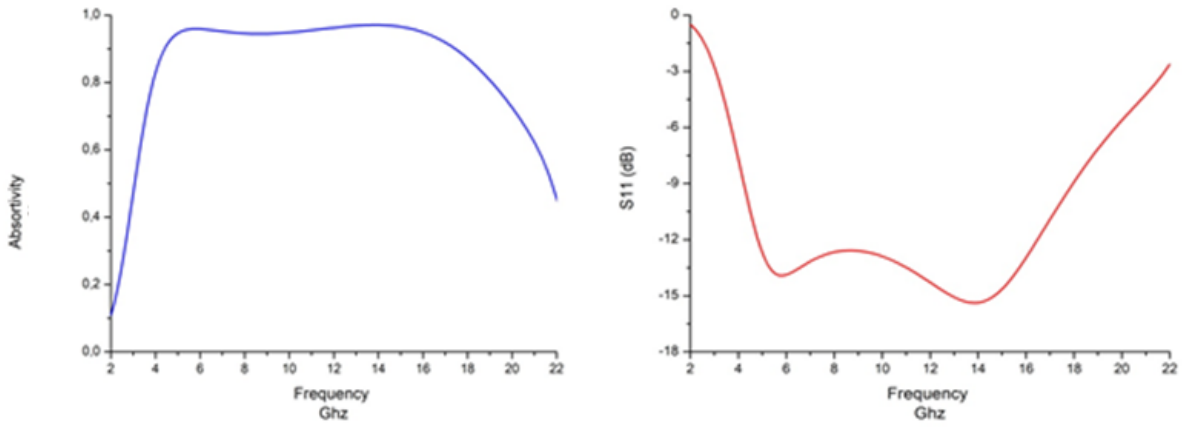

Figure 3.11: Simulated absorption and S11 of the flexible absorber.

a)Effect of oblique incidence wave:

Figure 3.12 depicts the absorber's absorptivity values as a function of incidence angle for TE polarization, where the incident angle covers from 0 degrees to 50 degrees by a factor of 10 degrees. At incidence angle 50 degrees, the absorption values are higher, with values more than 0.8 at two separate frequencies and frequency ranges.

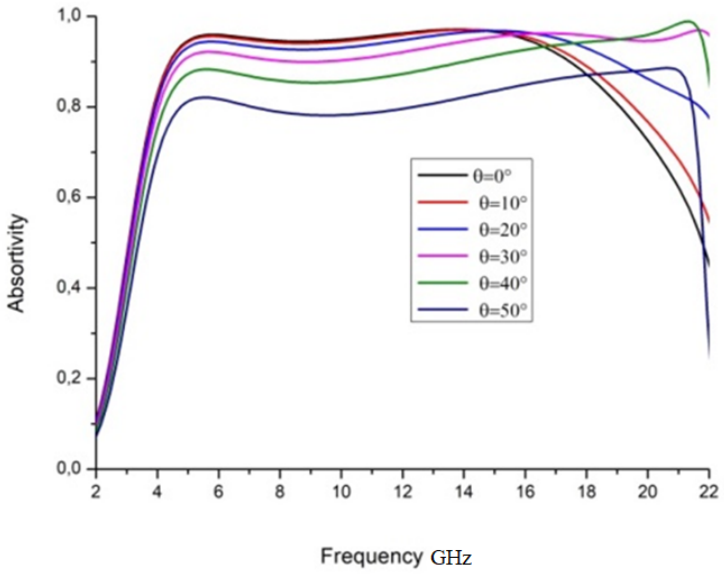

Figure 3.12: The estimated absorptivity when the incident angle is changed for TE polarization.

b)Effect of the polarization angle:

Absorption efficiency changes as a function of polarization angle for normal incidence are seen in Figure 3.13. Here, the microwave moves in a path parallel to the z axis, while the electric field and magnetic field maintain a constant angle with respect to the x and y axes. It is important to remark that the absorption curves coincide precisely for a variety of polarization orientations. This is due to the fact that the flexible absorber's surface resonant unit cell has a radially symmetrical pattern. So, the suggested structure has great absorption performance despite polarization. The preceding research shows that the planned absorber has a large polarization operating area.

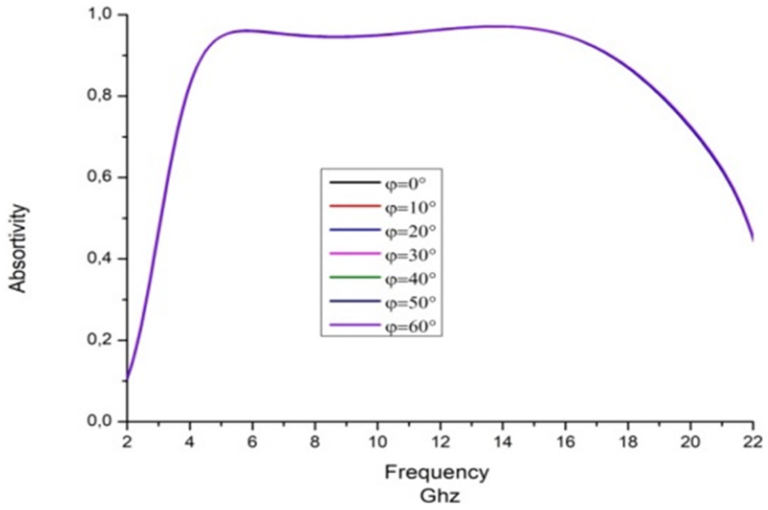

Figure 3.13: The estimated absorptivity when the polarization angles is changed.

d)surface current distribution:

Studying the surface current distribution of the suggested structure helps to further comprehend the radiation process of the device. Figure 3.14 shows that at 17 GHz, the current is located around the cross-shaped resonatorsbecause the greatest surface current is highest near in the middle of the SRR.

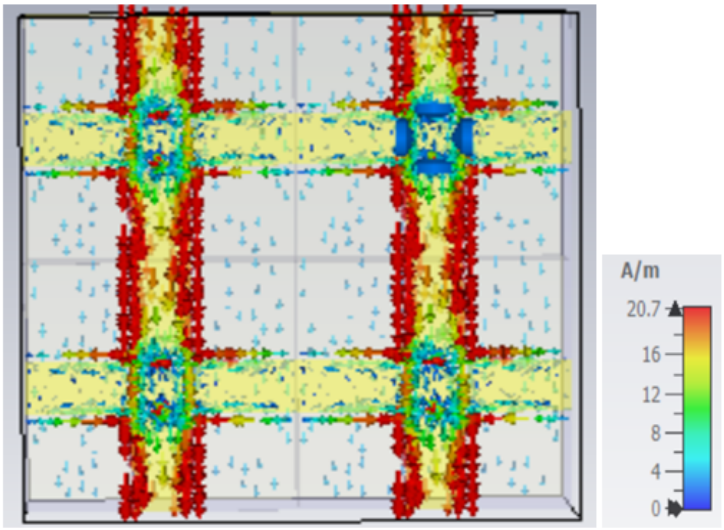

Figure 3.14: surface current distribution at 17 Ghz.

3.5.3 Comparison with others study

Table 3.4 Illustrates the differences between the suggested absorber configuration and other presented absorber designs. The technique discussed here is innovative in that it produces a wide absorption bandwidth with fewer resistors while having smaller electrical dimensions and thickness

Table 3.4: Comparison of Electrical Size, Electrical Thickness, and Fractional Bandwidth

Study	**Electrical Size**	**Electrical Thickness**	**Fractional Bandwidth**
[85]	$0.16\lambda_0$	$0.41\lambda_0$	91.6%
[83]	$0.14\lambda_0$	$0.098\lambda_0$	82.6%
Original structure [84]	$0.8\lambda_0$	$0.88\lambda_0$	123%
Our Modified structure	$0.14\lambda_0$	$0.6\lambda_0$	127%

3.6 Conclusion

This chapter thoroughly looked at multiple types of metamaterial absorbers, with particular focus on theoretical modeling and practical simulations to improve performance in diverse applications. We started by examining the fundamental design concepts and doing a parametric analysis. Through this process, we identified the key elements thathave an important effect on the absorption efficiency of MMAs. These factors include the incidence angle, substrate thickness, and material selection. The implementation of an extremely thin absorber designed for flexible applications in the Ka frequency range showcased the capability of metamaterial absorbers (MMAs) to achieve significant absorption rates while preserving a compact and adaptable shape.

As we move to the next chapter, we will shift focus towards developing new designs through wideband performance simulations and further optimization. Building on the theoretical insights gained in this chapter, the next chapter will delve deeper into the design and simulation of wideband flexible MMAs, highlighting how these concepts can be refined for enhanced performance and practical applications.

Chapitre 4 Design, simulation and experimental validation of wideband flexible of MMA

4.1 Introduction

This chapter explores into the comprehensive process of developing effective metamaterial absorbers devloped in this study, starting from the theoretical design and simulation to the optimization of absorber parameters and finally the fabrication of the optimized structures. The efficacy of metamaterial absorbers depends on their capacity to modulate electromagnetic waves via specific structures, often represented using equivalent circuit or transmission line models.

This chapter starts by presenting the proposed design in details then describe the equivalent transmission line model of the absorber, which provides an additional perspective of how the absorber's structure works with the incoming electromagnetic waves. By decomposing the complex shape of the absorber into manageable transmission line sections, we can systematically examine the impedance matching, resonance characteristics, and overall absorptivity.
Based on the theoretical model, we investigate the electromagnetic field distributions within the absorber. Our focus is on analyzing the electric field, magnetic field, and surface current distributions.Next, we analyze the normalized impedance of the absorber when it is subjected to normal incidence. This factor is essential for obtaining minimum reflection and maximum absorption; also examines the efficient permittivity and permeability of the absorber, which are important factors that define the absorber's reaction to electromagnetic fields and impact its capacity to absorb.

Finally, the chapter covers the fabrication process of the optimized MA, outlining the practical challenges and solutions encountered during the materialization of theoretical designs into physical prototypes. This comprehensive approach not only demonstrates the potential of metamaterial absorbers in practical applications but also provides insights into the integrated process of design, simulation, optimization, and fabrication.

4.2 Presentation of The Structure

4.2.1 Design description

The design we presented for the metamaterial absorber (Figure 4.1) included a wire-coil resonator structure. The wire coil resonator is an unfamiliar element used in the construction of metamaterials. We selected it based on its ability to produce strong magnetic resonances, which are essential for improving the material's absorption capacities. In our design, we made accurate modifications to the size of the SRR in order to improve its capacity to control electromagnetic waves within the specified frequency range of 16.5 GHz to 27.3 GHz. The suggested unit cell of the flexible wideband MMA consists of a single layer with 3 turns of split wire resonator on the top side, which is placed on a terephthalate (PET) substrate. Polyethylene terephthalate (PET) is used as the dielectric substrate due to its advantageous combination of flexibility and

affordability. The goal was to improve the resonance frequencies of the FSS in order to achieve maximum absorptivity within the specified frequency range [86].

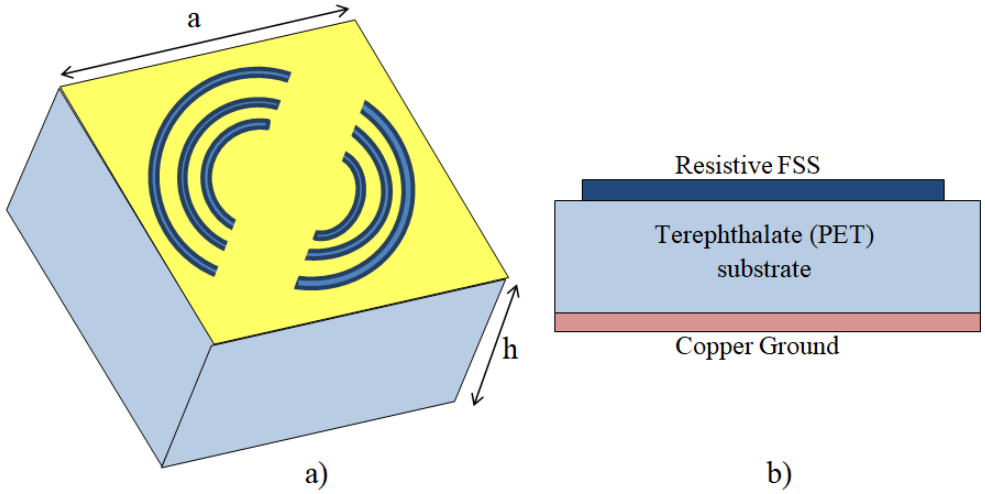

Figure 4.1: The Structure of the proposed MMA, as seen from two different perspectives. a) A view from the side. b) A look at the front.

The key parameters adjusted in the design included:

- The inner radius (R0) was tuned to a specified value of 0.3 mm. This optimization allows for tuning the higher resonant mode to the upper end of the frequency spectrum.
- The wire coil end angle was configured to 180 degrees, determining the angle at which the wire coil terminates and impacting the inductive characteristics of the coil.
- Wire coil start angle: The wire coil's beginning angle was optimized to 90 degrees, which directly affected the initial inductance and the total resonance.
- The parameter "Wire coil angle" is set to a particular value in degrees, and it directly influences the magnetic resonance by determining the angular extent of the wire coil.
- Wire coil turns (N): The wire coil was configured with a precise number of turns, namely 3, which plays a critical role in calculating the inductive coupling and, therefore, the resonant frequency.
- The trace width (Ws) of the wire coil was configured at 0.1 mm, which directly impacted the resistance and inductance of the coil.
- The wire coil trace (t) was set to a specified value of 0.035 mm. This number represents the height of the trace and has a significant impact on the overall electromagnetic characteristics of the coil.

- Wire coil progress (g): This parameter, when set to a given value, governs the movement of the wire coil along the structure, hence modifying the system's inductance and capacitance.

4.2.2 Simulation Setup

The unit cell architecture of the proposed design was simulated systematically using CST MICROWAVE STUDIO™ 2021. To simulate the electromagnetic wave propagation along the z-axis, open space boundary conditions were applied in the z direction. Meanwhile, periodic boundary conditions were set along the x and y directions to represent the unit cell structure. Table 4.1 contains the requested simulation settings.

Table 4.1: Specifications and parameters used in the simulation.

Name	**Value**
Frequency Range	15-30 GHz
Substrate Material	Terephthalate (PET) substrate ($\varepsilon_r = 3.5$ and $\tan\delta = 0.015$)
Substrate Thickness	1.6 mm
Conductivity of SRR	Copper; 0.035 mm
Boundary Conditions	The open-space
The wire_coil_end_angle	180 degrees
The wire_coil_start_angle	90 degrees
Wire_coil_angle (E)	45 degrees
Wire_coil_turns	3
Wire_coil_progress	0.4 mm
Inner Radius of Spiral	0.3 mm
Trace Width	0.1 mm
Wire_coil_trace_height	0.035 mm
a	12.5 mm

4.2.3 Simulation Processs

Implementing the wire-coil structure on a dielectric substrate was a crucial step in the modeling process. The substrate material was selected based on its appropriate dielectric characteristics, including permittivity and loss tangent, to facilitate the necessary frequency functioning. The absorber's performance is evaluated based on its ability to achieve an absorption efficiency greater than 90%. As illustrated in Figure 4.3, the absorption bandwidth extends from 16.5 GHz to 27.3 GHz, resulting in an absolute bandwidth of 10.8 GHz. The fractional bandwidth (WFRA) [55] is calculated using the formula WFRA = 2(fU - fL) / (fU + fL), where fU and fL represent the upper and lower frequency limits for absorption above 90%. The calculated WFRA is around 50%, indicating ultra-wideband absorption.With a thickness of 1.67 mm, which is approximately 0.09 times the wavelength of the lowest absorption frequency (16.5

GHz), the proposed design fulfills the criteria for subwavelength structures, making it a promising candidate for a wideband metamaterial absorber.

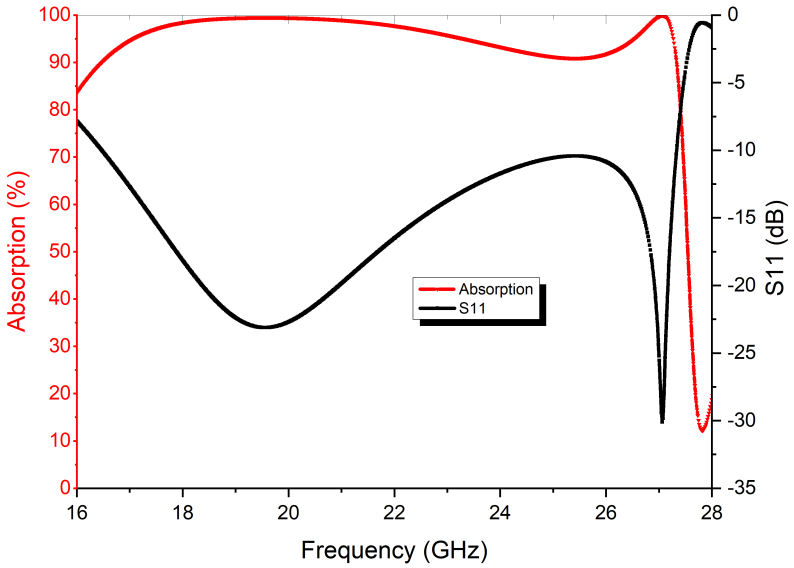

Figure 4.2: the simulated Absortivity and reflection coefficient S11 of the PMA

4.3 Analysis and discussion

4.3.1 Equivalent Transmission Line Model

To assess the structural performance of the proposed absorber, simulations were carried out using Keysight's PathWave Advanced Design System (ADS) software. As depicted in Figure 4.3, the unit cell consists of a three-turn open-loop split-ring resonator (SRR). Each SRR is modeled as a series combination of RLC components, connected in parallel. The dielectric substrate is represented as a transmission line with a characteristic impedance of 300 ohms. The inductor in the final stage of the model accounts for the spacing between the coils, offering a comprehensive representation of the absorber's structure and behavior. The inductances L1, L2, and L3 were calculated from the outer ring, outer ring additional components, and inner rings, respectively, using Equation (4.2) [87].

$$L_i(\text{nH}) = 1.257 \times 10^{-3} \times r_{i\text{mean}} \left[\ln \left(\frac{r_{i\text{mean}}}{w_i + t_{\text{cu}}} \right) + 0.078 \right], \quad K_{gi} = 1, 2 \tag{4.1}$$

The variables $r_{i\text{mean}}, w_i,$ and t_{cu} represent the dimensions of the i-th SPAR ring in micrometers. Specifically,they correspond to the mean radius, width, and copper thickness of the ring, respectively. Kg is the adjustment factor that takes into consideration the existence of the ground plane. The capacitances C1, C2, and C3 represent the values for the lowest, middle, and highest frequencies, respectively, as calculated using Equation (4.2), where f indicates the resonance frequency [88].

$$C = \frac{1}{4\pi^2 f^2 L_{ms}} \tag{4.2}$$

To calculate the input impedance required for fabricating the unit cell, both the ohmic loss (Ro) of the area occupied by the SRRs and the dielectric loss (Rd) of the substrate must be considered. These factors are critical in accurately determining the unit cell's impedance and ensuring optimal performance in practical applications.

$$R_0 = \frac{\text{Cell area}}{\text{metallic area of SRR}} \left(\frac{1}{\sigma\delta}\right) \quad (4) \tag{4.3}$$

In the case of a metallic split-ring resonator (SRR),The conductivity (σ), skin depth (δ), and surface resistance $\left(\frac{1}{\sigma\delta}\right)$ are important parameters in the study of electromagnetic materials and metamaterials.. Surface resistance refers to the resistance of the non-metallic region within the resonator. The total resistance is inherently tied to the surface resistance at each resonance frequency, as it directly influences the absorption behavior of the unit cell. This relationship can be described as: ;

$$R = R_0 \left(\frac{P}{S}\right)^2 \tag{4.4}$$

In this context, S represents the total length of the resonator, while P denotes the period of the unit cell. The dielectric loss (Rd)can be efficiently calculated using simulation data based on the unloaded capacitance of the SRR. Rd is treated as a variable resistor in the simulation, allowing for adjustments to achieve the desired S values, thus simplifying the overall calculation process [89]. During the simulation, a 50-ohm impedance is connected to the output of the circuit design to provide impedance matching. In the S-parameter simulation setup, certain start and stop frequencies are selected. The frequencies range from 16 GHz to 30 GHz, with an increment of 2 GHz.

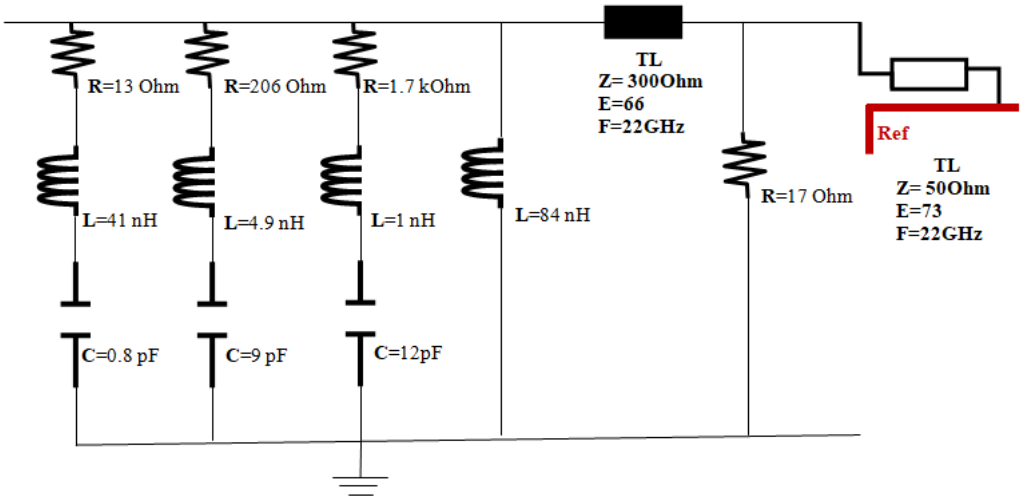

Figure 4.3: The equivalent circuit model for the geometry of the PMMA

To determine the equivalent resistance in an RLC circuit, the absorptivity was adjusted to observe how changes in its magnitude whether an increase or decrease

affect the overall behavior. The estimated parameters were fine-tuned to approximate the S11 curve obtained from CST simulations. Figure 4.4 shows a comparison between the absorption rate calculated through full-wave modeling and the Equivalent Circuit Model. The close similarity between the two absorption curves confirms the accuracy of the equivalent circuit approach.

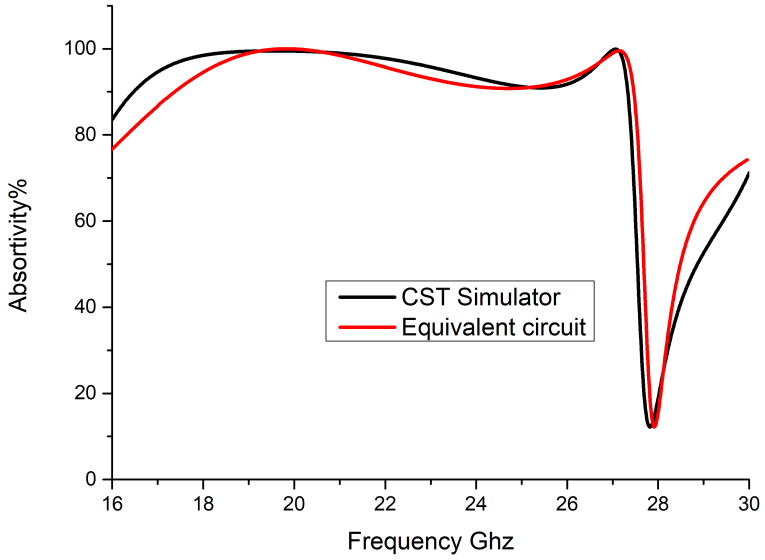

Figure 4.4: Evaluation of absorption characteristics through numerical simulations using CST and ADS.

4.3.2 Electric Field,Magnetic Field and Surface Current Distribution.

a)Electric Field and Magnetic Field Distribution

To gain a thorough understanding of the device's wide absorption range, we analyzed the electric and magnetic field distributions at three specific frequencies: 19.4 GHz, 21.7 GHz, and 27 GHz. The modeling results indicate that 19.4 GHz and 27 GHz represent key points within the absorption spectrum, corresponding to the highest absorption levels. The 21.7 GHz frequency falls between these two peaks.

In Figure 4.5, at the first peak frequency of 19.4 GHz, the distributions of the electric field (E-field) and magnetic field (H-field) are primarily concentrated at the outer edges of the structure. This suggests a strong resonance effect, with the interaction between the electric and magnetic fields at the edges of the unit cell being critical for energy absorption.

For the second peak at 27 GHz, as illustrated in Figure 4.5, both the electric and magnetic fields are focused in a specific region within the unit cell. This indicates a

more intense interaction among the internal components of the structure, enhancing absorption at this higher frequency. The notable interaction in the central part of the fundamental element at 27 GHz underscores the significant role of surface Resonator configuration in achieving broad-spectrum absorption.

In contrast, at the intermediate frequency of 21.4 GHz, shown in Figure 4.5(c), the electric and magnetic fields are less concentrated than at the peak frequencies. The field distribution across the structure is more even, resulting in lower absorption compared to the peaks at 19.4 GHz and 27 GHz. This highlights the importance of field concentration in influencing the efficiency of the absorption process at different frequencies within the spectrum.

b)Surface Current Distribution

An analysis of the surface current distributions at the same frequencies has been completed to clarify the absorption behavior of the metamaterial absorber being suggested. This analysis is shown in Figure 4.6. At a frequency of 19.4 GHz, the current distribution is mostly focused on the surface of the spiral wire-coil components. These elements play a crucial role in creating the lower absorption band. The robust surface currents in this area demonstrate the substantial contribution of these constituents to the energy absorption process.

At a frequency of 27 GHz, a similar pattern is seen, where the surface currents are mostly concentrated around the SRR structures, but with a higher level of strength in comparison to 19.4 GHz. This indicates that there is an increased resonance effect at higher frequencies, which causes a wider range of frequencies being absorbed. Furthermore, at both frequencies of 19.4 GHz and 27 GHz, the surface currents in the top resistive layer and the metal ground plane converge in opposing directions, resulting in the formation of magnetic resonance. The counterflow of currents plays a crucial role in the absorber's capacity to efficiently capture and disperse electromagnetic energy.

In contrast, at the intermediate frequency of 21.7 GHz, the surface current is less intense and more evenly distributed across the structure. This reduced concentration of current correlates with the lower absorption observed at this frequency, as less energy is gathered and dissipated compared to the peak frequencies. Notably, the current intensity in the lower layer is consistently lower than in the upper resistive layer at all three frequencies. This indicates that a significant portion of the energy is absorbed by the upper resistive layer before reaching the lower layer, which contributes to the absorber's capacity to handle a wide range of frequencies.

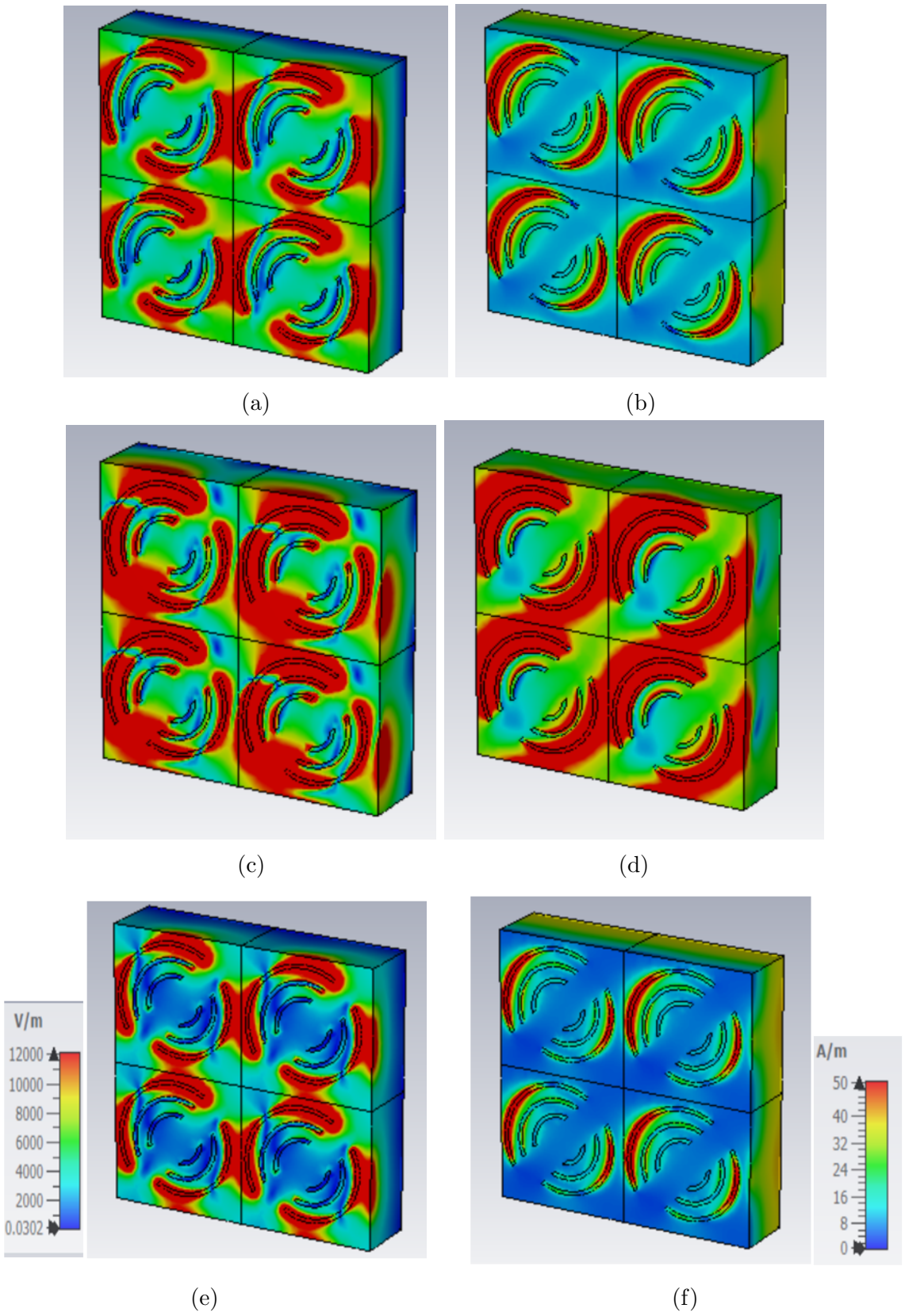

Figure 4.5: (a,c and e)Electric field at 19.4 , 27 and 21.7 GHz respectively.(b,d and f) magnetic field distribution at 19.4 ,27 and 21.7 GHz respectively.

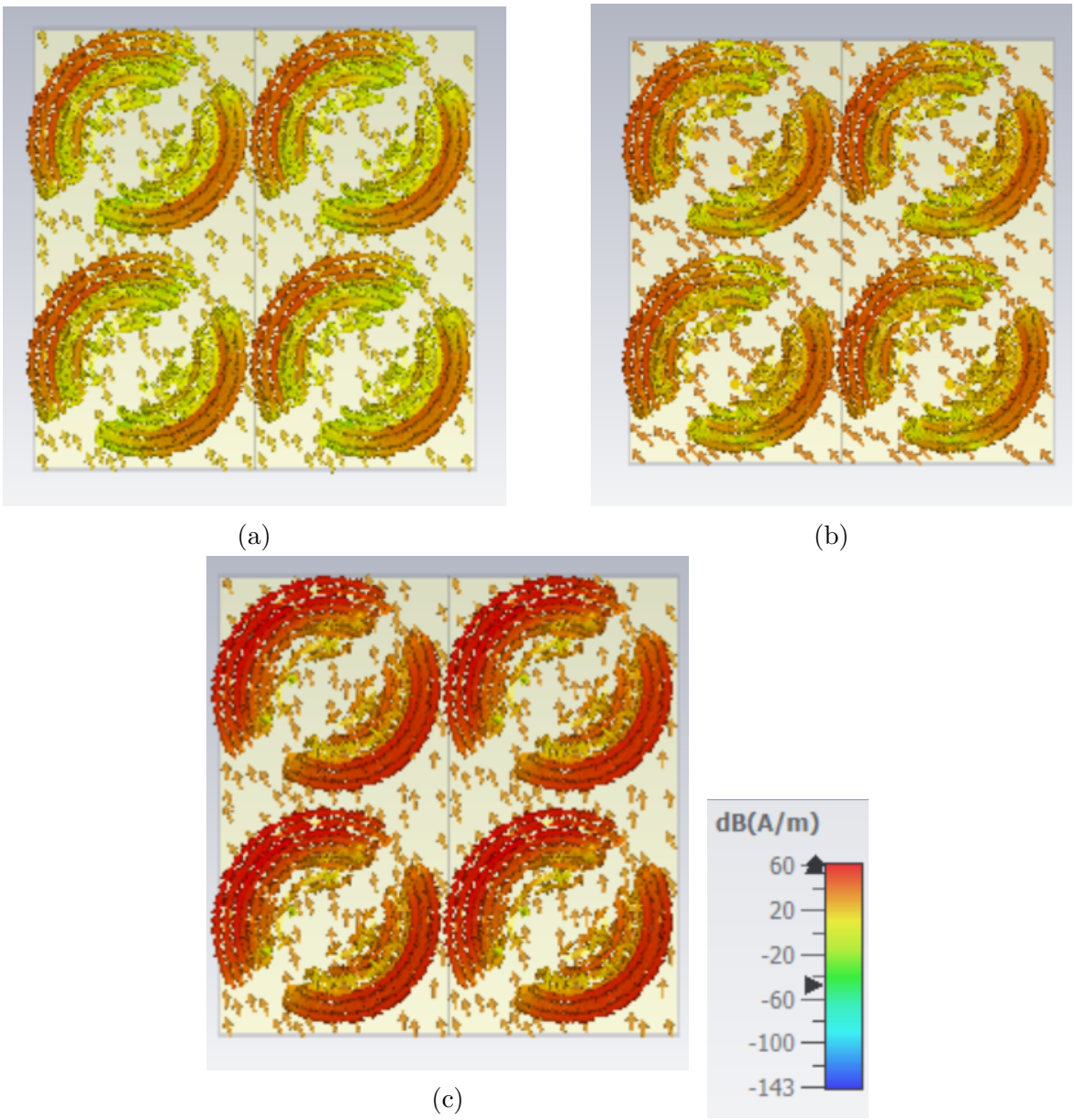

Figure 4.6: Surface current distribution at (a) 19.4 and (b) 27 GHz and (c) 21.7 GHz.

4.3.3 Normalized Impedance at Normal Incidence

Equation 4.5 illustrates the scattering characteristics used to calculate the normalized input impedance (Zin) of the proposed absorber, as depicted in Figure 4.7. The input impedance of the absorber is nearly equivalent to the impedance of free space (377 + j0), indicating minimal power reflection from the structure. As a result, maximum absorption occurs within the targeted frequency range, where the real part of the normalized input impedance is approximately equal to one (around 1) and the imaginary part is close to zero.

$$Z(f) = \sqrt{\frac{(1 + S_{11}(f))^2 - S_{21}^2(f)}{(1 - S_{11}(f))^2 - S_{21}^2(f)}} \tag{4.5}$$

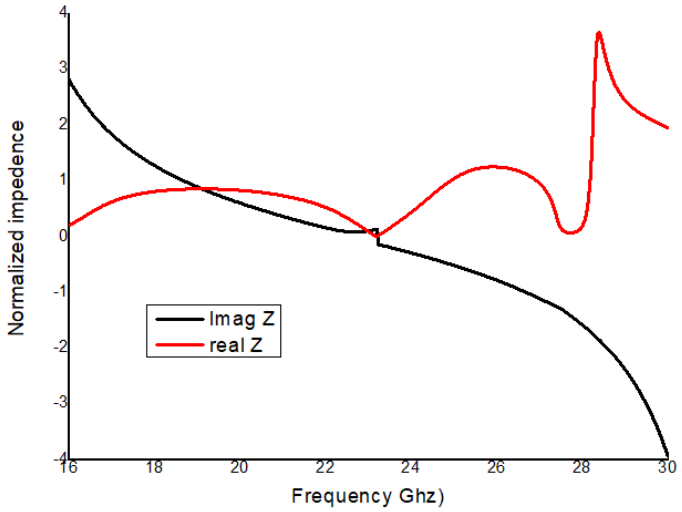

Figure 4.7: The normalized impedance of the proposed absorber at normal incidence.

4.3.4 Effective Permittivity and Permeability

To provide more knowledge of the absorption character, the effective permeability (μ_{eff}) and permittivity (ϵ_{eff}) of the suggested structure are shown in Figure 4.8 (a) and (b). These were generated using the following equations [89].

$$\epsilon_{\text{eff}}(f) = \frac{c}{i\pi f d}\left(\frac{1 - S_{21} - S_{11}}{1 + S_{21} + S_{11}}\right) \tag{4.6}$$

$$\mu_{\text{eff}}(f) = \frac{c}{i\pi f d}\left(\frac{1 - S_{21} + S_{11}}{1 + S_{21} - S_{11}}\right) \tag{4.7}$$

At the absorption frequencies, the real components of both permittivity and permeability approach zero ($\epsilon_{\text{eff}} < -0.004$; $\mu_{\text{eff}} < 0.02$), signifying negligible reflection. In other words, when the real parts of the permittivity and permeability exhibit nearly opposite signs within the absorption band, it results in no transmission.

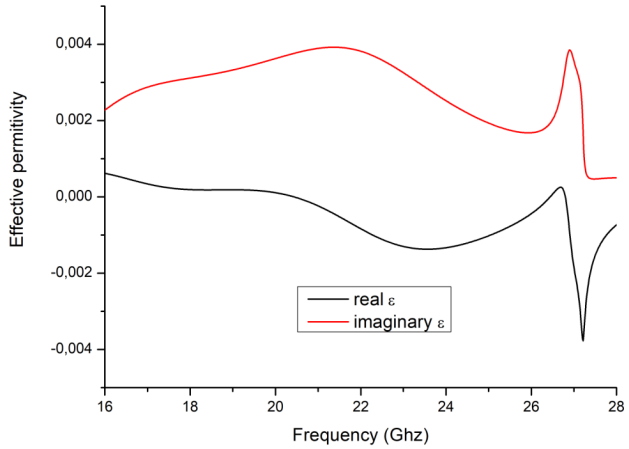

(a)

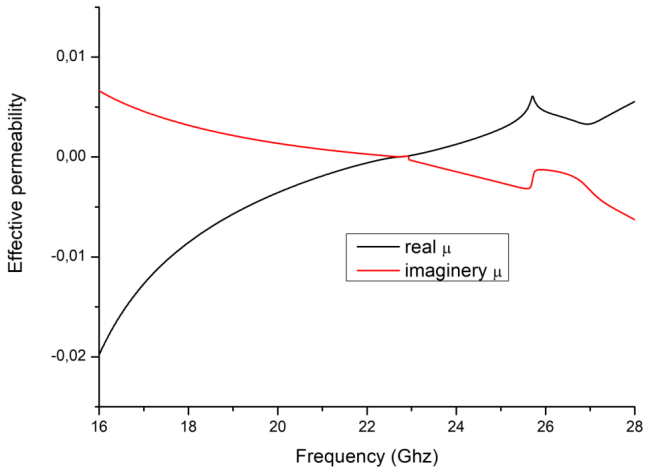

(b)

Figure 4.8: a)Effective permitivity and b) Effective permittivity of the designed absorber

4.3.5 Polarization and incident angle stability

Figure 4.10 demonstrates the absorptivity of the prototype at various polarization angles. This was carried out to confirm that the suggested wideband absorber is not influenced by changes in polarization. During these experiments, the electric field and magnetic field are positioned at right angles to the x and y axes, while the microwave propagation takes place along the z axis. It is significant that the absorption curves maintain consistency regardless of the polarization angles, indicating that they exhibit the same behavior regardless of the direction of polarization. The unit cell's surface resonance pattern exhibits rotational symmetry around its central axis, which explains its constant performance. Consequently, the suggested absorber design has excellent absorption properties that are not affected by polarization, ensuring stable performance across different polarization states.

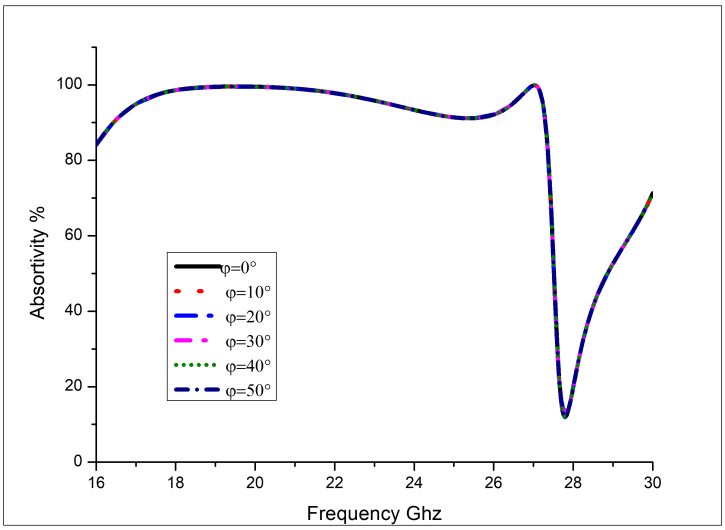

Figure 4.9: The polarisation angle's effect on absorption performance under normal incidence.

The previous study demonstrates that the proposed absorber performs effectively over a wide range of polarization and incident angles, accommodating both TE and TM modes.

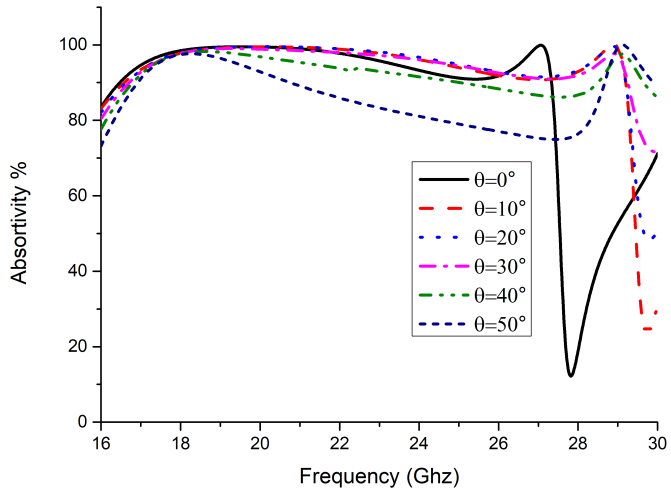

(a)

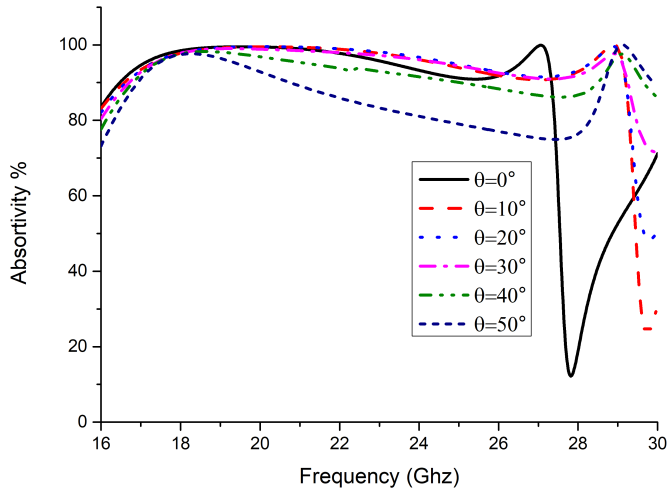

(b)

Figure 4.10: The Proposed MMA absorption spectra for a)TE and b)TM polarizations at different incident angles.

Figure 4.10 illustrates the absorption responses of TM and TE polarizations for oblique incidence angles from 0° to 50°, with a fixed angle of 0° for phi. Figure 4.10a illustrates the change in angle when light is incident at an oblique angle. We use rotational displacement to alter the magnetic field and wave propagation vector, while simultaneously maintaining a consistent direction for the electric field.

4.3.6 The substrate thikness

The Figure 4.11 depicts the absorptivity of the metamaterial absorber in relation to the thickness of the substrate (h), which varies from 0.8 mm to 1.6 mm. The data unambiguously demonstrates a significant increasing in absorptivity with increasing substrate thickness. The increase in substrate thickness results in a decrease in the absorber's capacity to adjust to the incoming electromagnetic waves, which therefore reduces the total absorption efficiency.

In addition, this figure demonstrates that the absorber's conformality decreases as the substrate thickness increases. The deterioration is probably caused by the greater separation between the resonant components and the ground plane, which changes the distribution of the electromagnetic field and reduces the interaction between the incoming waves and the absorber's resonant structure.

In order to enhance the absorption efficiency and ensure a wide range of absorption frequencies, a thin and flexible substrate measuring 1.6 mm in thickness was used. The use of a thinner substrate not only increases the absorption bandwidth, but also maintains the flexibility of the absorber, allowing it to adapt to different surfaces. This flexibility is important for practical applications that need the absorber to be mounted on curved or irregular surfaces.

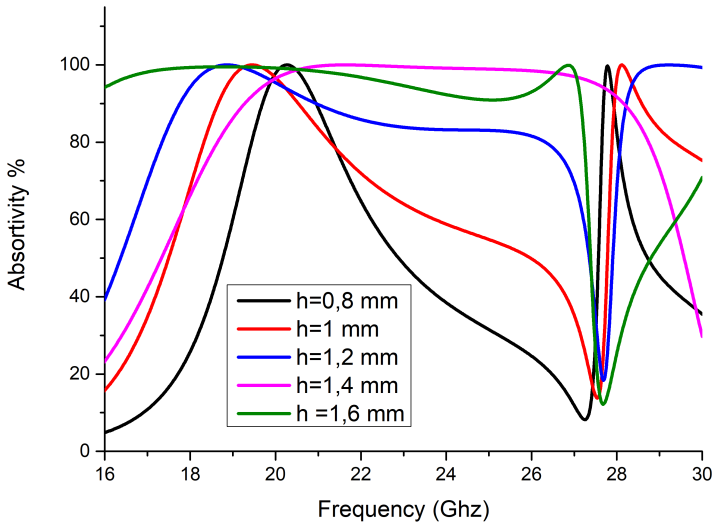

Figure 4.11: The absorption spectra for differences thickness of the substrate.

4.4 Comparison with Literature

Table 4.2: Comparison analysis with state-of-the-art metamaterial absorbers

MA	Total Thickness (mm)	Bandwidth Absorptivity spans (GHz)	Flexible	Design property
[90]	3.8	4.8 to 11.1 GHz (6.3)	NO	Circuit equivalent based on IoT
[91]	8	8.2 to 16 GHz (7.8)	NO	Polyimide film, PET and Ground separated by PMI layers
[85]	7.5	3.9 to 10.5 GHz (6.6)	YES	Circle and a slotted sector, loaded with lumped resistors
[92]	2.7	6.68 to 18 GHz (11.32)	YES	Copper, rubber substrate, PET, resistive film
[83]	3.302	7.6 to 18.3 GHz (10.35)	YES	Silicone rubber, Polyimide, resistive FSS with four lumped elements
[84]	8.23	3.25 to 16.3 GHz (10.35)	YES	Foam, PET, cross-shaped resonator loaded with lumped resistors
Proposed design	1.67	16.5 to 27.3 GHz (10.8)	YES	PET, spiral coil SRR

A comparative analysis has been carried out between the suggested metamaterial absorber, which depends on a wire coil construction, and other flexible metamaterial absorbers (MMAs) that use various resonator forms. The comparison is clearly shown in Table 4.2, which emphasizes the distinctive characteristics and benefits of the suggested design. The table illustrates many essential characteristics that differentiate the suggested absorber as an innovative addition to the field.

Initially, the frequency selection of the suggested absorber is fine-tuned to specifically target essential bands that are significant for diverse practical purposes. The exact frequency targeting of this design improves its relevance and efficacy in comparison to other designs. Moreover, the suggested absorber has a compact design, which makes it ideal for situations where limited space is of utmost importance. Furthermore, the suggested design provides a greater bandwidth, allowing it to effectively capture a broader spectrum of frequencies. The wideband performance is especially beneficial in situations that need absorption of many frequencies. The design's simplicity is a notable quality that not only simplifies manufacturing but also decreases production costs, making the absorber more accessible for wider application. In addition, the suggested absorber has exceptional polarization stability, ensuring constant performance independent of the polarization angle of the incoming wave. Ensuring stable functioning is essential in real-world circumstances where polarization angles may fluctuate. Ultimately, the absorber's pliability enhances its adaptability, enabling seamless incorporation into curved or uneven surfaces while maintaining optimal functionality. The suggested wire coil-based metamaterial absorber represents a substantial improvement over existing flexible MMAs, since it combines a set of highly desired qualities that are suitable for many applications.

4.5 Optimization of the MMA Parameters

The flexible broadband MMA, illustrated in Figures 4.12, comprises two main layers: a resistive frequency selective surface (FSS)layer and a polyethylene terephthalate (PET) substrate. The top layer features a spiral coil design. Notably, a copper layer in the background acts as a reflective surface, effectively bouncing back the incoming wave. The PET substrate has a thickness of 1.6 mm, a permittivity of 3.5, and a loss tangent of 0.015. The copper layers on both the top and bottom are 0.035 mm thick. the absorber is optimized for the widest possible absorption band.The wire coil width (Ws) is precisely set to 0.2 mm. Additional geometric parameters include a unit cell size (a) of 3.5 mm, an inner spiral radius (R0) of 0.3 mm, a wire coil connection space (Wc) of 0.8 mm, and a wire coil progression (g) of 0.4 [93].

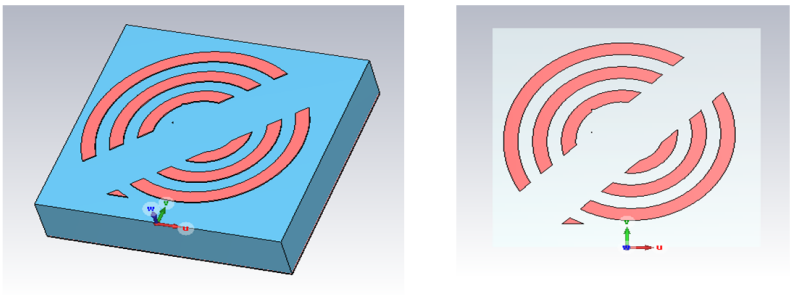

Figure 4.12: The optemized strecture

Unit-cell boundary conditions were applied to the x and y axes, with the electromagnetic wave (EMW) propagating along the negative z-axis. The metamaterial (MM) exhibited reflection $R(\omega)$ and transmission $T(\omega)$, expressed as follows:

$$R(\omega) = |S_{11}(\omega)|^2 \tag{4.8}$$

$$T(\omega) = |S_{21}(\omega)|^2 \tag{4.9}$$

The transmission parameter S_{21} can be described as a function of the material thickness d:

$$S_{21} = \frac{1}{\cos(nkd) - \frac{i}{2}\left(\frac{Z+1}{Z}\right)\sin(nkd)} \tag{4.10}$$

In this equation, n represents the complex refractive index, expressed as:

$$n = n' + in'' \tag{4.11}$$

and Z denotes the complex impedance, expressed as:

$$Z = Z' + iZ'' \tag{4.12}$$

When the absorber's impedance equals the impedance of free space, $Z(\omega)$ becomes 1. In this condition, where Z_0 is the characteristic impedance of free space, the equations governing the reflection and transmission of the wave within the material are given as:

$$R(\omega)_{(Z(\omega)\to 1)} = |S_{11}|^2 = \left(\frac{Z(\omega)-1}{Z(\omega)+1}\right)^2 = 0 \tag{4.13}$$

$$T(\omega)_{(n_2\to\infty)} = |S_{21}|^2 = |e^{in'kd} - e^{-in''kd}|^2 = \lim_{n_2\to\infty} e^{-2n''kd} = 0 \tag{4.14}$$

When n'' approaches infinity, it indicates that the absorbing structure possesses a high level of EM wave attenuation. The absorption rate A is given by:

$$A(\omega) = 1 - R(\omega) - T(\omega) = 1 \tag{4.15}$$

Broadband absorbers are frequently evaluated based on their bandwidth, which is determined by measuring the absorption rate and aiming for values greater than 90%. The optimized absorber in this case demonstrates a wide range of effective absorption, spanning from 17.9 to 27.9 GHz, as shown in Figure 4.13. The bandwidth has a fixed value of 10 GHz, meeting the criteria for wideband absorption. The absorber has a thickness of just 1.6 mm, which is approximately 0.095 times the wavelength at its operating frequency of 17.9 GHz. This thickness meets the criteria for a subwavelength structure. Therefore, the proposed design is a thin broadband metamaterial absorber.

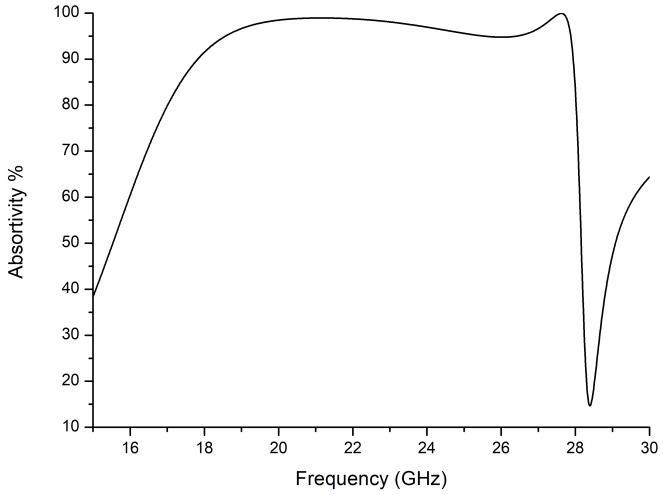

Figure 4.13: The new Absorption simulated at standard incidence conditions.

Figure 4.14 illustrates the core unit of the absorber structure, which consists of a three-turn coil open-loop resonator (SRR). This SRR is modeled using a series combination of resistance (R), inductance (L), and capacitance (C) elements, connected in parallel. The dielectric substrate in the proposed absorber is modeled as a transmission line with a characteristic impedance of 417 ohms. Furthermore, the inclusion of the final inductor in the model accounts for the distance between the coils, offering a detailed view of the absorber's structure and its interaction with EM waves.

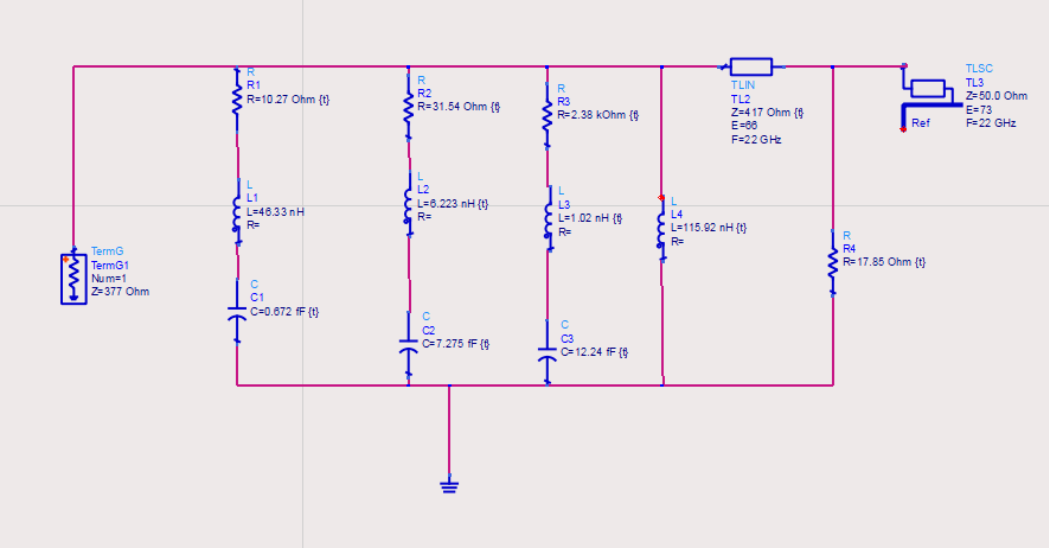

Figure 4.14: Topological representation of the equivalent circuit for the geometry of the Proposed MMA

The accuracy of the modeling approach is validated by comparing the absorption rates obtained through full-wave modeling and the equivalent circuit model. Figure 4.15 presents this comparison, showing the absorption rate curves derived from both methods. The close alignment of the two curves demonstrates the validity of the equivalent circuit concept, confirming that the simplified RLC representation accurately captures the absorber's behavior.

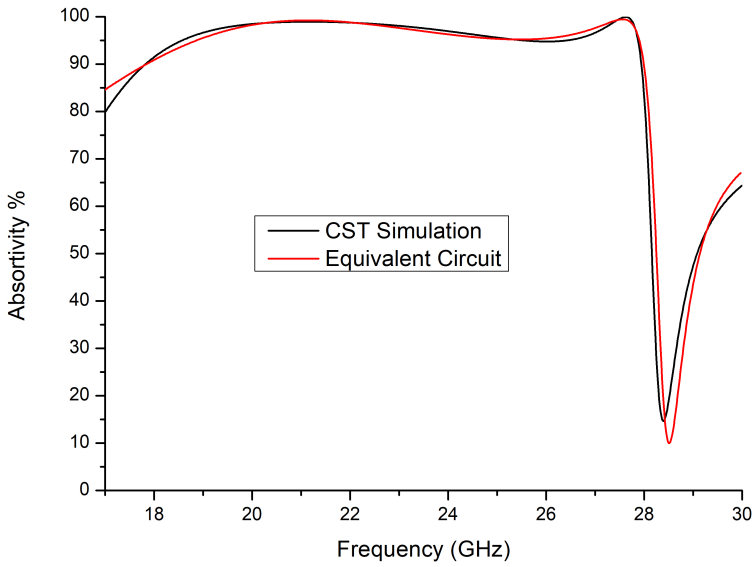

Figure 4.15: Comparative analysis of absorption rates using numerical simulations in CST and ADS.

4.6 Fabrication Process Overview

4.6.1 Experimental Setup and Measurement Outcomes

To verify the efficacy of the Proposed MMA, a prototype was fabricated using the photolithography process, incorporating optimal geometric properties. Initially, the PCB method was employed to create a sample consisting of 40 × 40 individual cells. The prototype was constructed using a PET substrate on both sides, with dimensions of 500 × 500 × 1.6 mm. Figure 4.16 shows the constructed prototype, while Figure 4.17 depicts the measuring equipment.

The S-parameters for the PMMA were acquired using a horn antenna and a vector network analyzer (AgilentFieldFox® model N9918A). Initially, S-parameters for an ideal reflector were established as a reference.Subsequently, the S-parameters for the PMMA were measured, and subtraction was employed to mitigate the influence of factors such as edge reflection, diffraction loss, and scattering loss between the two sets of measured data.

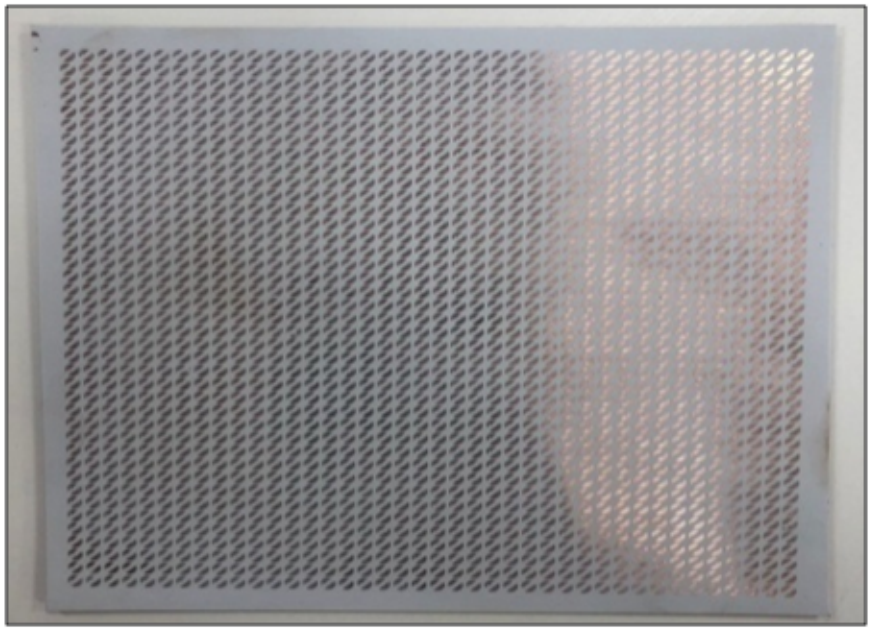

Figure 4.16: Photographic representation of the constructed PMMA.

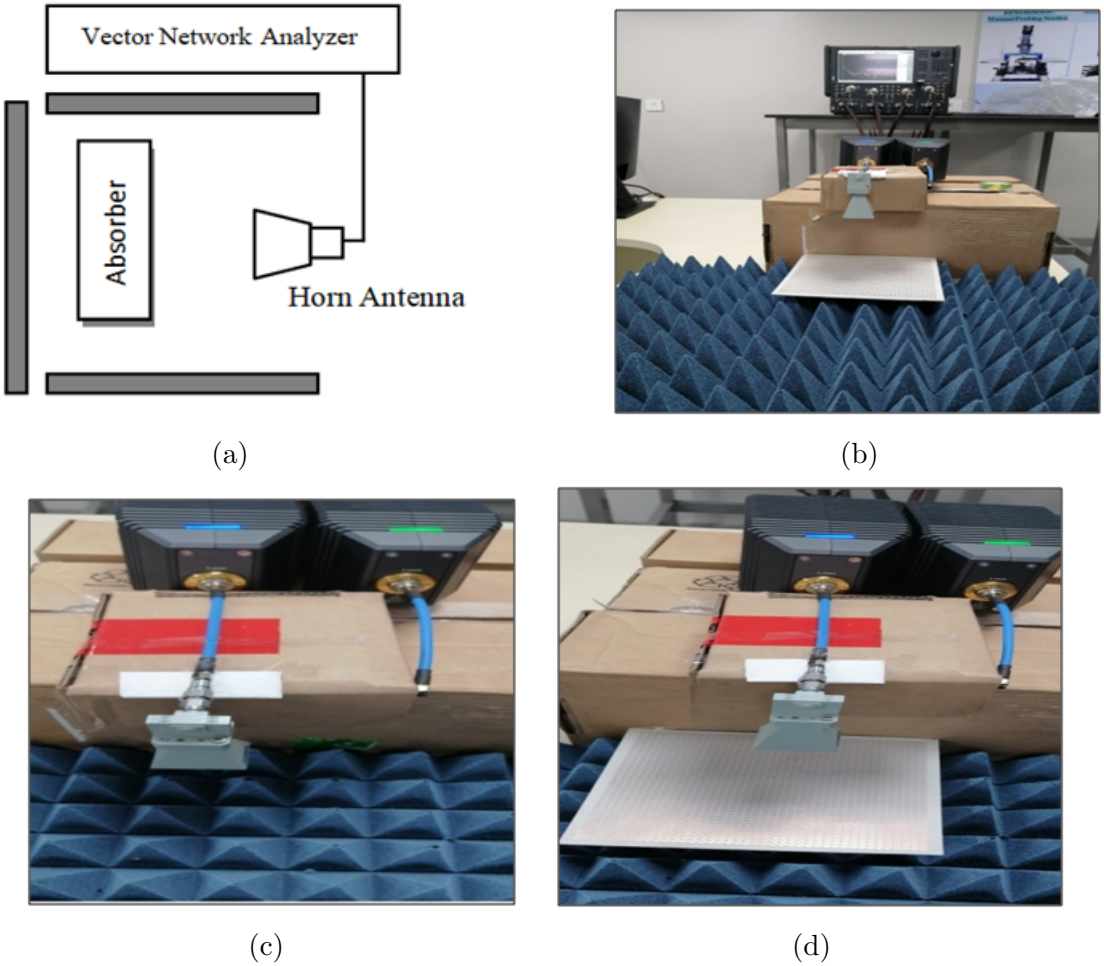

Figure 4.17: Visual representation of the experimental setup: (a) Complete experimental configuration, (b) Measurement setup for absorptivity, (c) Zero-backscattering reference ($S_{\text{Back}} = -\infty$ dB), (d) Backscattering coefficient of the test surface.

Figure 4.18 presents the observed absorption of the PMMA in contrast to the estimated values, demonstrating a significant degree of concurrence. The prototype's absorption spectra were measured, highlighting the difference between the observed and expected results for the planar absorber.The measured results closely match the broadband absorption pattern observed in the calculations, although the absorption rate is somewhat reduced at specific frequencies. The difference in the results can be attributed to diffraction and scattering of waves [94], as the sample's inability to match the conditions for infinite geometry leads to edge diffraction during characterization, resulting in minor variations observed during the manufacturing phase. Additionally, the PMMA can be modified by adjusting the frequency range it functions within through the incorporation of an active component, such as a varactor diode [95].

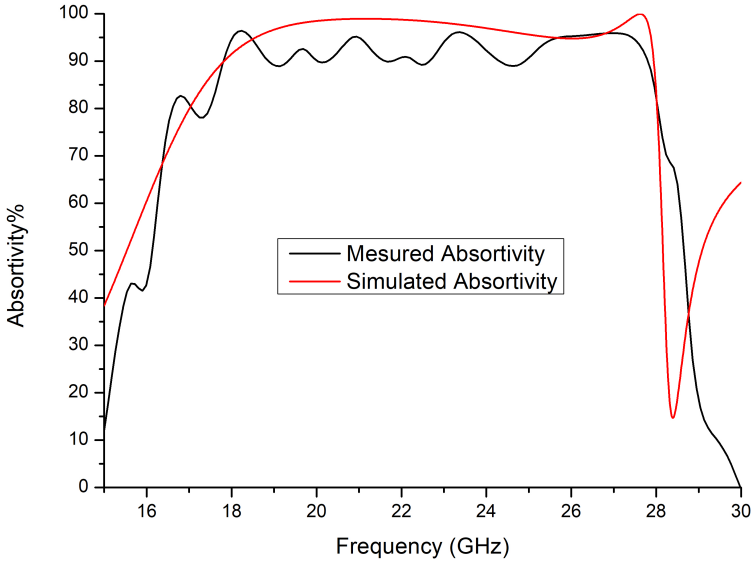

Figure 4.18: The absorptivity of the proposed MMA, as determined via both measurement and simulation.

Table 4.3 provides a comprehensive comparative study of several MMAs, focusing on important factors such as absorption bandwidth, unit cell size, thickness, and design propriety. The table also indicates whether the examined absorbers are constructed using multilayered or lumped element designs. The current MMA design offers distinct advantages, including small thickness, perfect absorptivity, and a broadband absorption response, achieved without the complexity of multiple layers or concentrated components.Comparing our study's frequency bandwidth of [17.9 to 27.9] GHz with literature findings reveals significant superiority. For instance, Zolfaghary pour et al. [96] ,Chen et al. [33], Singh et al. [37] [97], and Nguyen et al. [98] reported bandwidths ranging from approximately [7.1 to 13.8] GHz,[7.1 to 18.3] GHz, [7.39 to 18] GHz,and [8 to 18] GHz, respectively. Our bandwidth exceeds these ranges by approximately [25 to 60]%, demonstrating our absorber's ability to efficiently operate over a broader spectrum. De Araújo et al. [99] and Saadeldin et al. [100] achieved narrower ranges of [11.4 to 20] GHz and [12 to 20.2] GHz, respectively, indicating a narrower performance compared to our study. Kalraiya et al. [85] had the narrowest bandwidth of [3.90 to 10.5] GHz, significantly less than our absorber. These comparisons underscore our MMA design's robust capability in accommodating diverse EM frequencies for enhanced absorption efficiency across a wide range of applications.

Table 4.3: Comparison of Various Metamaterial Absorbers

Study	Frequency Bandwidth (GHz)	Unit Cell Dimension ($\times 10^{-3}$ m)	Thickness ($\times 10^{-3}$ m)	Multi-layered / Lumped Elements
Zolfaghary et al. [96]	7.1 - 13.8	15 × 15	6	NO / NO
Singh et al. [97]	7.39 - 18	14 × 14	3.2	YES / NO
Nguyen et al. [98]	8 – 18	9.7 × 9.7	2.5	NO / YES
De Araújo et al. [99]	11.4 – 20	3.65 × 3.65	1.6	NO / NO
Saadeldin et al. [100]	12 – 20.2	3.7 × 3.7	1.6	NO / NO
Kalraiya et al. [85]	3.90 - 10.5	12.5 × 12.5	7.57	YES / YES
Present Study	17.9 - 27.9	12.5 × 12.5	1.6	NO / NO

4.7 Conclusion

In this chapter, we looked at the structure and efficiency of the suggested metamaterial absorber, with especially focused on its ability to absorb a broad range of frequencies. The transmission line model, which is analogous, offers a theoretical foundation for comprehending the interaction between the structure and electromagnetic waves. Through the analysis of the electric and magnetic field distributions at certain frequencies, we have shown that field concentration is crucial in attaining significant absorption. The evaluation of normalized impedance and effective material characteristics also showcased the absorber's effectiveness and its ability to work regardless of polarization. The investigation on the impact of substrate thickness emphasized the significance of a thin substrate in keeping efficient absorption and flexibility. In summary, this chapter provides evidence that the suggested absorber is well engineered to provide dependable, broad-band absorption for a range of uses.

Conclusion and Perspectives

As we conclude this exploration into metamaterial absorbers, our research signifies a notable advancement in the field of electromagnetic materials and their applications. This thesis has delved deeply into the design, simulation, optimization, and fabrication of metamaterial absorbers, offering new insights and solutions that push the boundaries of current technology.

A key achievement of this work is the development and successful fabrication of a wideband metamaterial absorber (MMA) that operates efficiently within the frequency range of 17.9 GHz to 27.9 GHz. By leveraging innovative design techniques and optimizing various parameters, we have achieved a level of absorption performance that surpasses previous benchmarks. The integration of a spiral coil split-ring resonator (SRR) within the absorber's structure has proven to be highly effective in broadening the absorption bandwidth while maintaining high performance.

Our empirical results demonstrate not only a significant enhancement in the absorber's bandwidth and absorption efficiency but also a robust fabrication process that ensures the practicality and reproducibility of our design. The meticulous optimization of parameters such as wire coil angles, trace widths, and substrate thickness has led to an absorber with superior performance characteristics, setting a new standard for future research and development in this field.

Central to our success is the innovative approach adopted in the design and fabrication processes. By combining advanced simulation techniques with precise fabrication methods, we have achieved a high degree of accuracy in aligning simulated predictions with experimental results. This approach highlights the effectiveness of integrating theoretical models with practical fabrication techniques to create high-performance metamaterial absorbers.

As we reflect on the significance of our work, it is clear that our research not only advances the understanding of metamaterial absorbers but also opens new possibilities for their application in various fields. The insights gained from this study offer a solid foundation for further exploration and development, paving the way for future innovations in electromagnetic materials and their applications. The methodologies and results presented here provide valuable contributions to the ongoing advancement of metamaterial technology and its practical implementations.

In perspective, future research could build on these findings by exploring additional design modifications, alternative materials, and expanded frequency ranges. The continued refinement of fabrication techniques and the exploration of novel applications for metamaterial absorbers hold the promise of further enhancing the capabilities and impact of these advanced materials in various technological domains.

Published Works

International publication

- Mebarki GH, and N. Benmostefa. A Spiral Wire coil Wideband Metasurface Absorber with Ultrathin and Flexible Feature for Microwave Applications. journal of Nano electronics and physics (2024).
- Ghada Fatima Zahra Mebarki, Naima Benmostefa, Mohammed Feham, Mohammed Ayad Alkhafaji, Serge Dzo Mawuefa Afenyiveh, Younes Menni; Design, simulation, and experimental validation of a wideband flexible metamaterial absorber for gigahertz electromagnetic waves. AIP Advances 1 September 2024; 14 (9)

Conferences

- Mebarki ghada , Benmostefa Naima ,An Ultrathin Metamaterial Absorber for Conformal Applications at Ka Frequency Band.The 1 st International Conference on Advances in Electronics, Control and Computer Technologies "ICAECCT'23"
- Mebarki ghada , Benmostefa Naima , Flexible and ultrathin metamaterial absorber for microwave application.Nationale conference on Télécommunications thier Applications (CNTA'22)
- Mebarki ghada , benmostefa naima ,Devloped wideband conformal metamaterial absorber using Resistor elements.",NCASE24 , algeria.

IEEE

Bibliography

[1] Victor Veselago, Leonid Braginsky, Valery Shklover, and Christian Hafner. Negative refractive index materials. *Journal of Computational and Theoretical Nanoscience*, 3(2):189–218, 2006.

[2] Wenshan Cai and Vladimir Shalaev. Optical metamaterials fundamentals and application. *Physics Today*, 63(9), 2010.

[3] Kaushal Gangwar, RPS Gangwar, et al. Metamaterials: Characteristics, process and applications. *Advance in Electronic and Electric Engineering*, 4(1):97–106, 2014.

[4] Mohammad Jakir Hossain, Mohammad Rashed Iqbal Faruque, and Mohammad Tariqul Islam. Perfect metamaterial absorber with high fractional bandwidth for solar energy harvesting. *PLoS One*, 13(11):e0207314, 2018.

[5] Wenshan Cai, Uday Chettiar, Alexander Kildishev, and Vladimir Shalaev. Optical cloaking with metamaterials. nat photonics 1:224-227. *Birck and NCN Publications*, 1, 04 2007.

[6] Vivek Prakash Yadav, Praveen Sharma, Gaurav Sahu, and Lovendra Solanki. Use of metamaterials in antenna design: A review. *JETIR*, 16(12), 12 2020.

[7] Fuyan Wu, Yahui Liu, Le Ling, Zhongxi Sheng, Zao Yi, Qianju Song, Shubo Cheng, Bin Tang, Sohail Ahmad, and Tangyou Sun. Spectrally selective ultra-broadband solar absorber based on pyramidal structure. *Advanced Photonics Research*, 5(3):2300305, 2024.

[8] Mohammad Sarwar Raeen, Anveshkumar Nella, and Rajagopal Maheswar. A fourfold star petal–shaped polarization-insensitive broadband plasmonic metamaterial absorber. *Plasmonics*, 18(3):1059–1074, 2023.

[9] D.R. Smith, J.B. Pendry, and M.C.K. Wiltshire. Metamaterials and negative refractive index. *Science (New York, N.Y.)*, 305:788–92, 09 2004.

[10] JL Volakis, A Chatterjee, and J Gong. A class of hybrid finite element methods for electromagnetics: A review. *Journal of electromagnetic waves and applications*, 8(9-10):1095–1124, 1994.

[11] Gwanho Yoon, Inki Kim, and Junsuk Rho. Challenges in fabrication towards realization of practical metamaterials. *Microelectronic Engineering*, 163:7–20, 2016.

[12] Sumeet Walia, Charan M Shah, Philipp Gutruf, Hussein Nili, Dibakar Roy Chowdhury, Withawat Withayachumnankul, Madhu Bhaskaran, and Sharath Sriram. Flexible metasurfaces and metamaterials: A review of materials and fabrication processes at micro-and nano-scales. *Applied Physics Reviews*, 2(1), 2015.

[13] Sneha Singh, Golakoti Pavan, and Chetan Chalurkar. Acoustic metamaterials for noise control applications. In *Handbook of Vibroacoustics, Noise and Harshness*, pages 1–25. Springer, 2023.

[14] Patrick Rufangura. Wide-band perfect metamaterial absorber for solar cells applications. Master's thesis, Middle East Technical University, 2015.

[15] Clifford M Krowne. Left-handed material use in monoatomic & iii-v ics. *III-Vs Review*, 17(3):26–27, 2004.

[16] Claire Watts. Metamaterials and their applications towards novel imaging technologies. *Boston College*, 2015.

[17] Simon Marcellin. *Métamatériaux" tout-diélectrique" pour le térahertz*. PhD thesis, Université Paris Saclay (COmUE), 2016.

[18] P ROS. Molecular orbital calculations on copper-ch lori de com plexes. *Theoretica chimica acta*, 1996.

[19] Ari Sihvola. Metamaterials in electromagnetics. *Metamaterials*, 1(1):2–11, 2007.

[20] Davi Bibiano Brito. *Metamaterial inspired improved antennas and circuits*. PhD thesis, Télécom ParisTech, 2010.

[21] Manvir S Kushwaha and Bahram Djafari-Rouhani. Surface plasmons in coaxial metamaterial cables. *Modern Physics Letters B*, 27(17):1330013, 2013.

[22] Muhammed Emin Gulduren. *Optically modulated terahertz metamaterials using liquid crystals*. PhD thesis, The University of Alabama in Huntsville, 2019.

[23] David R Smith, Willie J Padilla, DC Vier, Syrus C Nemat-Nasser, and Seldon Schultz. Composite medium with simultaneously negative permeability and permittivity. *Physical review letters*, 84(18):4184, 2000.

[24] Martin A Green. Solar cells: operating principles, technology, and system applications. *Englewood Cliffs*, 1982.

[25] Richard W Ziolkowski. Double negative metamaterial design, experiments, and applications. In *IEEE Antennas and Propagation Society International Symposium (IEEE Cat. No. 02CH37313)*, volume 2, pages 396–399. IEEE, 2002.

[26] Wenshan Cai, Vladimir Shalaev, and Dilip Paul. Optical metamaterials: Fundamentals and applications. *Physics Today - PHYS TODAY*, 63, 09 2010.

[27] Md Mehedi Hasan, Mohammad Rashed Iqbal Faruque, and Mohammad Tariqul Islam. Dual band metamaterial antenna for lte/bluetooth/wimax system. *Scientific reports*, 8(1):1240, 2018.

[28] Shridhar E Mendhe and Yogeshwar Prasad Kosta. Metamaterial properties and applications. *International Journal of Information Technology and Knowledge Management*, 4(1):85–89, 2011.

[29] Tian Hong Loh. High impedance surface electromagnetic band gap metamaterials: Design approach and applications for antenna engineering. *Invited Paper*, 2011.

[30] Withawat Withayachumnankul and Derek Abbott. Metamaterials in the terahertz regime. *IEEE Photonics Journal*, 1(2):99–118, 2009.

[31] Costas M Soukoulis and Martin Wegener. Past achievements and future challenges in the development of three-dimensional photonic metamaterials. *Nature photonics*, 5(9):523–530, 2011.

[32] Jeremiah P Turpin, Jeremy A Bossard, Kenneth L Morgan, Douglas H Werner, and Pingjuan L Werner. Reconfigurable and tunable metamaterials: a review of the theory and applications. *International Journal of Antennas and Propagation*, 2014(1):429837, 2014.

[33] Liyang Li, Jun Wang, Jiafu Wang, Hua Ma, Hongliang Du, Jieqiu Zhang, Shaobo Qu, and Zhuo Xu. Reconfigurable all-dielectric metamaterial frequency selective surface based on high-permittivity ceramics. *Scientific Reports*, 6(1):24178, 2016.

[34] Peng Yu, Lucas V Besteiro, Yongjun Huang, Jiang Wu, Lan Fu, Hark H Tan, Chennupati Jagadish, Gary P Wiederrecht, Alexander O Govorov, and Zhiming Wang. Broadband metamaterial absorbers. *Advanced Optical Materials*, 7(3):1800995, 2019.

[35] Claire M Watts, Xianliang Liu, and Willie J Padilla. Metamaterial electromagnetic wave absorbers. *Advanced materials*, 24(23):OP98–OP120, 2012.

[36] Bachir BELKADI. *Etude et conception de filtres hyperfréquences à base de nouveaux matériaux.* PhD thesis, Université de Sidi Bel Abbès-Djillali Liabes, 2019.

[37] Sylvain Lannebere. *Étude théorique de métamatériaux formés de particules diélectriques résonantes dans la gamme submillimétrique: magnétisme artificiel et indice de réfraction négatif.* PhD thesis, Université Bordeaux 1, 2011.

[38] John E Akin. *Finite element analysis for undergraduates.* Academic Press Inc, 1986.

[39] Shu Li, Zhihui Liu, Lei Han, and Guoqing Jing. Enhanced measurement and optimization of railway profile parameters for large tamping machine operations. *Measurement Science and Technology*, 2024.

[40] Hervé Dret. *The Galerkin Method*, pages 93–109. springer, 05 2018.

[41] Hervé Le Dret. *La méthode de Galerkin*, pages 83–97. Springer Berlin Heidelberg, Berlin, Heidelberg, 2013.

[42] Solène Miaskiewicz. *Or et azacycles: vers la synthèse totale de molécules naturelles*. PhD thesis, Université de Strasbourg, 2017.

[43] Peter Markoš and Costas M Soukoulis. Transmission properties and effective electromagnetic parameters of double negative metamaterials. *Optics express*, 11(7):649–661, 2003.

[44] D Robert Smith, Sheldon Schultz, P Markoš, and Costas M Soukoulis. Determination of effective permittivity and permeability of metamaterials from reflection and transmission coefficients. *Physical review B*, 65(19):195104, 2002.

[45] GENERIC-ENSMSE. *Tolérance et accumulation des métaux lourds par la végétation spontanée des friches métallurgiques : vers de nouvelles méthodes de bio-dépollution*. PhD thesis, Universit de france, 2006.

[46] Emilie Masson. *Etude de la propagation des ondes électromagnétiques dans les tunnels courbes de section non droite pour des applications métro et ferroviaire*. PhD thesis, Université de Poitiers, 2010.

[47] A Elouadih, A Oulad-Said, and MM Hassani. Design and simulation by hfss of a miniaturized bi-mode pifa antenna for the gsm 900 and ism 2.4 ghz bands. *AMSE journal of modeling and simulation série A, en attente de publication dans*, 86(1), 2013.

[48] Manh Cuong Tran and Thi Thuy Hang Phuong. Two-layered dual-band perfect metamaterial absorber at k band frequency. *Advanced Electromagnetics*, 7(2):25–27, 2018.

[49] Ali Valipour, Mohammad H Kargozarfard, Mina Rakhshi, Amin Yaghootian, and Hamid M Sedighi. Metamaterials and their applications: an overview. *Proceedings of the Institution of Mechanical Engineers, Part L: Journal of Materials: Design and Applications*, 236(11):2171–2210, 2022.

[50] WenXuan Tang, ZhongLei Mei, and TieJun Cui. Theory, experiment and applications of metamaterials. *Science China Physics, Mechanics & Astronomy*, 58:1–11, 2015.

[51] John B Pendry, David Schurig, and David R Smith. Controlling electromagnetic fields. *science*, 312(5781):1780–1782, 2006.

[52] Alexandre Sellier. *Absorbants à métamatériaux: étude théorique et expérimentale*. PhD thesis, Université Paris Sud-Paris XI, 2014.

[53] Jussi Säily and Antti Räisänen. *Studies on specular and non-specular reflectivities of radar absorbing materials (RAM) at sub-millimetre wavelengths*. Helsinki University of Technology, 2003.

[54] W Emerson. Electromagnetic wave absorbers and anechoic chambers through the years. *IEEE Transactions on Antennas and Propagation*, 21(4):484–490, 1973.

[55] Muhammad Tariq and Muhammad Noaman Zahid. Design and performance analysis of band pass filter using frequency selective surface for 5g communication. *Proceedings of Engineering and Technology Innovation*, 23:15–22, 01 2023.

[56] Asuka Namai, Shunsuke Sakurai, Makoto Nakajima, Tohru Suemoto, Kazuyuki Matsumoto, Masahiro Goto, Shinya Sasaki, and Shin-ichi Ohkoshi. Synthesis of an electromagnetic wave absorber for high-speed wireless communication. *Journal of the American Chemical Society*, 131(3):1170–1173, 2009.

[57] Nathan I Landy, Soji Sajuyigbe, Jack J Mock, David R Smith, and Willie J Padilla. Perfect metamaterial absorber. *Physical review letters*, 100(20):207402, 2008.

[58] Ruixiang Deng, Meiling Li, Badar Muneer, Qi Zhu, Zaiying Shi, Lixin Song, and Tao Zhang. Theoretical analysis and design of ultrathin broadband optically transparent microwave metamaterial absorbers. *Materials*, 11(1):107, 2018.

[59] C. Linton. Wave propagation. from electrons to photonic crystals and left-handed materials, by p. markos and c.m. soukoulis. *Contemporary Physics*, 50, 09 2009.

[60] D.M. Pozar. *Microwave Engineering*. Wiley, 2012.

[61] Constantine A Balanis. *Advanced engineering electromagnetics*. John Wiley & Sons, 2012.

[62] Nitinkumar Jivarajbhai Bathani. *Design and Analysis of Electromagnetic wave Absorbers based on Frequency selective surfaces*. PhD thesis, GUJARAT TECHNOLOGICAL UNIVERSITY AHMEDABAD, 2022.

[63] Howard A Tanner. Fibrous microwave absorber, 3 1961. US Patent 2,977,591.

[64] W Dallenbach and W Kleinsteuber. Reflection and absorption of decimeter-waves by plane dielectric layers. *Hochfreq. u Elektroak*, 51:152–156, 1938.

[65] Winfield W Salisbury. Absorbent body for electromagnetic waves. *International Journal for Environmental Rehabilitation and Conservation*, 1952.

[66] Krishna Naishadham and Prasad K Kadaba. Measurement of the microwave conductivity of a polymeric material with potential applications in absorbers and shielding. *IEEE Transactions on Microwave Theory and Techniques*, 39(7):1158–1164, 1991.

[67] John B Pendry, Anthony J Holden, David J Robbins, and William J Stewart. Magnetism from conductors and enhanced nonlinear phenomena. *IEEE transactions on microwave theory and techniques*, 47(11):2075–2084, 1999.

[68] Richard A Shelby, David R Smith, and Seldon Schultz. Experimental verification of a negative index of refraction. *science*, 292(5514):77–79, 2001.

[69] Anthony Grbic and George V Eleftheriades. A backward-wave antenna based on negative refractive index lc networks. In *IEEE Antennas and Propagation Society International Symposium (IEEE Cat. No. 02CH37313)*, volume 4, pages 340–343. IEEE, 2002.

[70] Jeremy N Munday and Harry A Atwater. Large integrated absorption enhancement in plasmonic solar cells by combining metallic gratings and antireflection coatings. *Nano letters*, 11(6):2195–2201, 2011.

[71] Christophe Caloz and Tatsuo Itoh. Transmission line approach of left-handed (lh) materials and microstrip implementation of an artificial lh transmission line. *IEEE Transactions on Antennas and propagation*, 52(5):1159–1166, 2004.

[72] Christophe Caloz. Dual composite right/left-handed (d-crlh) transmission line metamaterial. *IEEE microwave and wireless components letters*, 16(11):585–587, 2006.

[73] Cédric Vandenbem and Jean Pol Vigneron. Mie resonances of dielectric spheres in face-centered cubic photonic crystals. *JOSA A*, 22(6):1042–1047, 2005.

[74] Haiyu Zheng, Thanh Son Pham, Liangyao Chen, and Youngpak Lee. Metamaterial perfect absorbers for controlling bandwidth: Single-peak/multiple-peaks/tailored-band/broadband. *Crystals*, 14(1):19, 2023.

[75] H Zhou, S-B Qu, J-F Wang, B-Q Lin, H Ma, Z Xu, P Bai, and W-D Peng. Ultra-wideband frequency selective surface. *Electronics letters*, 48(1):11–13, 2012.

[76] Han Xiong, Jin-Song Hong, Chao-Ming Luo, and Lin-Lin Zhong. An ultrathin and broadband metamaterial absorber using multi-layer structures. *Journal of Applied Physics*, 114(6), 2013.

[77] Yulong Fan, Yunkun Xu, Meng Qiu, Wei Jin, Lei Zhang, Edmund Y Lam, Din Ping Tsai, and Dangyuan Lei. Phase-controlled metasurface design via optimized genetic algorithm. *Nanophotonics*, 9(12):3931–3939, 2020.

[78] Wei Wang, Kejia Wang, Zhenggang Yang, and Jinsong Liu. Experimental demonstration of an ultra-flexible metamaterial absorber and its application in sensing. *Journal of Physics D: Applied Physics*, 50(13):135108, 2017.

[79] Zefeng Xu and Yu-Sheng Lin. A stretchable terahertz parabolic-shaped metamaterial. *Advanced Optical Materials*, 7(19):1900379, 2019.

[80] Saima Hafeez, Jianguo Yu, Fahim Aziz Umrani, Abdul Majeed, and Wang Yun. A broadband meta-absorber for curved terahertz stealth applications. *Electronics*, 13(15):2966, 2024.

[81] Niti Rani, Aashish Kumar Bohre, and Aniruddha Bhattacharya. An ultra-thin substrate-based conformal meta-absorber for emi shielding and rcs minimization in c and x band. *Plasmonics*, pages 1–10, 2023.

[82] Yuqiang Deng, Qing Sun, Jing Yu, Yandong Lin, and Jinghui Wang. Broadband high-absorbance coating for terahertz radiometry. *Optics Express*, 21(5):5737–5742, 2013.

[83] Huijie Chen, Xiaoqing Yang, Shiyue Wu, Di Zhang, Hui Xiao, Kama Huang, Zhanxia Zhu, and Jianping Yuan. Flexible and conformable broadband metamaterial absorber with wide-angle and polarization stability for radar application. *Materials Research Express*, 5(1):015804, 2018.

[84] Sachin Kalraiya, Raghvendra Kumar Chaudhary, and Mahmoud A Abdalla. Resistor loaded wideband conformal metamaterial absorber for curved surfaces application. *AEU-International Journal of Electronics and Communications*, 143:154033, 2022.

[85] Sachin Kalraiya, Raghvendra Kumar Chaudhary, and Mahmoud A Abdalla. Design and analysis of polarization independent conformal wideband metamaterial absorber using resistor loaded sector shaped resonators. *Journal of Applied Physics*, 125(13), 2019.

[86] GH Mebarki and N Benmostefa. A spiral wire_coil wideband metasurface absorber with ultrathin and flexible feature for microwave applications. *journal of nano and electronic physics*, 2024.

[87] I.J. Bahl and Prakash Bhartia. *Microwave Solid State Circuit Design*. wiley, 01 2003.

[88] Mohammad Lutful Hakim, Mohammad Tariqul Islam, Touhidul Alam, Sharul Kamal Abdul Rahim, Badariah Bais, Md Shabiul Islam, and Mohamed S Soliman. Triple-band square split-ring resonator metamaterial absorber design with high effective medium ratio for 5g sub-6 ghz applications. *Nanomaterials*, 13(2):222, 2023.

[89] Giampaolo Pisano, Christopher Dunscombe, Peter Hargrave, Alexey Shitvov, and Carole Tucker. Thin flexible multi-octave metamaterial absorber for millimeter wavelengths. *Applied Optics*, 62(9):2317–2328, 2023.

[90] Jingda Wen, Yinpeng Wang, and Yuhang Wang. Advanced engineering design of the metamaterial absorbers. In *Metamaterial Technology and Intelligent Metasurfaces for Wireless Communication Systems*, pages 136–179. IGI Global, 2023.

[91] C Zhang, J Yang, W Yuan, J Zhao, J Y Dai, T C Guo, J Liang, G Y Xu, Q Cheng, and T J Cui. An ultralight and thin metasurface

for radar-infrared bi-stealth applications. *Journal of Physics D: Applied Physics*, 50(44):444002, oct 2017.

[92] Ling-ling Wang, Shao-Bin Liu, Zhang Feng, Xiang-Kun Kong, and Lu-lu Liu. High-impedance surface-based flexible broadband absorber. *Journal of Electromagnetic Waves and Applications*, 31:1–16, 07 2017.

[93] Ghada Fatima Zahra Mebarki, Naima Benmostefa, Mohammed Feham, Mohammed Ayad Alkhafaji, Serge Dzo Mawuefa Afenyiveh, and Younes Menni. Design, simulation, and experimental validation of a wideband flexible metamaterial absorber for gigahertz electromagnetic waves. *AIP Advances*, 14(9):095108, 09 2024.

[94] Alparslan Cınar and S Cumhur Basaran. Textile-based quad-band electromagnetic absorber design for wearable applications. *The Journal of The Textile Institute*, pages 1–5, 2023.

[95] Tianlong Wu, Wei Li, Shaowen Chen, and Jianguo Guan. Wideband frequency tunable metamaterial absorber by splicing multiple tuning ranges. *Results in Physics*, 20:103753, 2021.

[96] Saeed Zolfaghary Pour, Ebrahim Chegini, and Mojtaba Mighani. Design of wideband metamaterial absorber using circuit theory for x-band applications. *IET Microwaves, Antennas and Propagation*, 17:n/a–n/a, 01 2023.

[97] Gaganpreet Singh, Harsh Sheokand, Kajal Chaudhary, Kumar Vaibhav Srivastava, Janakarajan Ramkumar, and S A Ramakrishna. Fabrication of non-wettable wearable textile based metamaterial microwave absorber. *Journal of Physics D: Applied Physics*, 52, 07 2019.

[98] Thi Kim Thu Nguyen, Thanh Nghia Cao, Ngoc Hieu Nguyen, Xuan Khuyen Bui, Chi Lam Truong, Dinh Lam Vu, Thi Quynh Hoa Nguyen, et al. Simple design of a wideband and wide-angle insensitive metamaterial absorber using lumped resistors for x-and ku-bands. *IEEE Photonics Journal*, 13(3):1–10, 2021.

[99] José Bruno O de Araújo, Glaucio L Siqueira, Erich Kemptner, Maurício Weber, Cynthia Junqueira, and Marbey Manhães Mosso.

An ultrathin and ultrawideband metamaterial absorber and an equivalent-circuit parameter retrieval method. *IEEE Transactions on Antennas and Propagation*, 68(5):3739–3746, 2020.

[100] A Samy Saadeldin, Amr M Sayed, Adnan M Amr, Menna O Sayed, Mohamed Farhat O Hameed, and SSA Obayya. Wideband ultrathin and polarization insensitive metamaterial absorber for ku-band applications. *Journal of Materials Science: Materials in Electronics*, 34(26):1797, 2023.